Quantum Interference in Semiconductor Rings

PhD Thesis

written by

Orsolya Kálmán

Supervisors:
Dr. Mihály Benedict
Dr. Péter Földi

Doctoral School of Physics

Department of Theoretical Physics
Faculty of Science and Informatics
University of Szeged
Szeged, Hungary
2009

Contents

Part I

Introduction

In most of the commonly used conductors the electric current is carried by electrons. Although electrons have a discrete charge, diffraction experiments also have demonstrated that they propagate as waves. The wave properties of individual electrons are hardly important in usual conductors the width of which is about ten million times the wavelength corresponding to an electron. The conductance of such a conductor is inversely proportional to its length and scales linearly with its cross-sectional area. The proportionality coefficient, or conductivity, characterizes the material the conductor is made of, and is independent of its dimensions. One may ask: What happens with this simple scaling law when one makes a conductor thinner and shorter so that the wave property of electrons becomes relevant? This question has been in the center of interest of scientists for a long time. Due to the development in miniaturization, it became possible to fabricate conductors whose dimensions are small enough not to follow the mentioned scaling law, but still much larger than microscopic objects like atoms. These are called *mesoscopic* conductors ("meso" stands for the mentioned intermediate length scale) [1,2]. The scaling law breaks down when the conductor size is small enough to allow coherent propagation of an electron across it in the given material. This happens when the dimensions of the conductor are comparable to the relevant wavelength, the mean free path and the phase relaxation length of the electrons. (These latter two notions describe the distance that an electron travels before its initial momentum or the phase of its wave function is destroyed, respectively.) The conductance of such small conductors is quantized in universal, material-independent units [3], and they operate as electron waveguides.

Although some of the pioneering experiments with mesoscopic conductors were performed using metallic conductors [4], recent works are mostly based on semiconductor heterostructures, such as AlGaAs/GaAs, or InGaAs/InAlAs. In these systems a highly mobile two-dimensional electron gas is present at the interface of the two semiconductor layers, which provides a good basis for the fabrication of mesoscopic conductors of various structure. Among these, ring shaped devices (often called *quantum rings*) are intensely studied due to their ability to show various types of quantum interference phenomena, such as the well-known Aharonov-Bohm effect [5], when the wave function of a charged particle passing around a magnetic flux experiences a phase shift as a result of the enclosed magnetic field.

Electrons – besides their wave nature – possess another quantum property, called spin. The idea of investigating, and possibly utilizing this additional feature in electronic transport led to the development of a new field of research: *spintronics* [6–9]. Devices, based on early results of spintronics are already commercially available, e.g., giant magnetoresistance (GMR) [10,11] led to computer hard drives that can store data with unprecedented surface density. An important common feature of these spintronic devices is that they use spin degree of freedom as a classical resource, quantum mechanical features play no role. In other words, spin states are "up" and "down" with respect to a certain quantization direction but their superpositions (preferably) play no role. The idea of utilizing spin as a quantum resource is a more recent direction in this field and may be related to the birth of quantum computing [12–15], which has attracted a lot of attention because of its potential to offer an exponential speedup over classical computation for certain problems [16, 17]. A quantum computational algorithm uses quantum bits (qubits), which are two-level quantum systems represented by a two-dimensional Hilbert space, i.e., their state is an arbitrary superposition of the logical "up" and "down" states. Among a variety of other possibilities, electron spin has been proposed as the qubit in a quantum computational system. From a practical point of view, using spin instead of charge in information processing applications may lead to less energy consumption, as spin flips require less energy than usual charge based operations. However, in order to achieve the ambitious goal of spin based computing, several problems have to be solved. Quantum information processing protocols [18] require coherent behavior, superpositions of the quantum bits must be available. From the transport point view, when the quantum mechanical information is being delivered by (spin) currents, the question whether these "flying qubits" are practically useful is related to the nature of the transport. In the diffusive regime, when the size of the device exceeds the (spin) coherence length, no coherent behavior can be expected. Coherent manipulation of spins is possible only if the coherence length is larger than the size of the device. Currently, high mobility samples have become available such that at cryogenic temperatures spin coherence lengths [19–21] of 100 μm have been found, which mean a promising perspective in the fabrication of devices of a few microns that are capable of coherent manipulation of spins.

Semiconductor heterostructures, which have an internal electric field perpendicular to the interface between the two layers, have found great interest in spintronic research. This is due to the fact that in such systems, the manipulation of the electron spin is possible via an effect of relativistic origin. This is called Rashba spin-orbit interaction [22]: in the particle's rest frame there is a magnetic field perpendicular to the electric field and the direction of movement. The spin direction precesses around the axis parallel to this magnetic field and the precession rate depends on the spin-orbit interaction strength, which can be controlled by an external gate voltage [23, 24].

A pioneering example of spintronic devices that make use of Rashba spin-orbit in-

teraction [25–28] is the spin field-effect transistor proposed by Datta and Das [25]. In this proposal, a spin-polarized electron is injected from a ferromagnetic source contact into a two-dimensional electron gas. The electron then undergoes spin precession due to the Rashba effect before it is collected by a ferromagnetic drain contact. By varying the strength of the spin-orbit coupling with an applied gate voltage, one can alter the degree of spin precession and thus modulate the current through the device. Another device that has received considerable attention is the spin-interference device proposed in Ref. [29]. This is a small ring (with a diameter of a micron) connected with two external leads fabricated in a semiconductor heterostructure with Rashba spin-orbit interaction. The key idea is that the phase difference between electrons traveling clockwise and counterclockwise would produce interference effects in the spin-sensitive electron transport. The conductance oscillations of such a ring, fabricated in InGaAs/InAlAs and in HgTe/HgCdTe, has been experimentally demonstrated in Refs. [30] and [31], respectively. Rectangular arrays of such rings have also been realized and measured experimentally [32,33]. Of the theoretical results concerning quantum rings with Rashba spin-orbit interaction here we mention Ref. [34] where it has been shown that the interference effects lead to the modification of the spin properties of the incoming electron by the spin-orbit interaction, resulting in a transformation of the qubit state carried by the spin [34], which can be varied by tuning the strength of the Rashba interaction, by changing the relative position of the leads, or the size of the ring.

The ongoing intensive experimental [31–33] and theoretical [35–37] interest in quantum rings with Rashba spin-orbit interaction and/or magnetic field motivated us to carry out further investigations regarding such rings. We wished to describe a quantum ring connected to two current-carrying leads, in which the probabilities for the electron to enter the two arms of the ring are not equal. We also wished to explore whether it is possible to polarize the spin of the electron by a quantum ring in which Rashba coupling is present. Additionally, we intended to calculate the conductance of rectangular arrays with Rashba spin-orbit interaction and a perpendicular magnetic field.

This dissertation is organized as follows. In Part I we summarize the results known form the literature: in Chapter 1 we give an introduction to the basic properties of transport in mesoscopic systems. Then, in Chapter 2 we overview interference effects that may be present in quantum rings and introduce one-dimensional models that are used in their theoretical description, which are based on the fact that when the width of the rings is much smaller than their radii, then, at low enough temperatures only the lowest radial mode takes part in the conduction. One of the models (Sec. 2.2) is able to take into account the imperfectness of the coupling between the current-carrying leads and the ring. It is also inherently able to account for scatterers in the arms of the ring. The other model (Sec. 2.3) considers no additional reflections at the junctions of the leads with the ring (when no scatterers are placed there directly), it simply fits the wave

functions and the currents at a given junction, and considers no scatterers in the arms of the ring. We will use this latter model to take into account spin-orbit interaction in the ring.

In Part II we present our own results: We extend the use of the above mentioned models in several aspects. In Chapter 3, we modify the model presented in Sec. 2.2 in order to be able to take into account asymmetric injection into the arms of a ring, in the presence of a magnetic field, and a scatterer in the ring. Chapter 4 is dedicated to the investigation of the effects related to a three-terminal quantum ring with Rashba spin-orbit coupling. In Section 4.1 we solve the scattering problem of such a ring with the model presented in Section 2.3. Then, in Section 4.2 we discuss our proposal for its utilisation, namely, spin-polarization: we show that the incoming electrons are forced to split into two different spatial parts and due to spin-sensitive quantum interference, electrons that are initially in a totally unpolarized spin state become polarized at the outputs with different spin directions. In Section 4.3 we analyze the physical origin of this spin polarizational effect, and demonstrate that it is due to spatial interference. In Section 4.4 we investigate the correlations between the spatial degree of freedom of the electron and its spin when leaving a three-terminal ring. We show that quantum intertwining between the spin direction and the output path can be present. In Chapter 5 we study electron transport through multi-terminal rectangular arrays of quantum rings in the presence of Rashba spin-orbit interaction and of a perpendicular magnetic field. We show that due to destructive and constructive interferences, the conductance shows oscillations as a function of the wave vector, the spin-orbit coupling strength, and the magnetic field.

Chapter 1

Transport in mesoscopic systems

In recent years miniaturization led to a dramatic increase of interest in the physics and applications of structures which can be described as "low-dimensional". In the case of electronic transport, this term refers to a system in which electrons are constrained by potential barriers so that they lose one or more degrees of freedom for motion; the system becomes two, one or even zero dimensional. Although a large variety of systems has been proposed, the majority of work on two- (and lower-) dimensional systems has been performed on semiconductor structures.

In this chapter we summarize the basic transport properties of low-dimensional systems relying mainly on Ref. [1]. We note that here we do not deal with zero-dimensional systems as they were not part of our investigations. In Section 1.1 we give an overview of the systems that are most frequently used as a basis for the fabrication of low-dimensional nanostructures. In Section 1.2 we present a simple theoretical description of two- and one-dimensional conductors, and then, in Section 1.3 we show the most important experimental measurements that are used for the characterization of these devices. In Section 1.4 we describe the characteristics of transport and then, in Section 1.5 we present the Landauer formula which relates the experimentally measurable conductance to the transmission probability through the conductor which can be obtained from its quantum mechanical description.

1.1 Semiconductor heterostructures

Currently, semiconductor heterostructures provide a good perspective for investigations of electrical conduction on short length scales. This was made possible by the availability of semiconducting materials of unprecedented purity and crystalline perfection. Such materials can be structured to contain a thin layer of highly mobile electrons. Motion perpendicular to the layer is quantized, and the electrons are constrained to move in a plane. This system combines a number of desirable properties, not shared by thin metal

films. It has a low electron density, which may be varied by means of an electric field. As we will see in Section 1.2 the low density implies a large wavelength corresponding to conduction electrons, that is comparable to the dimensions of the nanostructures that can be fabricated today. Additionally, compared to bulk samples, the electron mean free path can be quite large in these systems. As a result, quantum effects are manifested in the experimentally measurable quantities, such as the conductance.

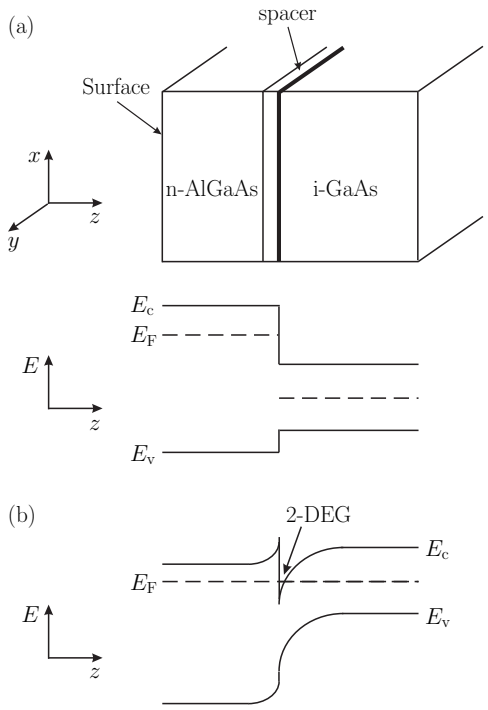

Figure 1.1: Conduction and valence band line-up at a junction between an n-type AlGaAs and intrinsic GaAs, (a) before and (b) after charge transfer has taken place. Note that this is a cross-sectional view.

One of the heterostructures that were first used for two-dimensional transport is composed of the two semiconductors, GaAs and $Al_xGa_{1-x}As$ which have nearly the same lattice parameter. In the latter material, a fraction x (commonly $x \simeq 0.3$) of the Ga atoms in the GaAs lattice is replaced by Al atoms. For $x < 0.45$ the semiconductor $Al_xGa_{1-x}As$ has a direct band gap, larger than that of GaAs, being approximately proportional to the Al content. Let us now consider the conduction and valence band line-up perpendicular to the interface (z-direction) when we first bring the layers in contact (Fig. 1.1(a)). The Fermi energy E_F in the widegap AlGaAs layer is higher than that in the narrowgap GaAs layer. Consequently, some of the electrons introduced by the donors in the n-AlGaAs are transferred into the lower-lying conduction band of the GaAs, leaving behind positively charged donors. This space charge gives rise to an electrostatic potential that causes the bands to bend as shown in Fig. 1.1(b), forming a nearly triangular well. At equilibrium the Fermi level is constant everywhere. The electron density is sharply peaked near the GaAs-AlGaAs interface (where the Fermi level is inside the conduction band) forming

a thin conducting layer which is usually referred to as the two-dimensional electron gas (2-DEG in short). In the narrow ($\sim$ 5 nm) well formed at the heterojunction, the energy spectrum for motion perpendicular to the interface is discrete (and in most cases only one electric subband is populated), whereas the motion along the interface is free-electron-like with an effective mass close to that of bulk GaAs conduction band electrons.

The carrier mobility of semiconductor heterostructures can be considerably larger than that of the corresponding bulk semiconductor; this is achieved by a technique generally referred to as "modulation doping". Modulation-doped heterostructures are obtained by introducing n-type dopant impurities (e.g., Si) into the wide-band-gap material, AlGaAs at some distance from the interface (the undoped AlGaAs is called the spacer), whereas the narrow-band-gap material (GaAs) remains free from intentional doping, as shown in Fig 1.1(a). Due to modulation doping, the mobile carriers in the heterostructure are spatially separated from their parent impurities [38] which leads to a reduction of scattering. Thus, high carrier mobilities can be obtained.

Although AlGaAs/GaAs has served as a model system for the majority of investigations of transport in low-dimensional structures, other material combinations have also received considerable attention. Important among these have been heterojunctions in InGaAs/InAlAs and HgTe/HgCdTe [39]. The InGaAs/InAlAs system has a number of potential technological advantages over AlGaAs/GaAs, such as a lower electron effective mass and a larger energy separation between conduction band minima in InGaAs/InAlAs compared with AlGaAs/GaAs, however, the presence of alloy scattering results in relatively low mobilities at low temperatures [40]. Work on HgTe/CdHgTe has indicated that many more subbands are occupied than what are usually observed in other heterojunction systems [41].

1.2 Effective mass equation, transverse modes

In order to determine theoretically the electronic states in solids, approximations of different accuracy have been developed. In this dissertation we will use the approximation that electrons are independent. In the single-electron picture it is also assumed that each electron feels the same periodic potential. Then, the wave function of an electron is a Bloch wave: the product of a plane wave and a lattice periodic function. For a given wave number (it is sufficient to consider only those in the first Brillouin zone) one can determine the corresponding energies. For bulk semiconductors these energies form bands, the two uppermost being the conduction and the valence band, which are separated by a band gap. As the Fermi level is inside the band gap, the valence band is full and the conduction band is empty. Conduction may only happen when valence electrons gain energy from thermal excitation. Only those electrons take part in the conduction, which have

an energy close to the minimum of the conduction band. For these conduction electrons the Hamiltonian can be approximated by an effective free-electron-like operator that is the sum of the energy corresponding to the conduction band edge and a kinetic term that incorporates the effect of the periodic lattice potential through the effective mass. The eigenfunctions of this Hamiltonian no longer reflect the periodicity of the crystal.

When two semiconductor crystals are placed adjacent to each other to form a heterojunction, then similar eigenvalue equations are valid in each, remembering that the effective mass could be a function of position. Thus, the dynamics of electrons in the conduction band can be described by an equation of the form

$$\left[E_{\mathrm{c}} + \frac{\boldsymbol{P}^2}{2m^*} + U(\boldsymbol{r})\right]\Psi(\boldsymbol{r}) = E\Psi(\boldsymbol{r}) \tag{1.1}$$

where $\boldsymbol{P}$ is the momentum operator of the electron, $U(\boldsymbol{r})$ is a model potential energy due to space-charge and confinement, E_{c} is the energy corresponding to the conduction band edge, and m^* is the effective mass. As we have already mentioned, the lattice potential, which is periodic on an atomic scale, does not appear explicitly in Eq. (1.1); its effect is incorporated through the effective mass m^* which we assumed here to be spatially constant. Any band discontinuity ΔE_{c} at heterojunctions is incorporated by letting E_{c} be position-dependent. We note that in the presence of a magnetic field $\boldsymbol{P}$ has to be replaced by $\boldsymbol{P} - e\boldsymbol{A}$, where e is the charge of the electron, which is the negative of the elementary charge, and $\boldsymbol{A}$ is the vector potential. Equation (1.1) is called a single-band effective mass equation.

In a 2-DEG shown in Fig.1.1(b), the electrons are free to propagate in the $x-y$ plane but are confined by some potential $U(z)$ in the z-direction. The electronic wave functions in such a structure can be written e.g., in the form

$$\Psi(\boldsymbol{r}) = \phi_l(z)e^{\mathrm{i}k_x x}e^{\mathrm{i}k_y y}, \tag{1.2}$$

with the dispersion relation:

$$E = E_{\mathrm{c}} + \varepsilon_l + \frac{\hbar^2}{2m^*}\left(k_x^2 + k_y^2\right). \tag{1.3}$$

The index l labels the different subbands each having a different wave function $\phi_l(z)$ in the z-direction and a cut-off energy ε_l. Usually at low temperatures with low carrier densities only the lowest subband with $l = 1$ is occupied and the higher subbands do not play any significant role. We can then ignore the z-dimension altogether and simply treat the conductor as a two-dimensional system in the $x - y$ plane. For a free electron gas the eigenfunctions are obtained from Eq. (1.1) by setting $U = 0$. The eigenfunctions

normalized to an area S have the form

$$\Psi(x,y) = \frac{1}{\sqrt{S}} e^{\mathrm{i}k_x x} e^{\mathrm{i}k_y y}, \tag{1.4}$$

with eigenenergies given by

$$E = E_\mathrm{s} + \frac{\hbar^2}{2m^*}\left(k_x^2 + k_y^2\right), \tag{1.5}$$

where $E_\mathrm{s} = E_\mathrm{c} + \varepsilon_1$.

At equilibrium the available states in a conductor are filled up according to the Fermi function

$$f_0(E) = \frac{1}{1 + e^{\frac{E-E_\mathrm{F}}{k_\mathrm{B}T}}}, \tag{1.6}$$

where E_F is the Fermi level, which, at $T = 0$ K, coincides with the Fermi energy. (We note that in the literature, instead of Fermi level often the terminology "chemical potential" is used, here however, the sample properties do not change significantly, therefore we will continue using "Fermi level".) In the low temperature limit ($e^{\frac{E_\mathrm{s}-E_\mathrm{F}}{k_\mathrm{B}T}} \ll 1$), the Fermi function inside the band ($E > E_\mathrm{s}$) can be approximated by

$$f_0(E) = \Theta\left(E_\mathrm{F} - E\right). \tag{1.7}$$

where Θ is the unit step function. We note that throughout this thesis we will remain within this limit.

At low temperatures the conductance is determined entirely by electrons with energy close to the Fermi level. The wavenumber of such electrons is referred to as the Fermi wavenumber (k_F):

$$k_\mathrm{F} = \frac{\sqrt{2m^*\left(E_\mathrm{F} - E_\mathrm{s}\right)}}{\hbar}. \tag{1.8}$$

As $E_\mathrm{F} - E_\mathrm{s}$ is proportional to the number of occupied states in two dimensions, and consequently to the equilibrium electron density n_s, we can express the Fermi wavenumber as:

$$k_\mathrm{F} = \sqrt{2\pi n_\mathrm{s}}. \tag{1.9}$$

In narrow conductors, besides the z-direction, electrons are also confined in a second direction. Let us consider a rectangular conductor that is uniform in the x-direction, which has some transverse confining potential $U(y)$ (see Fig. 1.2(a)). Then, the solutions of the effective mass equation (1.1) can be expressed in the form of plane waves

$$\Psi(x,y) = \frac{1}{\sqrt{L}} e^{\mathrm{i}kx} \chi(y), \tag{1.10}$$

where L is the length of the conductor over which the wavefunctions are normalized. In general, for arbitrary confining potentials $\chi(y)$ can not be determined analytically. However, for a parabolic potential $U(y) = \frac{1}{2}m^*\omega_0^2 y^2$, which is often a good description of the actual potential in narrow conductors, analytic solutions can be written down. The eigenenergies and eigenfunctions are well-known from the theory of the harmonic oscillator [42].

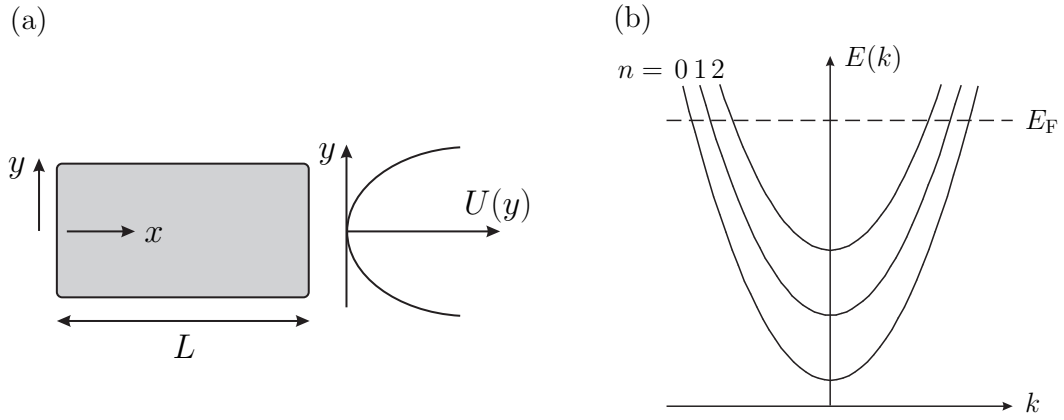

Figure 1.2: (a) A rectangular conductor assumed to be uniform in the x-direction and having some transverse confining potential $U(y)$. (b) Dispersion relation, $E(k)$ as a function of k for electric subbands arising from parabolic confinement. The different subbands are indexed by n.

The dispersion relation is sketched in Fig. 1.2(b). States with different index n are said to belong to different subbands just like the subbands that arise from the confinement in the z-direction. The spacing between two subbands is equal to $\hbar\omega_0$. The tighter the confinement, the larger ω_0 is, and the further apart the subbands are. Usually the confinement in the z-direction is very tight (electrons are confined into a layer of width of $\sim 5 - 10$ nm) so that the corresponding subband spacing is large (~ 100 meV) and only one or two subbands are customarily occupied. In all our discussions we will assume that only one z-subband is occupied. The y-confinement is relatively weaker and the corresponding subband spacing is smaller so that a number of these may be occupied under normal operating conditions. The subbands are called *transverse modes* in analogy with the modes of an electromagnetic waveguide, and such conductors are often referred to as *electron waveguides*.

As a simple estimation for the number of transverse modes in a narrow quantum wire of width W, one may also consider the transverse confining potential as an infinite well, the discrete energies of which are given as $n_{\rm W}^2\hbar^2\pi^2/(2m^*W^2)$ ($n_{\rm W} = 1, 2, ...$). Then, the energy difference between the first and second energy levels in the case of a narrow wire of width $W = 50$ nm, is approximately twice as much as the Fermi energy (for a Fermi energy of 11.13 meV in case of an effective mass $m^* = 0.023m$ of InGaAs), however, as W is increased, this ratio is decreased, so that in the case of $W = 100$ nm, two of these modes may be occupied.

1.3 Experimental characterization

In this section we summarize some of the experimental tools which are used to determine the characteristic parameters of the two-dimensional electron gas formed at the interface of semiconductor heterostructures. We will describe magnetoresistance measurements in low and high magnetic fields, from which the mobility and the carrier concentration in the sample can be derived.

The mobility (at low temperatures) provides a direct measure of the momentum relaxation time, which is limited by impurities and defects. Let us first briefly explain the meaning of mobility. In equilibrium the conduction electrons move in a random way, not producing any current in any direction. An applied electric field $\boldsymbol{E}$ gives them a drift velocity $\boldsymbol{v}_\mathrm{d}$ in the direction of the force $e\boldsymbol{E}$. In order to relate the drift velocity to the electric field we note that, at steady-state, the rate at which the electrons receive momentum from the external field is exactly equal to the rate at which they lose momentum due to scattering processes:

$$\left[\frac{d\boldsymbol{p}}{dt}\right]_{\text{scattering}} = \left[\frac{d\boldsymbol{p}}{dt}\right]_{\text{field}}. \tag{1.11}$$

From this follows that

$$\frac{m^*\boldsymbol{v}_\mathrm{d}}{\tau_\mathrm{m}} = e\boldsymbol{E}, \tag{1.12}$$

where τ_m is the momentum relaxation time. The drift velocity of electrons is thus given by

$$\boldsymbol{v}_\mathrm{d} = \frac{e\tau_\mathrm{m}}{m^*}\boldsymbol{E}. \tag{1.13}$$

The mobility is defined as the ratio of the drift velocity to the electric field:

$$\mu = \left|\frac{\boldsymbol{v}_\mathrm{d}}{\boldsymbol{E}}\right| = \frac{|e|\,\tau_\mathrm{m}}{m^*}. \tag{1.14}$$

Mobility measurement using the Hall effect (see Section 1.3.1) is a basic characterization tool for semiconductor samples, since, if the mobility is known, the momentum relaxation time can easily be deduced from Eq. (1.14).

In bulk semiconductors as we decrease the temperature, at first, the momentum relaxation time increases due to the suppression of scattering on phonons. However, it does not increase any further when the scattering on phonons becomes weak enough so that scattering on impurities becomes the dominant mechanism. In undoped samples, the mobilities are higher, but these are less useful since there are very few conduction electrons. In a 2-DEG, on the other hand, mobilities may be two orders of magnitude larger than in undoped samples. This is due to modulation doping, i.e., the spatial separation between the donor atoms in the AlGaAs layer and the conduction electrons in the GaAs layer, which reduces the scattering on impurities.

1.3.1 Hall measurement

The measurement of conductivity in a weak magnetic field (generally referred to as a Hall measurement) is one of the basic tools used to characterize semiconductor samples. This is due to the fact that it allows the determination of the carrier density n_s and the mobility μ individually, while the conductivity measured without a magnetic field only gives the product of these two.

In a magnetic field at steady-state, the rate at which the electrons receive momentum from the external field is equal to the rate at which they lose momentum due to scattering processes:

$$\frac{m^* \boldsymbol{v}_\mathrm{d}}{\tau_\mathrm{m}} = e\left(\boldsymbol{E} + \boldsymbol{v}_\mathrm{d} \times \boldsymbol{B}\right). \tag{1.15}$$

Assuming $\boldsymbol{B} = \hat{\boldsymbol{z}} B$ and using the fact that the current density $\boldsymbol{J}$ is related to the electron density n_s by the relation $\boldsymbol{J} = e\boldsymbol{v}_\mathrm{d} n_\mathrm{s}$, we can rewrite Eq. (1.15) in the form

$$\begin{pmatrix} E_x \\ E_y \end{pmatrix} = \frac{1}{\sigma} \begin{pmatrix} 1 & -\mu B \\ \mu B & 1 \end{pmatrix} \begin{pmatrix} J_x \\ J_y \end{pmatrix}, \tag{1.16}$$

where $\sigma \equiv |e|\, n_\mathrm{s} \mu$ is the conductivity, and $\mu \equiv |e|\, \tau_\mathrm{m}/m^*$. Since the resistivity tensor ρ is defined by the relation $\boldsymbol{E} = \rho \boldsymbol{J}$, we can write from Eq. (1.16)

$$\rho_{xx} = \rho_{yy} = 1/\sigma, \tag{1.17}$$

$$\rho_{yx} = -\rho_{xy} = \mu B/\sigma = B/\left(|e|\, n_\mathrm{s}\right). \tag{1.18}$$

Thus this simple Drude model predicts that the longitudinal resistance is constant while the Hall resistance increases linearly with the magnetic field.

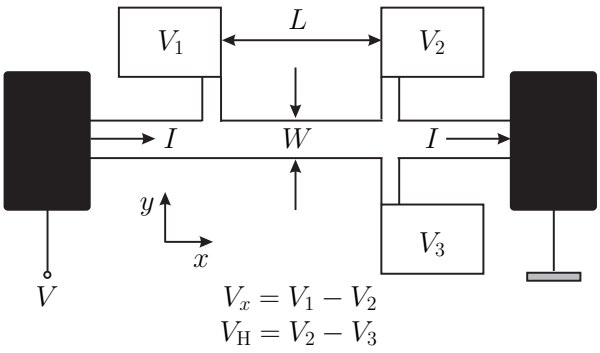

Figure 1.3: Rectangular Hall bar for magnetoresistance measurements. The magnetic field is in the z-direction, perpendicular to the plane of the conductor.

Experimentally, the resistivity tensor is measured by preparing a rectangular sample, setting up a uniform current flow along the x-direction and measuring the longitudinal voltage drop $V_x = V_1 - V_2$ and the transverse (or Hall) voltage drop $V_\mathrm{H} = V_2 - V_3$, as shown in Fig. 1.3. Since $J_y = 0$, $I = J_x W$, $V_x = E_x L$ and $V_\mathrm{H} = E_y W$, where W is

the width of the sample, the resistivities ρ_{xx} and ρ_{yx} are related to the longitudinal and transverse voltages by

$$\rho_{xx} = \frac{V_x}{I}\frac{W}{L}, \tag{1.19}$$

$$\rho_{yx} = \frac{V_{\rm H}}{I}. \tag{1.20}$$

The carrier density n_s and the mobility μ can be obtained from the measured resistivities ρ_{xx} and ρ_{yx} using Eqs. (1.17) and (1.18):

$$n_{\rm s} = \left[|e|\,\frac{d\rho_{yx}}{dB}\right]^{-1} = \frac{I}{|e|\,\frac{dV_{\rm H}}{dB}} \tag{1.21}$$

$$\mu = \frac{1}{|e|\,n_{\rm s}\rho_{xx}} = \frac{IL}{|e|\,n_{\rm s}V_xW} \tag{1.22}$$

For this reason, Hall measurement is a basic characterization tool for semiconducting samples.

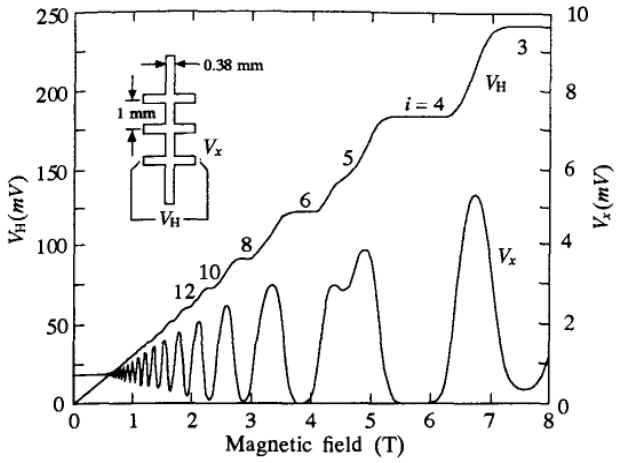

Figure 1.4: Measured longitudinal and transverse voltages for a modulation-doped GaAs sample at $T = 1.2$ K ($I = 25.5$ μA) [43].

Figure 1.4 shows the measured longitudinal voltage V_x and transverse voltage $V_{\rm H}$ for a modulation-doped GaAs sample using a rectangular Hall bar with $W = 0.38$ mm and $L = 1$ mm and a current of $I = 25.5$ μA [43]. At low magnetic fields the longitudinal voltage is nearly constant while the Hall voltage increases linearly in agreement with the predictions of the semiclassical Drude model described above. At high fields, however, the longitudinal resistance shows an oscillatory behavior, referred to as *Shubnikov-deHaas (or SdH) oscillations*, while the Hall resistance exhibits plateaus corresponding to the minima in the longitudinal resistance. These features are usually absent at room temperature but quite evident at cryogenic temperatures. These features can be understood by taking into account the formation of Landau levels.

1.3.2 High-field magnetoresistance

As we have mentioned in the previous section the comparison of the experimental data shown in Fig. 1.4 is in disagreement with the predictions of the Drude model at high magnetic fields. There are (SdH) oscillations in the longitudinal resistivity ρ_{xx}. The minimum longitudinal resistivity ρ_{xx} is very close to zero and plateaus appear in the Hall resistivity ρ_{yx} whenever ρ_{xx} goes through a minimum.

As it is well-known from quantum mechanics, at high magnetic fields, the energy of electrons becomes quantized, forming the so-called *Landau levels* [44], which have the same form as those of the quantum harmonic oscillator. In a 2-DEG, which is confined in the z-direction, they can be written as

$$E_{n_l} = E_{\mathrm{s}} + \hbar\omega_{\mathrm{c}}\left(n_l + \frac{1}{2}\right), \quad n_l = 0, 1, 2, ... \tag{1.23}$$

where $\omega_{\mathrm{c}} = |e|\, B/m^*$ is the cyclotron frequency. Landau levels are degenerate, the number of electrons per level (N) is directly proportional to the strength of the applied magnetic field [45]

$$N = \frac{2\,|e|\, B}{h}. \tag{1.24}$$

The SdH oscillations that can be seen in Fig. 1.4, arise because the step-like density of states associated with a 2-DEG breaks up into a sequence of peaks spaced by $\hbar\omega_{\mathrm{c}}$, due to the formation of Landau levels. This is illustrated in Fig. 1.5. The spikes are ideally delta functions, but in practice scattering processes spread them out in energy. As the magnetic field B is changed, the spacing of Landau levels increases. The resistivity ρ_{xx} goes through one cycle of oscillation as the Fermi level moves from the center of one Landau level to the center of the next one. This provides a simple method to calculate the electron density n_{s} from the oscillations in ρ_{xx}.

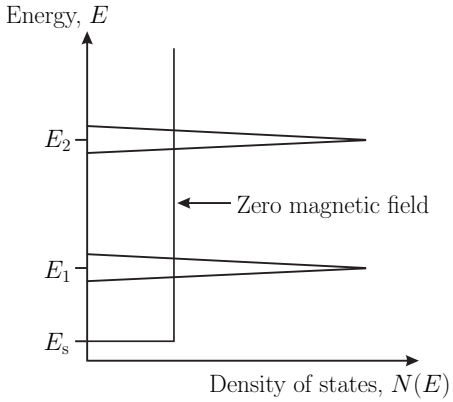

Figure 1.5: Density of states as a function of the energy for a 2-DEG in a magnetic field.

As we change the magnetic field B the number of occupied Landau levels changes. The resistivity ρ_{xx} goes through a maximum every time this number is a half-integer and

the Fermi level lies at the center of a Landau level. Therefore, the magnetic field values B_1 and B_2 corresponding to two successive peaks must be related by

$$\frac{n_\mathrm{s}}{2\left|e\right|B_1/h} - \frac{n_\mathrm{s}}{2\left|e\right|B_2/h} = 1 \tag{1.25}$$

so that

$$n_\mathrm{s} = \frac{2\left|e\right|}{h}\frac{1}{\frac{1}{B_1}-\frac{1}{B_2}}. \tag{1.26}$$

We could choose many different values B_1 and B_2 corresponding to any pair of successive peaks. They should all yield approximately the same result for the carrier density. The usual procedure is to plot the positions of the maxima in ρ_{xx} as a function of $1/B$, then the slope of the resulting straight line gives the electron density.

1.4 Transport characteristics

We have seen in Sec. 1.3 that for a given sample the electron density n_s and the mobility μ can be measured experimentally, and the momentum relaxation time τ_m can be derived. Since impurities, lattice vibrations (phonons) or electron-electron interaction lead to "collisions" that scatter the electron from one state to another, thereby changing its momomentum, the momentum relaxation time τ_m is related to the collision time τ_c (the average time between two collisions) by a relation of the form

$$\frac{1}{\tau_\mathrm{m}} = \frac{1}{\tau_\mathrm{c}}\alpha, \tag{1.27}$$

where $0 \leq \alpha \leq 1$ denotes the "effectiveness" of an individual collision in destroying momentum: if the collisions are such that the electrons are scattered only by a small angle, then very little momentum is lost in an individual collision, i.e., α is very small so that τ_m is much longer than τ_c. The mean free path L is the distance that an electron travels before its initial momentum is destroyed, that is,

$$L = v_\mathrm{F}\tau_\mathrm{m}, \tag{1.28}$$

where v_F is the Fermi velocity (the velocity of electrons at the Fermi level), which, for a free two-dimensional electron gas, can be given in the following way:

$$v_\mathrm{F} = \frac{\hbar k_\mathrm{F}}{m^*} = \frac{\hbar}{m^*}\sqrt{2\pi n_\mathrm{s}}. \tag{1.29}$$

When estimating L we used the fact that at low temperature, electrons with energies close to the Fermi level are responsible for the conduction. However, L is usually smaller than what we can calculate from Eq. (1.28), as the velocity of an electron is generally

smaller than v_{F}. In high mobility semiconductors at low temperature, the typical value of the mean free path is $10-100$ μm. In samples, which are smaller than L, electrons are transported essentially without disturbance, i.e., *ballistically*.

The mean free path is related to the momentum relaxation of the electrons. If however, we want to treat the electrons quantum mechanically, there is another characteristic length, the one that is related to phase relaxation. Let us consider the process, when the phase of the wave function of the electron is initially well-defined, but becomes more and more random as a consequence of scattering events. The characteristic time of this phenomenon is the phase relaxation time τ_φ, which can be related to τ_{c} by:

$$\frac{1}{\tau_\varphi} = \frac{1}{\tau_{\mathrm{c}}}\beta. \tag{1.30}$$

In general, τ_{m} and τ_φ are not necessarily of the same magnitude. One way to visualize the destruction of phase is in terms of a thought experiment involving interference. For example, let us suppose that we split a beam of electrons into two paths of equal length and then recombine them. In a perfect crystal the two paths would be identical resulting in constructive interference. By applying a magnetic field perpendicular to the plane containing the paths, one can change their relative phase, thereby changing the interference alternately from constructive to destructive and back. Now let us suppose that we are not in a perfect crystal but in a real one with collisions due to impurities, phonons etc. We would expect the interference amplitude to be reduced by a factor $e^{-\frac{\tau_{\mathrm{t}}}{\tau_\varphi}}$, where τ_{t} is the transit time that the electron spends in each arm of the interferometer.

Let us investigate what happens if we introduce impurities and defects randomly into each arm. The two arms are then no longer identical so that the interference may not be constructive at zero magnetic field. But as long as the impurities and defects are static, there is a well-defined phase-relationship between the two paths, and as we increase the magnetic field we would go through alternate cycles of constructive and destructive interference, whose amplitude is unaffected by the length of each arm. We may thus conclude that for static scatterers $\beta = 0$ in Eq. (1.30).

The situation is different when we take into account the effect of dynamic scatterers, like lattice vibrations (phonons). The phase-relationship between the scattered waves in the two arms then varies randomly with time so that there is no stationary interference pattern. At a fixed value of the magnetic field the scattered waves show random variations from constructive to destructive interference which time-average to zero. Interference can only be observed between the unscattered components, whose amplitude decreases exponentially with the length of each arm.

If the internal state of a scatterer can be changed as a result of a collision with an electron, then it can ruin the interference. This is related to the fact that interference can be expected only if there is no way to tell which path the electron took. But if there is a

high probability that the electron changes the internal state of a scatterer in one arm of the interferometer, then in principle, one could tell which path it took.

Another important source of phase-randomizing collisions is electron-electron interaction. Electrons are scattered by other electrons due to their mutual Coulomb repulsion. Interestingly, the mean free path (L) is not affected by such processes. This is because they do not lead to any loss in the net momentum, as any momentum lost by one electron is picked up by another. Consequently, the effectiveness factor α is zero for such processes though β is non-zero.

We have seen that the characteristic time of momentum and phase depend in a different way on the different type of scattering mechanisms, thus in general, they are not the same. In certain low-mobility semiconductors, often $\tau_\varphi \gg \tau_\mathrm{m}$, then, as a result of numerous elastic scattering events with static scatterers, the corresponding classical motion is quasi-random, but the phase coherence is kept. In high-mobility samples however, in general $\tau_\mathrm{m} \approx \tau_\varphi$, and the phase-relaxation length L_φ is given by

$$L_\varphi = v_\mathrm{F}\tau_\varphi, \tag{1.31}$$

and it is essentially equal to the mean free path L. In this case the size of the sample determines whether the behavior is coherent or incoherent. If the electrons are transported in samples that are much larger than L_φ, then no quantum effects can be expected. But if the size of the sample is smaller than L_φ, then quantum mechanical description is necessary.

1.5 The Landauer formula

In this section we describe the Landauer formula [46] that has proved to be very useful in describing mesoscopic transport. In this approach, the current through a conductor is expressed in terms of the probability that an electron can be transmitted through it.

Let us consider a piece of conductor placed between two large contact pads as shown in Fig. 1.6(a). If the dimensions of the conductor were large, then its conductance would be given by $G = \sigma d/l$, where the conductivity σ is a parameter characteristic of the material but independent of the dimensions of the sample. If this ohmic scaling relation were to hold as the length (l) is reduced, then we would expect the conductance to grow indefinitely. Experimentally, however, it is found that the measured conductance approaches a limiting value G_c, when the length of the conductor becomes much shorter than the mean free path. This is rather counterintuitive since a ballistic conductor (that is, a conductor with no scattering) should have zero resistance.

The resistance G_c^{-1} arises from the interface between the conductor and the contact pads which are very dissimilar materials. For this reason it is referred to as *contact*

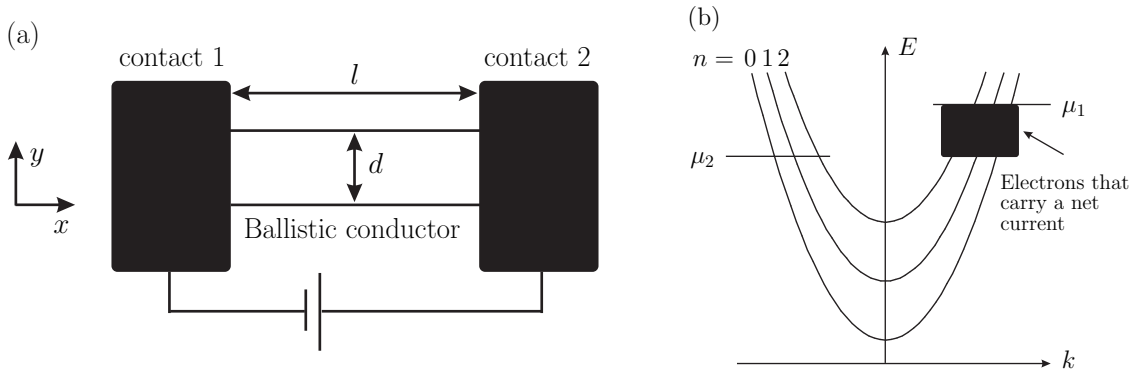

Figure 1.6: (a) A conductor is placed between two contacts across which an external bias is applied. (b) Dispersion relations for the different transverse modes (or subbands) in the narrow conductor.

resistance. The current is carried in the contacts by infinitely many transverse modes, but inside the conductor by only a few modes. This requires a redistribution of the current among the current-carrying modes at the interface leading to the interface resistance.

To determine the contact resistance G_c^{-1} we consider a ballistic conductor and calculate the current through it for a given applied bias $(\mu_1 - \mu_2)/e$. It is straightforward to calculate this current if we assume that the contacts are "reflectionless", that is, the electrons can enter them from the conductor without suffering reflections. We use the quotes to remind that the reflection is negligible only when transmitting from the narrow conductor to the wide contact. Going the other way from the contact to the conductor, the reflections can be quite large.

For "reflectionless" contacts, we have a simple situation: $+k$ states in the conductor are occupied only by electrons originating in the left contact while $-k$ states are occupied only by electrons originating in the right contact. This is because electrons originating in the right contact populate the $-k$ states and empty without reflection into the left contact while electrons originating in the left contact populate the $+k$ states and empty without reflection into the right contact (note that k denotes the wavenumber in the x-direction, shown in Fig. 1.6(a)).

We will now argue that the Fermi level for the $+k$ states is always equal to μ_1 even when a bias is applied (Fig. 1.6(b)). Suppose both contacts are at the same potential μ_1. There is no question then that the Fermi level for the $+k$ states (or any other state) is equal to the potential μ_1. Now if we change the potential at the right contact to μ_2, this can have no effect on the Fermi level for the $+k$ states since there is no causal relationship between the right contact and the $+k$ states. No electron originating from the right contact ever makes its way to a $+k$ state. Similarly, we can argue that the Fermi level for the $-k$ states is always equal to μ_2. Hence at low temperatures the current is equal to that carried by all the $+k$ states lying between μ_1 and μ_2.

To calculate the current we note that the states in the narrow conductor belong to different transverse modes or subbands, as discussed in Section 1.2. Each mode has a dispersion relation $E(n,k)$ as sketched in Fig. 1.2(b) with a cut-off energy

$$\varepsilon_n = E(n, k = 0), \tag{1.32}$$

below which it cannot propagate. The number of transverse modes at an energy E is obtained by counting the number of modes having cut-off energies smaller than E:

$$M(E) = \sum_n \Theta(E - \varepsilon_n). \tag{1.33}$$

We can evaluate the current carried by each transverse mode (labeled by n) separately and add them up.

Let us consider a single transverse mode whose $+k$ states are occupied according to some function $f^+(E)$ (in the low temperature limit this function is given by $f^+(E) = \Theta(\mu_1 - E)$). A uniform electron gas with n_e electrons per unit length moving with a velocity v carries a current equal to $en_\mathrm{e}v$. Since the electron density associated with a single k-state in a conductor of length l is $n_\mathrm{e} = 1/l$, and its velocity is given by $v = \frac{1}{\hbar}\frac{dE}{dk}$, we can write the current I carried by the $+k$ states as

$$I = \frac{e}{l}\sum_k v f^+(E) = \frac{e}{l}\sum_k \frac{1}{\hbar}\frac{\partial E}{\partial k} f^+(E). \tag{1.34}$$

Assuming periodic boundary conditions and converting the sum over k into an integral according to the usual prescription

$$\sum_k \to 2\frac{l}{2\pi}\int dk,$$

where the factor 2 takes into account the spin of the electron, we obtain

$$I = \frac{2e}{h}\int_{max(\varepsilon_n,\mu_2)}^{\infty} f^+(E)dE, \tag{1.35}$$

where ε_n is the cut-off energy of the waveguide mode. If $\varepsilon_n < \mu_2$, and we are in the low-temperature limit, then we can easily calculate the integral (1.35):

$$I = \frac{2e}{h}(\mu_1 - \mu_2). \tag{1.36}$$

From this follows that the contact resistance is

$$G_\mathrm{c}^{-1} = \frac{(\mu_1 - \mu_2)/e}{I} = \frac{h}{2e^2}. \tag{1.37}$$

For a single-moded conductor the contact resistance is ~ 12.9 kΩ, which is certainly not negligible. This is the resistance one would measure if a single-moded ballistic conductor were placed between two conductive contacts.

Assuming that M modes carry the current the contact resistance (which is the resistance of a ballistic waveguide) is given by

$$G_{\mathrm{c}}^{-1} = \frac{h}{2e^2 M}, \tag{1.38}$$

i.e., it is inversely proportional to the number of modes. This means that in the macroscopic limit, when M is very large, the contribution of the contact resistance to the full resistance is negligible. If however, M is sufficiently small, then the appearance of a new mode leads to a measurable decrease in the resistance.

It is important to note that the contact resistance arises because on one side the current is carried by infinitely many modes, while on the other side it is carried only by a few modes. The details of the geometry are not important as long as the contacts are "reflectionless" as explained earlier.

Let us now consider the case when there is scattering inside the ballistic conductor (e.g. due its geometry or impurities). Then those electrons which have entered the conductor not necessarily exit from it. This leads to a resistance greater than G_{c}^{-1}. As we explained above, the current that enters the conductor is

$$I_{in} = \frac{2e}{h} M \left(\mu_1 - \mu_2\right). \tag{1.39}$$

If, for simplicity, we consider the probability T that an electron transmits the conductor to be equal for each mode, then the current which flows out of the conductor is

$$I_{out} = T \frac{2e}{h} M \left(\mu_1 - \mu_2\right), \tag{1.40}$$

from which for the conductance we get

$$G = \frac{2e^2}{h} MT. \tag{1.41}$$

This is the *Landauer formula*. The factor T represents the probability that an electron injected at one end of the conductor will be transmitted to the other end. If the transmission probability is unity, we recover the correct expression for the resistance of a ballistic conductor including the contact resistance (see Eq. (1.38)).

1.6 Spin-orbit interaction

In this section we recall a relativistic effect, namely, spin-orbit interaction, that is common in semiconductor heterostructures either due to the inversion asymmetry in the bulk crystal, or to the asymmetry in the growth direction of the heterostructure. As we will see in the next chapters, devices with such interactionmay find interesting applications.

Taking an expansion of the Dirac equation up to second order in $\boldsymbol{P}^2/m^2c^2$ [47, 48], the most important correction to the nonrelativistic (Pauli) limit is the appearance of the term in the Hamiltonian called the *spin-orbit interaction*[1]:

$$H_{SO} = -\frac{\hbar}{4m^2c^2}\boldsymbol{\sigma}\cdot(\boldsymbol{P}\times\boldsymbol{\nabla}V) \tag{1.42}$$

as it induces a splitting of the energy levels due to spin, even in the absence of an external magnetic field. The other second order corrections are spin independent and in a perturbative treatment yield only additive constants, and have no effect on the spectrum. Therefore we have the following effective Hamiltonian for an electron in the potential V:

$$H = \frac{1}{2m}\left(\boldsymbol{P}-e\boldsymbol{A}\right)^2 + V - \mu\boldsymbol{\sigma}\boldsymbol{B} - \frac{\hbar}{4m^2c^2}\boldsymbol{\sigma}\left(\boldsymbol{P}\times\boldsymbol{\nabla}V\right) \tag{1.43}$$

and the wave function will be a two-component *spinor*:

$$\Psi = \begin{pmatrix}\psi_1\\ \psi_2\end{pmatrix}. \tag{1.44}$$

In a single-electron picture of a solid, essentially the same equation can be used to describe the motion of an electron, replacing m with the effective mass m^* in the first and last terms. One splits the potential $V = V_0(\boldsymbol{r}) + V_{\text{ext}}(\boldsymbol{r})$ into the periodic crystal potential V_0 and an aperiodic part V_{ext}, which contains the potential due to impurities, confinement, boundaries, and external electrical field (e.g. gate voltage). One then tries to eliminate the crystal potential as much as possible and to describe the charge carriers in terms of the band structure. The simplest systems of this kind are electrons in cubic direct-gap semiconductors, where the conduction band and the valence band are separated by a band gap E_0 at $\boldsymbol{k}=0$. In a perturbation theory around $\boldsymbol{k}=0$ [49] the lowest order terms that couple to the spin are expected to be linear in $\boldsymbol{k}$:

$$H_{\text{SO}} = -\boldsymbol{b}(\boldsymbol{k})\cdot\boldsymbol{\sigma}. \tag{1.45}$$

[1]The terminology is explained by the fact that in an atom, the potential giving rise to the electric field is central $V = V(r)$ and this term reduces to the form

$$H_{\text{SO}} = \frac{1}{2m^2c^2}\frac{1}{r}\frac{dV}{dr}\boldsymbol{S}\cdot\boldsymbol{L},$$

with $\boldsymbol{L} = \boldsymbol{R}\times\boldsymbol{P}$ being the orbital angular momentum.

Time reversal symmetry requires $\boldsymbol{b}(-\boldsymbol{k}) = -\boldsymbol{b}(\boldsymbol{k})$. If, in addition, the system has an inversion symmetry $\boldsymbol{b}(-\boldsymbol{k}) = \boldsymbol{b}(\boldsymbol{k})$ then the only possible solution is $\boldsymbol{b}(\boldsymbol{k}) = 0$. Thus, for the term (1.45) to be nonzero the inversion symmetry needs to be broken.

For a three-dimensional system, $\boldsymbol{b}$ can only be present if the inversion symmetry of the host crystal is broken. This is called *bulk inversion asymmetry*. In the case of a two-dimensional system, $\boldsymbol{b}$ can also result from an asymmetry in the confinement, or with other words, from *structural inversion asymmetry*. Here we focus on electrons confined to two dimensions.

In zinc blende structures (such as GaAs), the bulk inversion asymmetry leads to the so-called Dresselhaus SO coupling [50] which manifests itself in a term linear in k:

$$H_{\mathrm{D1}} = \beta \left(k_x \sigma_x - k_y \sigma_y \right), \tag{1.46}$$

and a term cubic in k:

$$H_{\mathrm{D2}} = \mathcal{B} k_x k_y \left(k_y \sigma_x - k_x \sigma y \right), \tag{1.47}$$

where $\mathcal{B} \approx 27$ eVÅ^3, for both GaAs and InAs [51, 52], and $\beta \approx -\mathcal{B}(\pi/d)^2$, with d being the width of the confinement. For small confinement width d, the main bulk inversion asymmetry contribution is the H_{D1} term.

Another spin-orbit coupling term arises if the confinement potential $V(z)$ along the z-direction (the growth direction of the heterostructure) is not symmetric, i.e., if there is a structural inversion asymmetry. This is the so-called Rashba Hamiltonian [22, 53–55]:

$$H_{\mathrm{R}} = \alpha \boldsymbol{\sigma} \cdot (\hat{\boldsymbol{z}} \times \boldsymbol{k}) = \alpha \left(k_y \sigma_x - k_x \sigma_y \right), \tag{1.48}$$

where the parameter α describes the strength of the spin-orbit coupling. The magnitude of α depends on the asymmetry of the quantum well potential [54] and it can be modified by applying an additional field via external gates [23]. In general, the level splitting due to the Rashba spin-orbit interaction is inversely proportional to the energy gap E_0. It has been pointed out that the Rashba mechanism becomes dominant in a narrow-gap semiconductor system [56, 57], and it can be particularly large, for example, in n-type InGaAs heterojunctions or quantum wells [58, 59] (with typical values in the range (0.5–2.0) $\times 10^{-11}$ eVm [23, 24]), or in HgTe quantum wells [60].

A very visible manifestation of the spin-orbit spin splitting is a beating pattern in Shubnikov–de Haas (SdH) oscillations due to two close frequency components with similar amplitudes arising from the spin-split levels. These provide in fact an experimental method for determining the value of the Rashba spin-orbit interaction strength α [60, 61].

Chapter 2

Models of quantum rings

In Section 2.1 of this chapter we give a review of quantum interference effects that emerge in ballistic rings (i.e., in rings, in which scattering is practically zero), which we will call *quantum rings* throughout this dissertation. We will show that the presence of a magnetic field, or Rashba spin-orbit coupling together with quantum interference leads to the appearance of oscillations in the conductance of such devices as a function of the magnetic field, or the external gate voltage, respectively. Then, we introduce two widely used models in the theoretical description of these rings. Both approaches are based on the assumption that the ring is formed by narrow leads in which the spacing between the discrete energy levels produced by the transverse confinement is much larger than the energy range of the longitudinal transport, so that only one such transverse mode takes part in the conduction (see Section 1.2). In such leads the single-electron Schrödinger equation reduces to a one-dimensional equation. Therefore, one often refers to such models as one-dimensional. First, in Section 2.2 we consider the method [62], which takes into account elastic scatterers in the arms of the ring and in the junctions of a lead with the ring. Then, in Section 2.3, we introduce a model, which inherently does not account for any scatterers in the arms of the ring or at the junctions, however, takes into account the presence of spin-orbit interaction.

2.1 Interference effects in quantum rings

We have seen in Section 1.4 that in ballistic conductors of multiply connected geometry interference effects are expected to appear. As these effects manifest themselves in oscillations of measurable quantities, e.g., the conductance, they have been in the center of interest since the first nanoscale metallic conductors were fabricated. In this section we give a review of interference effects that emerge as a result of the presence of a magnetic field or Rashba spin-orbit interaction in quantum rings.

2.1.1 Quantum rings

The first quantum rings were fabricated from normal metals [4, 63]. Later, due to the development of semiconductor nanotechnology, it became possible to prepare quantum rings in semiconductor heterointerfaces e.g. in AlGaAs/GaAs [64–66], InGaAs/InAlAs [32] and HgTe/HgCdTe [31], by techniques such as etching [32, 67], patterning by a scanning force microscope [68], or optical and electron beam lithography [31]. The usual radii of such rings range from a hundred nanometers to a few micrometers, while their usual widths range from a few tens to a few hundreds of nanometers.

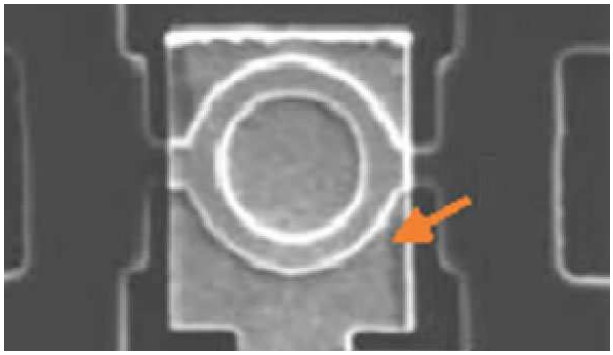

Figure 2.1: Scanning electron microscope picture of a quantum ring fabricated in InGaAs/InAlAs. The radius of the ring is 340 nm, the width of the arms is 200 nm [30].

Figure 2.1 shows a scanning electron microscope picture of an experimentally realized quantum ring in InGaAs/InAlAs, with a radius of 340 nm, and an arm width of 200 nm. The ring was fabricated by electron beam lithography and electron cyclotron resonance dry etching [30].

2.1.2 The effect of magnetic field

In a quantum ring which encloses a well-defined flux Φ the conductance has a fundamental periodicity

$$G(\Phi) = G(\Phi + n\Phi_0), \quad (n = 1, 2, 3, ...)\,, \tag{2.1}$$

as a function of the perpendicular magnetic field $\boldsymbol{B}$ (or the flux $\Phi = BS$ through the area S enclosed by the conductor), where $\Phi_0 = h/|e|$ is called the magnetic flux quantum. This is due to the Aharonov-Bohm effect [5, 69], which shows how an electron can be influenced by the presence of a vector potential even if the external $\boldsymbol{B}$ field is exculded from the region where the electron is moving. In most of the actual experiments however, the magnetic field penetrates the arms of the ring as well as its interior so that deviations from Eq. (2.1) can occur. Since in many situations such deviations are small, at least in a limited field range, these magnetoconductance oscillations are still referred to as Aharonov-Bohm (AB) oscillations [4, 64–66].

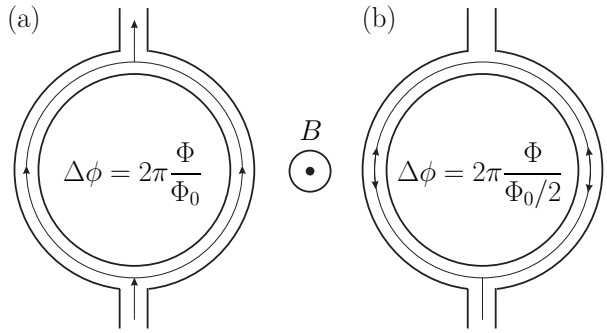

Figure 2.2: Illustration of the effect of a magnetic field in a ring geometry. (a) The phase difference between interfering trajectories responsible for the conductance oscillations with $\Phi_0 = h/|e|$ periodicity in the enclosed flux Φ. (b) The phase difference of the pair of time-reversed trajectories which lead to oscillations with $\Phi_0/2 = h/2|e|$ periodicity.

The fundamental periodicity

$$\Delta\Phi_{\mathrm{AB}} = \Phi_0 = \frac{h}{|e|} \tag{2.2}$$

in the magnetic flux is caused by the interference between trajectories which make a half-revolution around the ring, as shown in Fig. 2.2(a). The first harmonic oscillation, which pertains to the periodicity

$$\Delta\Phi_{\mathrm{AAS}} = \frac{\Phi_0}{2} = \frac{h}{2|e|}, \tag{2.3}$$

results from interference after one complete revolution, as shown in Fig. 2.2(b). The main difference between these two types of oscillations is that in non-ideally ballistic samples, the phase of the one with $h/|e|$ periodicity (2.2) is not fixed relative to zero magnetic field, it is sample-specific. The magnitude of this phase depends on the microscopic details of the impurity configuration. On the other hand, as the oscillations with $h/2|e|$ periodicity (2.3) arise from the interference of trajectories that make a full revolution in the ring, they always result in a conductance minimum at $B = 0$, independently of the sample. Consequently, in a geometry with many rings in series (or in parallel) the $h/|e|$ oscillations average out, but the $h/2|e|$ oscillations remain [70]. The oscillations with $h/2|e|$ periodicity are often referred to as Al'tshuler-Aronov-Spivak (AAS) [63, 71, 72] oscillations, as these authors were the first to suggest that such oscillations should survive when conductors are disordered. Such conductance oscillations have been observed in metal cylinders [73, 74] and honeycomb networks [75, 76] as well as square loop and ring arrays fabricated in semiconductor heterostructures [32, 77].

2.1.3 Spin-dependent interference

As we have mentioned in Section 1.6, in certain heterostructures spin-orbit interaction is present at the heterointerface as a result of the inversion asymmetry of the bulk crystal

(Dresselhaus coupling), or of the asymmetry of the confining potential in the growth direction (Rashba coupling), or both. It was found that in most of the cases the dominant contribution comes from the Rashba term [57,58,78]. Additionally, this type of spin-orbit interaction is tunable with external gate electrodes [23,24], which makes it very attractive for applications in spintronics [6,8,9,79,80].

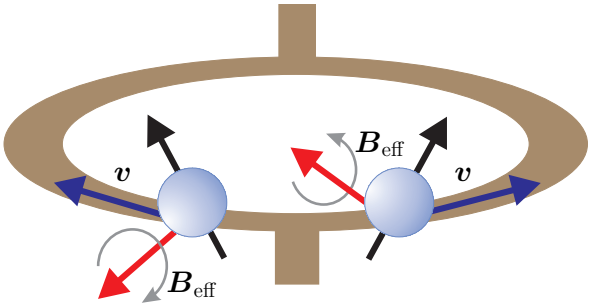

Figure 2.3: Quantum ring with Rashba spin-orbit interaction [81]. The electric field originating from the asymmetric confinement potential is perpendicular to the plane of the heterointerface, where the ring is frabricated. From the rest frame of the electron there is an effective magnetic field in the plane of the interface, perpendicular to the direction of movement. The precession angles in the left and right branches are different, leading to spin-dependent interference.

If the electron is restricted to move on a ring within the heterointerface, where Rashba-type spin-orbit interaction is present – as suggested by Nitta et al. [29, 81] – then the interference will be spin dependent as a function of the external gate voltage that is applied by a gate electrode which covers the ring. This can most easily be understood if we look at the effect of spin-orbit coupling from the rest frame of the electron (see Fig. 2.3). As a result of the asymmetric confinement potential there is an electric field perpendicular to the heterointerface. The electron sees this field as an effective magnetic field B_{eff} that is parallel to the plane of the interface (perpendicular to the electric field) and perpendicular to the direction of its movement, consequently, its spin will precess around it with a rate that depends on the strength of the Rashba coupling α. Since the direction of the magnetic field seen by the electron is different in every point of the ring (as the direction of the velocity is always tangential) the phases acquired in the left and right arms of the ring are not the same: they have opposite signs because the precession orientation is opposite. This leads to the oscillation of the conductance as a function of the external gate voltage (Rashba coupling strength), which has been verified by experiments with single rings [31] and ring arrays [32,33].

2.2 Model of a quantum ring with elastic scatterers

We have discussed in Section 1.4 that a scatterer placed in the arm of the ring (or the local application of a gate that affects the properties of one arm) may introduce phase

shifts in the electron wave function and change drastically the position and/or amplitude of the Aharonov-Bohm oscillations [31, 67, 82–85]. The general one-dimensional model of quantum rings we present here, which was introduced by Büttiker et al. [62], is able to take into account such elastic scatterers in the arms of the ring as well as in the junctions, thereby describing the imperfectness of the coupling between the current-carrying leads and the ring. We will use this model in Section 3 to describe asymmetric injection into the arms of the ring.

In order to describe elastic scattering in the arms of the ring, the model uses – instead of a potential $V(x)$ – a transfer matrix $\mathbf{t}$ [86], which relates the amplitudes β_{in}, β_{out} of the wave function to the left of the scatterer, to the amplitudes $\tilde{\beta}_{\text{out}}$, $\tilde{\beta}_{\text{in}}$ to the right of the scatterer (see Fig. 2.4)

$$\mathbf{t}\begin{pmatrix}\beta_{\text{in}}\\ \beta_{\text{out}}\end{pmatrix} = \begin{pmatrix}\tilde{\beta}_{\text{out}}\\ \tilde{\beta}_{\text{in}}\end{pmatrix}. \tag{2.4}$$

By taking into account the conservation of probability and time reversal symmetry [87,88], $\mathbf{t}$ is given by

$$\mathbf{t} = \begin{pmatrix} \frac{1}{t^*} & -\frac{r^*}{t^*} \\ -\frac{r}{t} & \frac{1}{t} \end{pmatrix}, \tag{2.5}$$

where

$$t = \sqrt{T_{\text{s}}}e^{\text{i}\chi} \tag{2.6}$$

is the transmission amplitude with T_{s} being the transmission probability through the scatterer, and χ the phase change in the transmitted wave.

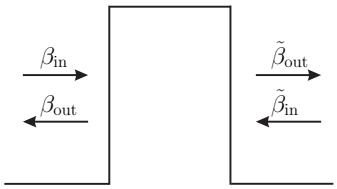

Figure 2.4: Schematic representation of the potential $V(x)$ of the scatterer.

An incoming wave from the left of the scatterer of amplitude 1 gives rise to a reflected wave with amplitude

$$r = e^{-\text{i}\frac{\pi}{2}}\sqrt{R_{\text{s}}}e^{\text{i}\chi}e^{\text{i}\chi_a}, \tag{2.7}$$

where $R_{\text{s}} = 1 - T_{\text{s}}$ is the reflection probability and χ_a is a possible additional phase difference between the transmitted and reflected amplitudes (note that in case of a symmetric potential $\chi_a = 0$). For an incoming wave to the right of the scatterer,

$$r' = e^{-\text{i}\frac{\pi}{2}}\sqrt{R_{\text{s}}}e^{\text{i}\chi}e^{-\text{i}\chi_a} \tag{2.8}$$

is the amplitude of the reflected wave. We note that for the case when the electron is

scattered on more scatterers in series, one may also determine a transfer matrix of the form (2.5), which relates the amplitudes on the left of the scatterers to the amplitudes on their right, thus it is enough to consider one transfer matrix in each arm of the ring.

2.2.1 Closed ring with Aharonov-Bohm flux

Let us consider the ring, shown in Fig. 2.5, which encircles an Aharonov-Bohm flux Φ (i.e., the magnetic field is zero in the ring). Let us assume that there are two scatterers in the ring, with transfer matrices denoted by $\mathbf{t}_1$ and $\mathbf{t}_2$. These transfer matrices give the amplitudes of the wave functions to the right of the scatterers in terms of the amplitudes of the wave functions to the left of the scatterers. If we denote the transfer matrix which yields the amplitudes to the left of the scatterer in terms of the amplitudes to the right by $\mathbf{t}_2'$, the two transfer matrices give rise to the combined scatterer $\mathbf{t} = \mathbf{t}_2'\mathbf{t}_1$.

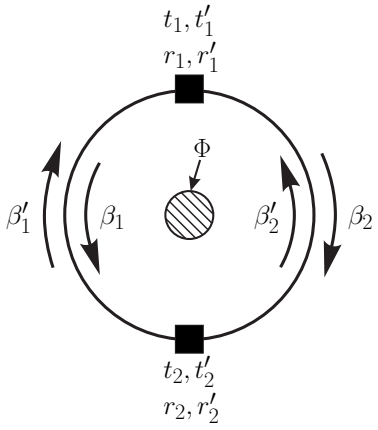

Figure 2.5: Closed ring with two elastic scatterers (denoted by the black squares) in the presence of an Aharonov-Bohm flux Φ.

As we follow the wave function around the ring, its phase changes by $2\theta = 2\pi\Phi/\Phi_0$. Therefore we can describe this closed ring with the following equation

$$\left[\mathbf{t}_2'\mathbf{t}_1 - e^{2\mathrm{i}\theta}\right] \begin{pmatrix} \beta_1' \\ \beta_1 \end{pmatrix} = 0, \tag{2.9}$$

which has nontrivial solutions only if

$$\det\left[\mathbf{t}_2'\mathbf{t}_1 - e^{2\mathrm{i}\theta}\right] = 0. \tag{2.10}$$

This is the eigenvalue equation of the closed ring. If we consider two equal scatterers $t_1 = t_2 = \sqrt{T_\mathrm{s}}e^{\mathrm{i}\chi}$, $r_1 = r_2 = r_1' = r_2' = e^{-\mathrm{i}\frac{\pi}{2}}\sqrt{R_\mathrm{s}}e^{\mathrm{i}\chi}$, where both χ and T_s are functions of the energy, then, Eq. (2.10) leads to

$$\cos^2\chi = T_\mathrm{s}\cos^2\theta, \tag{2.11}$$

from which, for a fixed value of θ, the discrete eigenenergies E_n of the closed ring can be determined. We note that when no scattering takes place in the arms of the ring, i.e., $T_s = 1$, then the phase χ is simply the geometrical phase, and the energy E is related to it by $\chi = \sqrt{2m^*E}\rho\pi/\hbar$ with ρ being the radius of the ring.

2.2.2 The scattering matrix method to couple leads to the ring

Now let us consider the case, when leads are attached to the ring. In the model of Ref. [62], at a junction of a lead with the ring (shown by the black triangles in Fig. 2.6), the three outgoing waves with amplitudes $(\alpha', \beta', \gamma')$ are related to the three incoming waves (α, β, γ) by a scattering matrix S:

$$\overrightarrow{\alpha}' = S\overrightarrow{\alpha}. \tag{2.12}$$

Current conservation implies that S is unitary, and time-reversal invariance implies, furthermore, that $S^* = S^{-1}$ [87, 88]. Consequently, the scattering matrix S has to be symmetric. As a result, in general, it depends on five independent parameters.

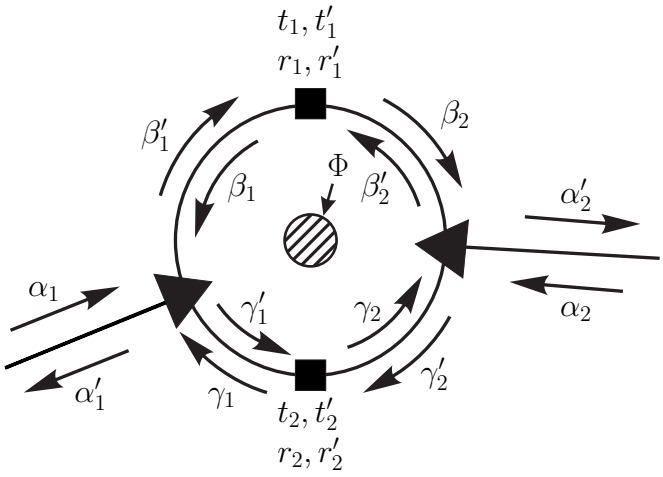

Figure 2.6: Ring connected to leads with elastic scatterers in the juctions and in the arms.

Büttiker et al. [62] assumed S to be symmetric with respect to the two arms of the ring, i.e., the probabilities of transmission from the incoming lead into the two arms and from the two arms into the incoming lead are considered equal, just as those from one arm to the other. In this way, the number of independent parameters is reduced to three. In addition to these, one may also assume that S is real, since the division of the elastic scattering between the S matrix and the $\mathbf{t}$ matrices is arbitrary. Consequently, the S

matrix can be written in the form

$$S = \begin{pmatrix} -(a+b) & \sqrt{\epsilon} & \sqrt{\epsilon} \\ \sqrt{\epsilon} & a & b \\ \sqrt{\epsilon} & b & a \end{pmatrix}, \tag{2.13}$$

with the following equations between its elements:

$$\begin{aligned} (a+b)^2 + 2\epsilon &= 1, \\ a^2 + b^2 + \epsilon &= 1, \\ 2ab + \epsilon &= 0. \end{aligned} \tag{2.14}$$

There are two types of solutions to Eqs. (2.14) for the coefficients a and b:

$$(a_1)_\pm = \pm\frac{1}{2}\left(\sqrt{1-2\epsilon} - 1\right), \tag{2.15}$$

$$(b_1)_\pm = \pm\frac{1}{2}\left(\sqrt{1-2\epsilon} + 1\right), \tag{2.16}$$

and

$$(a_2)_\pm = \pm\frac{1}{2}\left(\sqrt{1-2\epsilon} + 1\right), \tag{2.17}$$

$$(b_2)_\pm = \pm\frac{1}{2}\left(\sqrt{1-2\epsilon} - 1\right). \tag{2.18}$$

These equations determine all real 3×3 S matrices that are symmetric with respect to the two arms of the ring as a function of a single parameter ϵ, where $0 \leq \epsilon \leq \frac{1}{2}$.

Let us first consider the solutions $a = (a_1)_\pm$, $b = (b_1)_\pm$. A wave of unit amplitude coming from the left lead (see Fig. 2.6) is reflected back with probability $(a+b)^2 = 1-2\epsilon$ and transmitted into the two arms of the ring with equal probability ϵ. For $\epsilon = 1/2$, the junction is completely transparent for incoming electrons and the lead is strongly coupled to the ring. On the other hand, for $\epsilon = 0$, electrons are totally reflected and there is no coupling between the lead and the ring. In this case, the transmission probability from one arm of the ring into the other is $b^2 = 1$ and electrons in the ring do not see the junction. Thus ϵ is a coupling parameter and the solutions $a = (a_1)_\pm$, $b = (b_1)_\pm$ describe the transition from the strong coupling limit $\epsilon = 1/2$ to the weak or zero coupling limit $\epsilon = 0$. The solutions $a = (a_2)_\pm$, $b = (b_2)_\pm$ describe a transition from strong coupling $\epsilon = 1/2$ to a situation where the leads and the two arms are completely decoupled: For $\epsilon = 0$ we find $a = (a_2)_+ = -(a_2)_- = 1$, $b = (b_2)_+ = -(b_2)_- = 0$. These latter two solutions will not be investigated here.

2.2.3 Transmission probability through the ring

Let us consider a wave of unit amplitude $\alpha_1 = 1$, incident from the left in Fig. 2.6. In order to find the transmission probability of the ring $T = |\alpha_2'|^2$ we take $\alpha_2 = 0$.

For the amplitudes at the junction to the right, with the help of Eqs. (2.12) and (2.13) we can express the γ_2's in terms of the β_2's as

$$\begin{pmatrix} \gamma_2' \\ \gamma_2 \end{pmatrix} = \frac{1}{b} \begin{pmatrix} (b^2 - a^2) & a \\ -a & 1 \end{pmatrix} \begin{pmatrix} \beta_2 \\ \beta_2' \end{pmatrix} = \mathbf{t}_j \begin{pmatrix} \beta_2 \\ \beta_2' \end{pmatrix}. \tag{2.19}$$

Using Eqs. (2.12) and (2.13) for the amplitudes at the junction to the left, we can express the β_1's in terms of the γ_1's

$$\begin{pmatrix} \beta_1' \\ \beta_1 \end{pmatrix} = \frac{\sqrt{\epsilon}}{b} \begin{pmatrix} b - a \\ -1 \end{pmatrix} + \mathbf{t}_j \begin{pmatrix} \gamma_1 \\ \gamma_1' \end{pmatrix}. \tag{2.20}$$

The flux Φ introduces phase shifts $e^{\mathrm{i}\theta_1}$ and $e^{-\mathrm{i}\theta_2}$ in the wave function in the two arms of the ring where $\theta_1 + \theta_2 = 2\pi\Phi/\Phi_0$. The phase changes θ_1 and θ_2, both taken in a counterclockwise sense, depend on the length of the arms, i.e., the position of the junctions of the ring with the leads. Thus the amplitudes in the upper and lower arm are transferred according to

$$\begin{pmatrix} \beta_2 \\ \beta_2' \end{pmatrix} = e^{-\mathrm{i}\theta_1} \mathbf{t}_1 \begin{pmatrix} \beta_1' \\ \beta_1 \end{pmatrix}, \qquad \begin{pmatrix} \gamma_1 \\ \gamma_1' \end{pmatrix} = e^{-\mathrm{i}\theta_2} \mathbf{t}_2' \begin{pmatrix} \gamma_2' \\ \gamma_2 \end{pmatrix}. \tag{2.21}$$

Note that in the second equation we have used the matrix which transfers the amplitudes from right to left. Using Eqs. (2.19), (2.20) and (2.21) yields an equation for β_1' and β_1 alone

$$\mathbf{\Pi} \begin{pmatrix} \beta_1' \\ \beta_1 \end{pmatrix} = -\frac{\sqrt{\epsilon}}{b} \begin{pmatrix} b - a \\ -1 \end{pmatrix}, \tag{2.22}$$

with

$$\mathbf{\Pi} = \left(\mathbf{t}_j e^{-\mathrm{i}\theta_2} \mathbf{t}_2' \mathbf{t}_j e^{-\mathrm{i}\theta_1} \mathbf{t}_1 - \mathbf{1} \right). \tag{2.23}$$

The transmitted amplitude is found by eliminating γ_2 from the equations obtained by using Eqs. (2.12) and (2.13) for the right junction, then using Eq. (4.44) to give β_2 and β_2' in terms of β_1' and β_1, and eventually by expressing β_1' and β_1 from Eq. (2.22):

$$\alpha_2' = \frac{\sqrt{\epsilon}}{b} \left[(b - a)\, \beta_2 + \beta_2' \right] = -\frac{\epsilon}{b^2} e^{-\mathrm{i}\theta_1} \frac{h}{\det(\mathbf{\Pi})}, \tag{2.24}$$

where

$$h = \det(\mathbf{\Pi}) \left(\pm 1, 1 \right) \mathbf{t}_1 \mathbf{\Pi}^{-1} \begin{pmatrix} \pm 1 \\ -1 \end{pmatrix}. \tag{2.25}$$

Here we have used the relationship $b - a = b_{\pm} - a_{\pm} = \pm 1$. The transmission probability of the ring is thus given by

$$T\left(E, \Phi, \epsilon\right) = \left|\alpha_2'\right|^2 = \frac{\epsilon^2}{b^4} \frac{\left|h\right|^2}{\left|\det\left(\mathbf{\Pi}\right)\right|^2}. \tag{2.26}$$

Thereby, knowing the specific form of the transfer matrices, which depend on the type of the scattering potential, one is able to determine the transmission probability through the ring.

The most simple case however, is when there are no scatterers in the arms of the ring, and the ring is diametric (the two arms are of the same length). In order to be able to compare the results of the model which we will introduce in the next section, and this model, here we present the transmission probability for this case. As $T_{\mathrm{s}} = 1$ the transfer matrices are responsible only for adding the geometrical phase $e^{\mathrm{i}\chi}$ to the wave function, i.e., $t_1 = t_2 = e^{\mathrm{i}\chi}$, $r_1 = r_2 = r_1' = r_2' = 0$. Furthermore, as the ring is diametric the phases resulting from the flux are equal in the two arms: $\theta_1 = \theta_2 = \theta = \pi\Phi/\Phi_0$. Substituting these into Eq. (2.26) the transmission probability is found to be

$$T\left(\chi, \Phi, \epsilon\right) = \frac{4\epsilon^2 \sin^2\chi \cos^2\theta}{\left[a^2 + b^2\cos 2\theta - (1-\epsilon)\cos 2\chi\right]^2 + \epsilon^2 \sin^2 2\chi}, \tag{2.27}$$

where χ is related to the energy E of the electron by $\chi = \sqrt{2m^* E}\rho\pi/\hbar$ with ρ being the radius of the ring.

2.3 Spin-dependent propagation in quantum rings

In this section we introduce a one-dimensional model for ballistic quantum rings, which takes into account the presence of spin-orbit interaction, and assumes that there are no elastic scatterers in the arms of the ring or at the junction of a lead with the ring. We will use this model in Chapter 4 and Chapter 5, where we consider quantum rings and ring-arrays in which Rashba-type spin-orbit interaction is present.

The model is based on the assumption that the ring is formed by one-dimensional leads in which no scatterers are present. Thus, the Hamiltonian of the ring can be easily given and its eigenvalues and eigenstates can be determined. As transport is assumed to be ballistic, the energy of the electron has to be conserved, so that when leads are attached to the ring, the wave functions in the arms of the ring will be given as superpositions of the eigenstates of the Hamiltonian corresponding to the energy of the incoming electron. (We note that the introduction of scatterers into the arms of the ring may be carried out in the same manner as in Section 2.2, i.e., by relating the wave functions on the two sides of the scatterer by the transfer matrix, which can be determined by solving the scattering

problem for the actual form of the potential describing the scatterer.)

At an intersection of a lead with the ring the model uses the following boundary conditions: (1) the wave functions are continuous and (2) the probability currents are conserved at the junctions. This latter assumption may be considered as an analogue of the classical Kirchoff's law. The probability currents in the leads and the ring can be obtained by determining the continuity equation from the Schrödinger equation. We note that these boundary conditions are often referred to as *Griffith's conditions* [89] in the literature. Their concrete form will be presented in Secs. 2.3.2 and 2.3.3, corresponding to the given problem.

As the model is based on solving the time-independent Schrödinger equation, in Section 2.3.1 we start by presenting the one-dimensional Hamiltonian of an electron in a ring. Then, in Section 2.3.2, in order to compare the results of this model and the one introduced in the previous section, we will consider a ring, in which only an Aharonov-Bohm flux is present. Finally, in Section 2.3.3 we present the solution of the scattering problem on a ring with two external leads, in which Rashba spin-orbit interaction is present.

2.3.1 The one-dimensional Hamiltonian of the ring in the presence of spin-orbit interaction

In this section we describe the procedure for obtaining the one-dimensional Hamiltonian in single-electron picture on a ring in the presence of a magnetic field and Rashba spin-orbit interaction [90].

The Hamiltonian for a single electron of effective mass m^* in the presence of Rashba spin-orbit interaction and a magnetic field $\boldsymbol{B}$ is given by (see Section 1.6 and Refs. [90,91])

$$H = \frac{1}{2m^*}\left(\boldsymbol{P} - e\boldsymbol{A}\right)^2 + \frac{\alpha}{\hbar}\boldsymbol{\sigma}\cdot\left[\hat{\boldsymbol{z}}\times\left(\boldsymbol{P} - e\boldsymbol{A}\right)\right] - \mu\boldsymbol{\sigma}\cdot\boldsymbol{B}, \tag{2.28}$$

where $\boldsymbol{A}$ is the vector potential, $\boldsymbol{B} = \boldsymbol{\nabla}\times\boldsymbol{A}$, α is the strength of the Rashba spin-orbit interaction, e is the charge of the electron (which is the negative of the elementary charge), and μ is the coupling constant of the Zeeman coupling (which is negative for the electron). The first term in Eq. (2.28) describes the kinetic energy, the second term is the Rashba Hamiltonian, and the third one is the Zeeman coupling.

Let us assume that $\boldsymbol{B}$ is pointing in the z-direction. This can be modeled, for example, by choosing the vector potential (in cylindrical coordinates) to be

$$A_r = A_z = 0, \quad A_\varphi = \frac{B_z r}{2} = \frac{\Phi}{2\pi r}, \tag{2.29}$$

where Φ is the magnetic flux through the ring. Then, the Hamiltonian (2.28) in cylindrical

coordinates, with $x = r\cos\varphi$ and $y = r\sin\varphi$ reads

$$H(r,\varphi) = -\frac{\hbar^2}{2m^*}\left[\frac{\partial^2}{\partial r^2}+\frac{1}{r}\frac{\partial}{\partial r}-\frac{1}{r^2}\left(\mathrm{i}\frac{\partial}{\partial\varphi}+\frac{\Phi}{\Phi_0}\right)^2\right]-\frac{\alpha}{r}\left(\sigma_x\cos\varphi+\sigma_y\sin\varphi\right)\left(\mathrm{i}\frac{\partial}{\partial\varphi}+\frac{\Phi}{\Phi_0}\right)$$
$$+\mathrm{i}\alpha\left(\sigma_y\cos\varphi-\sigma_x\sin\varphi\right)\frac{\partial}{\partial r}+\frac{\hbar\omega_\mathrm{B}}{2}\sigma_z, \tag{2.30}$$

where $\Phi_0 = h/|e|$ is the flux quantum, σ_x, σ_y and σ_z are the Pauli matrices, and $\omega_\mathrm{B} = -2\mu B_z/\hbar$ (which is positive, as μ is negative for the electron).

In order to find the correct form for the one-dimensional Hamiltonian we need to add a potential $V(r)$ – that is small in a narrow region around $r = \rho$ and large outside this region – which forces the electron wave functions to be localized on the ring in the radial direction. For a narrow ring (steep confining potential) the confining energy in the radial direction is much larger than the spin-orbit interaction energy, the Zeeman energy, and the kinetic energy in the azimuthal direction. This allows us to solve the Hamiltonian for the radial wave function first, and treat the other terms in the Hamiltonian (2.30) as a perturbation. Here we do not present the details of such a calculation [90], we only mention that in the limit of a very narrow ring, electrons will be in the lowest radial mode $R_0(r)$. By calculating the matrix element of the perturbation Hamiltonian in this radial state, we are lead to the following Hamiltonian

$$H_\mathrm{1D}(\varphi) = \frac{\hbar^2}{2m^*\rho^2}\left(\mathrm{i}\frac{\partial}{\partial\varphi}+\frac{\Phi}{\Phi_0}\right)^2+\frac{\hbar\omega_\mathrm{B}}{2}\sigma_z-\frac{\alpha}{\rho}\left(\sigma_x\cos\varphi+\sigma_y\sin\varphi\right)\left(\mathrm{i}\frac{\partial}{\partial\varphi}+\frac{\Phi}{\Phi_0}\right)$$
$$-\mathrm{i}\frac{\alpha}{2\rho}\left(\sigma_y\cos\varphi-\sigma_x\sin\varphi\right). \tag{2.31}$$

This is the form of the one-dimensional Hamiltonian for electrons on a ring, in the presence of Rashba coupling and a perpendicular magnetic field [90].

2.3.2 Two-terminal ring with Aharonov-Bohm flux

In this section we show how the model we introduced above can be applied to solve the scattering problem in the case of a quantum ring, which encircles a magnetic flux Φ, as shown in Fig. 2.7. We assume that no spin-orbit interaction is present now, in order to be able to relate the results obtained with the model of Section 2.2.

Let us suppose, that $\boldsymbol{B} = 0$ in the region where the electron moves, i.e., no Zeeman term is present in the Hamiltonian given by Eq. (2.31):

$$H = \frac{\hbar^2}{2m^*\rho^2}\left(-\mathrm{i}\frac{\partial}{\partial\varphi}-\frac{\Phi}{\Phi_0}\right)^2. \tag{2.32}$$

For the sake of simplicity, let us consider the dimensionless Hamiltonian $\tilde{H} =$

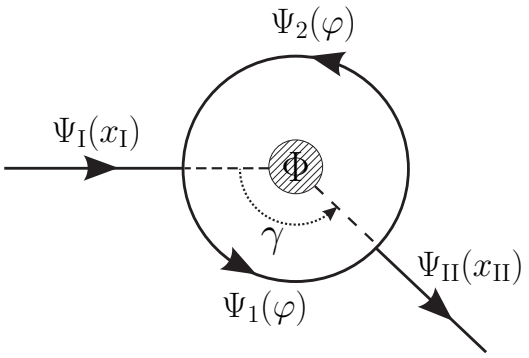

Figure 2.7: One-dimensional ring with an Aharonov-Bohm flux and the notations used for the wave functions in the different sections of the ring. The arrows indicate the directions of the local coordinates.

$H/\left(\hbar^2/2m^*\rho^2\right)$. Then, the eigenfunctions determined from the time-independent Schrödinger equation can be written as plane waves $\Psi(\varphi) = e^{{\rm i}n\varphi}$, where n is an integer, and the corresponding energy eigenvalues depend on the flux as

$$E\left(n,\Phi\right) = \left(n - \frac{\Phi}{\Phi_0}\right)^2, \quad (n \in \mathbb{Z}). \tag{2.33}$$

These are the eigenenergies of the closed ring, which can easily be shown to be the same as those obtained from Eq. (2.11) of Section 2.2 when no scatterers are present in the ring.

Now we turn to the case, when leads are attached to the ring. As we have mentioned in Section 1.2, the wave function of the electron in such narrow conductors can be given as a plane wave with wave vector $k = \sqrt{2mE/\hbar^2}$, E being the energy of the electron. Thus, the wave function in the left lead in Fig. 2.7 can be written in general as:

$$\Psi_{\rm I}(x_{\rm I}) = fe^{{\rm i}kx_{\rm I}} + re^{-{\rm i}kx_{\rm I}}, \tag{2.34}$$

where the direction of the local coordinate $x_{\rm I}$ in lead I is shown by the arrow, i.e., f (r) denotes the amplitude of the incoming (reflected) wave. On the other side of the ring, we assume that no incoming wave is present:

$$\Psi_{\rm II}(x_{\rm II}) = te^{{\rm i}kx_{\rm II}}. \tag{2.35}$$

Conservation of energy requires that the energy of the incoming electron $E = \hbar^2k^2/2m^*$ be equal to the eigenenergies $(\hbar^2/2m^*\rho^2)E(n,\Phi)$ of the Hamiltonian (2.32), from which follows that the wave numbers in the ring have two allowed values

$$n_\pm = \frac{\Phi}{\Phi_0} \pm k\rho. \tag{2.36}$$

Note that the wave numbers $n_\pm$ in the ring are no longer integers.

As we mentioned before, the wave functions $\Psi_1(\varphi)$, $\Psi_2(\varphi)$ pertaining to the same energy E in the different domains of the ring are built up as the linear combination of the eigenstates of $\tilde{H}$ with wave vectors $n_\pm$ determined by Eq. (2.36):

$$\Psi_i(\varphi) = a_{i,+}e^{\mathrm{i}n_+\varphi} + a_{i,-}e^{\mathrm{i}n_-\varphi}, \quad i = 1, 2. \tag{2.37}$$

According to the model, at the junctions of the leads with the ring, the wave functions have to be fitted and the net probability currents need to vanish. For example, for the left juction this means that

$$\Psi_{\mathrm{I}}(0) = \Psi_1(0) = \Psi_2(2\pi), \tag{2.38}$$

$$J_{\mathrm{I}}(0) - J_1(0) + J_2(2\pi) = 0, \tag{2.39}$$

where the form of the probability currents

$$J_l(x_l) = 2\rho\mathcal{R}e\left\{\Psi_l^*(x_l)\left(-\mathrm{i}\frac{\partial}{\partial x_l}\right)\Psi_l(x_l)\right\}, \quad (l = \mathrm{I,II}), \tag{2.40}$$

$$J_i(\varphi) = 2\mathcal{R}e\left\{\Psi_i^*(\varphi)\left(-\mathrm{i}\frac{\partial}{\partial\varphi} - \frac{\Phi}{\Phi_0}\right)\Psi_i(\varphi)\right\}, \quad (i = 1,2), \tag{2.41}$$

is determined from the continuity equations obtained from the respective Schrödinger equations.

Solving the set of equations (2.38) and (2.39) that we get for the two junctions, the amplitude t of the transmitted wave, and consequently, the transmission probability through the ring, can be determined. If we assume that the incoming amplitude is $f = 1$, and the ring is diametrical ($\gamma = \pi$) – which we have already examined with the model presented in Section 2.2 – the transmission probability is given by

$$T = |t|^2 = \frac{4\sin^2(k\rho\pi)\cos^2\left(\frac{\Phi}{\Phi_0}\pi\right)}{\left[\frac{1}{4} + \cos\left(\frac{\Phi}{\Phi_0}2\pi\right) - \frac{5}{4}\cos(2k\rho\pi)\right]^2 + \sin^2(2k\rho\pi)}. \tag{2.42}$$

If we compare this to the result (2.27) obtained with the model of Section 2.2, with $\chi = \sqrt{2m^*E}/\hbar\rho\pi = k\rho\pi$, which is the phase accumulated in one arm, then we can see that the result (2.42) obtained here without the assumption of scatterers in the juctions, is equal to (2.27) if the coupling parameter ϵ is 4/9, i.e., it corresponds to a strong, but not maximal coupling between the leads and the ring. This is due to the property of the Griffith's conditions, that they consider the lead and arms joining in a junction to be completely equivalent, thereby, besides the transmitted amplitude, they lead to a reflected one as well in each of the wires (corresponding to an S matrix with $\epsilon < 1/2$). At the same

time, in the case when a lead is maximally coupled to the arms (which is desrcibed by an S matrix with $\epsilon = 1/2$), it is treated to be inequivalent from the other wires (the arms of the ring), as no reflected amplitude results from the incoming one in the lead, there are only transmitted amplitudes from the arms.

2.3.3 Two-terminal ring with Rashba spin-orbit interaction

In this section we present the solution of the scattering problem in a two-terminal quantum ring, in which only Rashba-type spin-orbit interaction is present [34].

In this case the one-dimensional Hamiltonian (2.31) derived in Section 2.3.1 (with $\Phi/\Phi_0 = 0$, $\omega_{\mathrm{B}} = 0$) can be written in the simplified form [92]:

$$H = \hbar\Omega \left[\left(-\mathrm{i}\frac{\partial}{\partial\varphi} + \frac{\omega_{\mathrm{SO}}}{2\Omega} \left(\sigma_x \cos\varphi + \sigma_y \sin\varphi \right) \right)^2 - \frac{\omega_{\mathrm{SO}}^2}{4\Omega^2} \right], \tag{2.43}$$

where $\Omega = \hbar/2m^*\rho^2$, and $\omega_{\mathrm{SO}} = \alpha/\hbar\rho$ is the frequency associated with the spin-orbit interaction. Apart from constants, this Hamiltonian is the square of the sum of the z component of the orbital angular momentum operator $L_z = -\mathrm{i}\partial/\partial\varphi$, and of $(\omega_{\mathrm{SO}}/\Omega)S_r$, where $S_r = \sigma_r/2$ is the radial component of the spin (both measured in units of $\hbar$).

In order to solve the eigenvalue equation of the Hamiltonian (2.43), it is practical to look for operators that commute with it. It can be shown that H commutes with $K = L_z + S_z$, the z component of the total angular momentum and with $S_{\theta,\varphi} = S_x \sin\theta\cos\varphi + S_y \sin\theta\sin\varphi + S_z\cos\theta$, the spin component in the direction determined by the angles θ, and φ, where θ is given by

$$\tan\theta = -\frac{\omega_{\mathrm{SO}}}{\Omega}. \tag{2.44}$$

It is easy to prove that the commutator $[K, S_{\theta,\varphi}] = 0$, therefore, simultaneous eigenstates of H, K and $S_{\theta,\varphi}$ exist. In the $\{|\uparrow\rangle, |\downarrow\rangle\}$ eigenbasis of S_z we can find these in the form

$$\psi(\kappa,\varphi) = e^{\mathrm{i}\kappa\varphi} \begin{pmatrix} e^{-\mathrm{i}\frac{\varphi}{2}} u^{(\mu)} \\ e^{\mathrm{i}\frac{\varphi}{2}} v^{(\mu)} \end{pmatrix}, \quad (\mu = 1, 2), \tag{2.45}$$

obeying

$$K\psi(\kappa,\varphi) = \kappa\psi(\kappa,\varphi), \tag{2.46}$$

$$S_{\theta,\varphi}\psi(\kappa,\varphi) = s(\kappa)\psi(\kappa,\varphi), \quad s(\kappa) = \pm\frac{1}{2}, \tag{2.47}$$

where

$$\frac{v^{(\mu)}}{u^{(\mu)}} = \left(\tan\frac{\theta}{2} \right)^{(\mu)} = \frac{1 + (-1)^\mu w}{\frac{\omega_{\mathrm{SO}}}{\Omega}}, \tag{2.48}$$

and $w = \sqrt{1 + (\omega_{\rm SO}/\Omega)^2}$. The corresponding energy eigenvalues are

$$E^{(\mu)}(\kappa) = \hbar\Omega \left(\kappa^2 + (-1)^\mu \kappa w + \frac{1}{4} \right), \quad (\mu = 1, 2). \tag{2.49}$$

In a closed ring $\kappa \pm 1/2$ must be an integer (we have seen this in the previous section), while if one considers leads connected to the ring, there is no such restriction: the energy E of the incoming electron is a continuous variable, with which, as a result of energy conservation, the eigenvalues of the ring Halmiltonian (2.49) have to be equal. Thus, the possible values of κ can be written as

$$\kappa_j^{(\mu)} = (-1)^{\mu+1} \left(\frac{w}{2} + (-1)^j q \right), \tag{2.50}$$

where $q = \sqrt{(\omega_{\rm SO}/2\Omega)^2 + E/\hbar\Omega}$. We can see, that the energy eigenvalues are fourfold degenerate: $j = 1, 2$ correspond to two distinct values of $|\kappa_j^{(\mu)}|$, while the additional degeneracy at a given j is resolved by the sign of $\kappa_j^{(\mu)}$. Since $(\tan\theta/2)^{(1)} = -(\cot\theta/2)^{(2)}$, we may choose to parametrize the components of the eigenvectors by $(\tan\theta/2)^{(1)} = (1-w)/(\omega_{\rm SO}/\Omega) = \tan\theta/2$. Then, the four eigenstates can be expressed as

$$\psi_j^{(1)}(\kappa_j^{(1)}, \varphi) = e^{{\rm i}\kappa_j^{(1)}\varphi} \begin{pmatrix} e^{-{\rm i}\frac{\varphi}{2}} \cos\frac{\theta}{2} \\ e^{{\rm i}\frac{\varphi}{2}} \sin\frac{\theta}{2} \end{pmatrix}, \qquad \psi_j^{(2)}(\kappa_j^{(2)}, \varphi) = e^{{\rm i}\kappa_j^{(2)}\varphi} \begin{pmatrix} e^{-{\rm i}\frac{\varphi}{2}} \sin\frac{\theta}{2} \\ -e^{{\rm i}\frac{\varphi}{2}} \cos\frac{\theta}{2} \end{pmatrix}. \tag{2.51}$$

This means that the Hamiltonian has two eigenspinors (determined by the value of μ), and to each of these spinors there are two wave numbers (specified by the value of j). We note that in the experimentally achievable range of the parameters (see text below) q is usually larger than $w/2$. Thus, for each eigenspinor, $j = 1$ and 2 results in wave numbers of different sign, i.e., a clockwise and a counterclockwise direction of rotation.

The wave functions in the upper and lower arms of the ring (using the same notations as in Fig. 2.7) can be written as linear combinations of the four eigenspinors corresponding to the given energy

$$\Psi_i(\varphi) = \sum_{\mu,j=1,2} a_{ij}^{(\mu)} \psi(\kappa_j^{(\mu)}, \varphi) \quad i = 1, 2. \tag{2.52}$$

The wave functions in the leads – similarly to Eqs. (2.34) and (2.35) presented in the previous Section – are built up as linear combinations of plane waves, but in this case with spin-dependent amplitudes, i.e., f, r, and t denoting two-component spinors:

$$\Psi_{\rm I}(x_{\rm I}) = \begin{pmatrix} f_\uparrow \\ f_\downarrow \end{pmatrix} e^{{\rm i}kx_{\rm I}} + \begin{pmatrix} r_\uparrow \\ r_\downarrow \end{pmatrix} e^{-{\rm i}kx_{\rm I}}, \qquad \Psi_{\rm II}(x_{\rm II}) = \begin{pmatrix} t_\uparrow \\ t_\downarrow \end{pmatrix} e^{{\rm i}kx_{\rm II}}. \tag{2.53}$$

In order to determine the transmission properties of the ring, we need to apply the

boundary conditions introduced at the beginning of Section 2.3, i.e., at the junctions of the leads with the ring we need to fit the wave functions, and require the conservation of the current densities. If we assume that there are no spin-flip processes at the junctions, then we can require the spin probability currents to be conserved. These conditions can be formulated similarly to Eqs. (2.38) and (2.39), but now the wave functions being given by Eqs. (2.52) and (2.53), and the probability currents being replaced by the spin probability currents:

$$J(x_l) = 2\rho\mathcal{R}e\left\{\Psi_l^\dagger(x_l)\left(-\mathrm{i}\frac{\partial}{\partial x_l}\right)\Psi_l(x_l)\right\}, \quad l = I, II, \tag{2.54}$$

$$J_i(\varphi) = 2\mathcal{R}e\left\{\Psi_i^\dagger(\varphi)\left(-\mathrm{i}\frac{\partial}{\partial\varphi} + \frac{\omega_{\mathrm{SO}}}{2\Omega}\sigma_r\right)\Psi_i(\varphi)\right\}, \quad i = 1, 2, \tag{2.55}$$

which can be found by determining the continuity equation from the Schrödinger equation [92]. We note that $\Psi^\dagger\Psi$ is the usual two-dimensional Hilbert space inner product.

By solving the set of equations (2.38) and (2.39) that we have for the two junctions, the spin-dependent amplitude t of the transmitted wave, and consequently, the 2×2 transmission matrix T which transforms the incoming spinor as $t = Tf$ can be determined:

$$T = |T_\gamma|\, e^{\mathrm{i}\frac{\delta_0}{2}} U, \tag{2.56}$$

where the matrix elements of U are given by

$$U_{\uparrow\uparrow} = U_{\downarrow\downarrow}^* = e^{-\mathrm{i}\frac{\gamma}{2}}\left[e^{-\mathrm{i}\frac{\delta}{2}}\sin^2\frac{\theta}{2} + e^{\mathrm{i}\frac{\delta}{2}}\cos^2\frac{\theta}{2}\right] \tag{2.57}$$

$$U_{\uparrow\downarrow} = -U_{\downarrow\uparrow}^* = \mathrm{i}e^{-\mathrm{i}\frac{\gamma}{2}}\sin\frac{\delta}{2}\sin\theta. \tag{2.58}$$

$|T_\gamma|$ and the phases δ_0 and δ are obtained as

$$|T_\gamma|\, e^{\mathrm{i}\delta_\pm} = \frac{4\mathrm{i}k\rho q}{y}e^{\pm\mathrm{i}\frac{w}{2}\gamma}\left[\sin\left(q\left(2\pi-\gamma\right)\right) - e^{\mp\mathrm{i}w\pi}\sin\left(q\gamma\right)\right] \tag{2.59}$$

$$\delta_0 = \delta_+ + \delta_-, \quad \delta = \delta_+ - \delta_-, \tag{2.60}$$

where

$$y = k^2\rho^2\left[\cos\left(2q\left(\pi-\gamma\right)\right) - \cos\left(2q\pi\right)\right] + 4\mathrm{i}k\rho q\sin\left(2q\pi\right) - 4q^2\left[\cos\left(w\pi\right) + \cos\left(2q\pi\right)\right].$$

Let us note that if $\gamma = \pi$ and $\omega_{\mathrm{SO}} = 0$, i.e., there is no spin-orbit coupling, then the off-diagonal elements of T are zero, and the diagonal elements are equal to the transmission probability we get from Eq. (2.42) in the case when $\Phi/\Phi_0 = 0$.

The important fact is that T can be written as the product of a complex number the

absolute value of which is a non-negative constant with $|T_\gamma| \leq 1$, which can be considered as the efficiency of the transformation, and a unitary matrix U, which performs a nontrivial spin transformation.

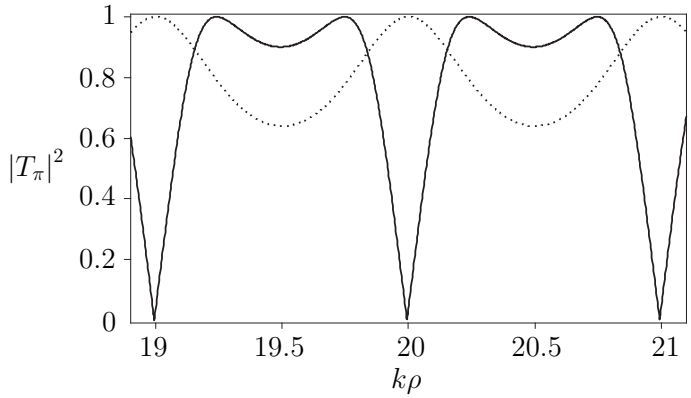

Figure 2.8: The transmission probability through a diametric ring ($\gamma = \pi$) as a function of $k\rho$ for $|\theta| = \pi/4$, where the transformation is a rotation of the spin around the y axis by $\pi/2$ (solid curve). The transmission probability of the same ring for zero spin-orbit coupling (dotted curve).

Figure 2.8 shows the transmission probability $|T_\pi|^2 = \frac{1}{2}Tr\left(TT^\dagger\right)$ through a diametric ring ($\gamma = \pi$) as a function of $k\rho$ around $k_F\rho = 20.4$, corresponding to a ring of radius 0.25 μm and a Fermi energy 11.13 meV of InGaAs, for $|\theta| = \pi/4$ (solid curve). It can be seen that for several values of $k\rho$ the transformation is strictly unitary, with $|T_\pi| = 1$. As compared to the case when no spin-orbit interaction is present (dotted curve) one can see, that for certain values of $k\rho$ the ring is completely opaque for the electrons.

Various types of rotations can be realized by tuning the strength of the Rashba coupling, changing the position of the junctions, or by fabricating rings with different sizes [34].

2.4 Conclusions

In this chapter we have introduced two widely used models of ballistic quantum rings, which are based on the assumption that narrow rings, in which only one radial mode takes part in the conduction, may be considered one-dimensional. One of the models (see Section 2.2) inherently contained elastic scatterers in the arms of the ring as well as in the junctions of the leads with the ring, and was able to account for the effect of a magnetic (Aharonov-Bohm) flux encircled by the ring. This model considered the injection of the electron from the leads into the two arms of the ring to be symmetric, by using a scattering matrix, in which the elements corresponding to these probabilities were equal. In Section 2.3 we have presented another model, which is more appriopriate for the theoretical description of spin-dependent transport through quantum rings. We have seen that this model does not account for any scatterers in the arms of the ring or

at the junctions. Instead of using a scattering matrix at the junctions, this model simply requires to fit the wave functions and the corresponding probability currents. We have used this model to solve the scattering problem of a two-terminal quantum ring which encircled an Aharonov-Bohm flux, and a ring, in which Rashba-type spin-orbit interaction was present. In the spin-dependent case we have seen that the wave functions in the arms of the ring are linear superpositions of the four eigenstates of the ring Hamiltonian that pertain to the fourfold degenerate energy eigenvalue, determined by the energy of the incoming electron. We have seen that this scattering problem can be solved analytically, and the transmission probability (or consequently, the conductance) can be determined. In the following part of the dissertation we will use the first model to take into account the possibility of asymmetric injection into the two arms of the ring, and the second model to solve the scattering problem of a ring with three terminals, and an array of rings.

Part II

Chapter 3

Aharonov-Bohm oscillations in a ring with asymmetric injection

In this chapter we study electron transport in the presence of an Aharonov-Bohm flux through quantum rings in which the probabilities of transmission from the leads into the two arms of the ring are different, and we also allow different propagation properties in the two arms [93]. In order to determine the transmission probability through such rings we use the model introduced in Section 2.2, i.e., we consider elastic scatterers in the junctions and in the arms of the ring. First, in Section 3.1 we define an appropriate scattering matrix to couple the leads to the ring, which is able to take into account the asymmetry of injection into the two arms. Then, in Section 3.2 we solve the scattering problem for two cases: when no scatterers are present in the arms of the ring (Section 3.2.1) and when a scatterer is placed in one of the arms of the ring (Section 3.2.2).

3.1 Introduction of arm-dependent asymmetry into the scattering matrix

In a real quantum ring the coupling between the current-carrying leads and the ring can be complicated. Reflections may be present at the junctions of the leads with the ring, and/or the probabilities of transmission from the leads into the two arms of the ring may be different. This asymmetry can be a consequence of fabrication defects but it can also be induced by the Lorentz force [35, 94].

In Section 2.2 we discussed a model which relates the three outgoing waves with amplitudes $(\alpha', \beta', \gamma')$ and the three incoming waves with amplitudes (α, β, γ) at each junction of a lead with the ring (indicated by the black triangles in Fig. 3.1) by a 3×3 scattering matrix S

$$\overrightarrow{\alpha}' = S \ \overrightarrow{\alpha}, \tag{3.1}$$

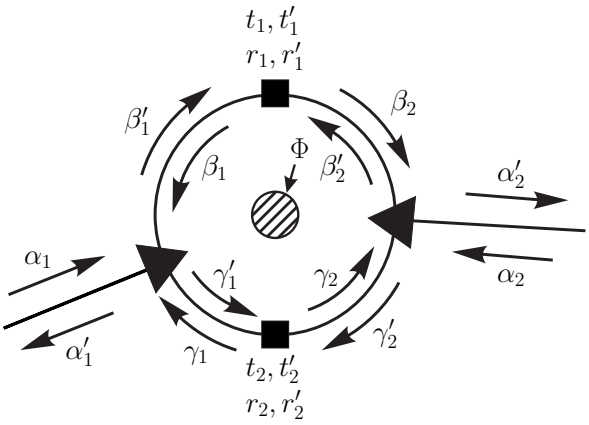

Figure 3.1: Ring connected to leads with elastic scatterers in the junctions and the ring.

which treats the two arms of the ring in a symmetric way, i.e., the matrix elements of S describing the transmission probability from the lead into the upper and lower arms being equal.

Based on the general requirements for the scattering matrix [87,88], here we define an appropriate S matrix, which treats the upper and lower arms of the ring in an asymmetrical way. Current conservation requires S to be unitary

$$S^{-1} = S^{\dagger}, \tag{3.2}$$

while time-reversal invariance demands that

$$S^{*} = S^{-1}. \tag{3.3}$$

As a result, S is necessarily a symmetric matrix. For the sake of simplicity, here we will further assume that it is real. Then S is given by

$$S = \begin{pmatrix} a & b & c \\ b & d & e \\ c & e & f \end{pmatrix}, \tag{3.4}$$

where the square of the diagonal elements are the reflection probabilities into the respective channels, while the square of the off-diagonal elements give the transmission probabilities from one channel to the other (e.g., b^2 is the transmission probability of the electron from the lead into the upper arm). The unitarity (3.2) of the S matrix leads to the following relations between its elements:

$$a^2 + b^2 + c^2 = 1, \tag{3.5}$$

$$b^2 + d^2 + e^2 = 1, \tag{3.6}$$

$$c^2 + e^2 + f^2 = 1, \tag{3.7}$$

$$ab + bd + ce = 0, \tag{3.8}$$

$$ac + be + cf = 0, \tag{3.9}$$

$$bc + de + ef = 0. \tag{3.10}$$

In order to introduce an asymmetry between the two arms, for convenience, we assume $b = \lambda c$ ($\lambda = 1$ meaning equivalent arms). Then, from Eqs. (3.9) and (3.10) we find

$$e = -\lambda (a + d), \tag{3.11}$$

$$f = -a - d \pm 1. \tag{3.12}$$

By using $b = \lambda c$ in Eq. (3.6) we can determine b as a function of λ and a:

$$b = \pm \frac{\lambda \sqrt{1 - a^2}}{\mu}, \tag{3.13}$$

where $\mu = \sqrt{\lambda^2 + 1}$, and in order for b to be real $|a| \leq 1$. Then Eqs. (3.6)-(3.7) and (3.11) determine d as

$$d = \frac{\lambda^2 a - 1}{\mu^2}. \tag{3.14}$$

Thus, each element of S can be expressed in terms of a and λ:

$$S = \begin{pmatrix} a & \lambda\nu & \nu \\ \lambda\nu & \eta - a & -\lambda\eta \\ \nu & -\lambda\eta & 1 - \eta \end{pmatrix}, \tag{3.15}$$

where $\nu = \frac{\sqrt{1-a^2}}{\mu}$, $\eta = \frac{a+1}{\mu^2}$, and $-1 < a < 1$.

The above equation for $\lambda = 1$ (i.e., symmetric arms) shows that the S matrix is indeed of the form given by Eq. (2.13). By taking this limit, we can also determine the realtionship between a and the coupling parameter ϵ of Section 2.2.2, namely

$$a^2 = 1 - 2\epsilon. \tag{3.16}$$

As a is the element of the S matrix which connects the incoming and outgoing amplitudes in the lead, the coupling between the lead and the ring is perfect when $a = 0$, while $a = 1$ corresponds to no coupling at the junction. These two limits correspond to those of ϵ in Section 2.2.2: $a = 1$ corresponding to $\epsilon = 0$, and $a = 0$ to $\epsilon = 1/2$.

3.2 Solution of the scattering problem with arm-dependent asymmetry

In the following, we show the detailed calculation of the transmission probability $T = |\alpha_2'|^2$ through the ring when there is an asymmetry between the arms included in the S matrix, derived in the previous Section. Based on the model of Section 2.2, we describe the elasctic scattering in each arm (indicated by the black squares in Fig. 3.1) by a transfer matrix of the form given by Eq. (2.5). For the usual scattering from the left we take the incoming amplitude $\alpha_1 = 1$, and assume that there is no incoming electron from the right, i.e., $\alpha_2 = 0$.

For the right junction from Eq. (3.1) we obtain

$$\alpha_2' = b\beta_2 + c\gamma_2, \tag{3.17}$$
$$\beta_2' = d\beta_2 + e\gamma_2, \tag{3.18}$$
$$\gamma_2' = e\beta_2 + f\gamma_2. \tag{3.19}$$

Using Eqs. (3.17) and (3.18) we can write

$$\begin{pmatrix} \gamma_2' \\ \gamma_2 \end{pmatrix} = \mathbf{t}_{j2} \begin{pmatrix} \beta_2 \\ \beta_2' \end{pmatrix}, \tag{3.20}$$

where the matrix $\mathbf{t}_{j2}$ is

$$\mathbf{t}_{j2} = \frac{1}{e} \begin{pmatrix} e^2 - fd & f \\ -d & 1 \end{pmatrix}. \tag{3.21}$$

For the left junction from Eq. (3.1) we obtain

$$\alpha_1' = a + b\beta_1 + c\gamma_1, \tag{3.22}$$
$$\beta_1' = b + d\beta_1 + e\gamma_1, \tag{3.23}$$
$$\gamma_1' = c + e\beta_1 + f\gamma_1. \tag{3.24}$$

Using Eqs. (3.23) and (3.24), we can write

$$\begin{pmatrix} \beta_1' \\ \beta_1 \end{pmatrix} = \frac{1}{e} \begin{pmatrix} be - dc \\ -c \end{pmatrix} + \mathbf{t}_{j1} \begin{pmatrix} \gamma_1 \\ \gamma_1' \end{pmatrix}, \tag{3.25}$$

where the matrix $\mathbf{t}_{j1}$ is given by (3.21) with d and f interchanged.

The connection between the amplitudes in the upper arm of the ring, i.e., the effect

of the scatterer, and the magnetic field can be written as

$$\begin{pmatrix}\beta_2\\ \beta_2'\end{pmatrix} = e^{-\mathrm{i}\theta_1}\mathbf{t}_1\begin{pmatrix}\beta_1'\\ \beta_1\end{pmatrix}, \tag{3.26}$$

while, for the amplitudes is the lower arm we can write

$$\begin{pmatrix}\gamma_1\\ \gamma_1'\end{pmatrix} = e^{-\mathrm{i}\theta_2}\mathbf{t}_2'\begin{pmatrix}\gamma_2'\\ \gamma_2\end{pmatrix}, \tag{3.27}$$

where $\mathbf{t}_1$ and $\mathbf{t}_2$ are the transfer matrices associated with propagation in the upper and lower arm (see Fig. 3.1), given by Eq. (2.5). θ_1 and θ_2 are the phase shifts introduced by the flux $\Phi = \pi\rho^2 B$ in the two arms, B being the perpendicular magnetic field and ρ the ring radius. These shifts satisfy the relation $\theta_1 + \theta_2 = 2\pi\Phi/\Phi_0$, where $\Phi_0 = h/|e|$ is the flux quantum.

Combining Eq. (3.20) and Eqs. (3.25)-(3.27) we can write

$$\mathbf{\Pi}\begin{pmatrix}\beta_1'\\ \beta_1\end{pmatrix} = -\frac{1}{e}\begin{pmatrix}be-dc\\ -c\end{pmatrix}, \tag{3.28}$$

with

$$\mathbf{\Pi} = \mathbf{t}_{j1}e^{-\mathrm{i}\theta_2}\mathbf{t}_2'\mathbf{t}_{j2}e^{-\mathrm{i}\theta_1}\mathbf{t}_1 - \mathbf{1}, \tag{3.29}$$

where $\mathbf{1}$ is the 2×2 unit matrix. The transmitted amplitude α_2' can be expressed from Eqs. (3.17) and (3.18):

$$\alpha_2' = \frac{1}{e}(be-cd, c)\begin{pmatrix}\beta_2\\ \beta_2'\end{pmatrix}, \tag{3.30}$$

from which, by using Eqs. (3.26) and (3.28) it can be determined as

$$\alpha_2' = \frac{1}{e}(be-cd, c)\, e^{-\mathrm{i}\theta_1}\mathbf{t}_1\mathbf{\Pi}^{-1}\left(-\frac{1}{e}\right)\begin{pmatrix}be-cd\\ -c\end{pmatrix}. \tag{3.31}$$

In what follows, we consider two cases: in Section 3.2.1 we suppose that no scatterers are present in the arms of the ring, then, in Section 3.2.2 we assume that a scatterer is present in one of the arms. (We note that the case with scatterers in both arms can be treated in the same way.) For the sake of simplicity, we restrict our calculations to diametric rings, i.e., rings with arms of equal length.

3.2.1 No scatterers in the arms

When no scatterers are present in the ring, the transfer matrices simply represent the geometrical phase χ attained by the wave function in the arms (which are of equal length),

i.e. $t_1 = t_2 = e^{i\chi}$, $r_1 = r_2 = r_1' = r_2' = 0$. This geometrical phase is related to the energy E of the electron by $\chi = \sqrt{2m^* E}\pi\rho/\hbar$. (We note that for a ring of radius $\rho = 0.25$ μm in InGaAs, where the Fermi energy is 11.13 meV, χ corresponds to 20.4π). The phases due to the encircled magnetic flux are $\theta_1 = \theta_2 = \pi\Phi/\Phi_0$. Then, using Eq. (3.31), the transmitted amplitude is given by

$$\alpha_2' = \frac{2\mathrm{i}\left(1-a^2\right)\Lambda e^{-\mathrm{i}\theta}\left(\lambda^2 + e^{2\mathrm{i}\theta}\right)\sin\chi}{\left(1+a\right)^2\Lambda_\theta - \Lambda^2\left[F\left(\chi,a\right)+2a\right]}, \tag{3.32}$$

where

$$\begin{aligned}\Lambda &= \lambda^2 + 1,\\ \Lambda_\theta &= \lambda^4 + 2\lambda^2\cos\left(2\theta\right) + 1,\end{aligned}$$

and

$$F\left(\chi,a\right) = \left(1+a^2\right)\cos\left(2\chi\right) - \mathrm{i}\left(1-a^2\right)\sin\left(2\chi\right).$$

Then, the transmission probability takes the following form:

$$T = \frac{4\left(1-a^2\right)^2\Lambda^2\Lambda_\theta\sin^2\chi}{\left[\left(1+a\right)^2\Lambda_\theta - \Lambda^2 a_\chi\right]^2 + \left(1-a^2\right)^2\Lambda^4\sin^2\left(2\chi\right)}, \tag{3.33}$$

where $a_\chi = \left(1+a^2\right)\cos\left(2\chi\right) + 2a$. It can be shown that the transmission probability given by Eq. (3.33) is invariant under the change $\lambda \to 1/\lambda$, representing the fact that asymmetry can favor the arms equally without changing the transmission properties of the ring.

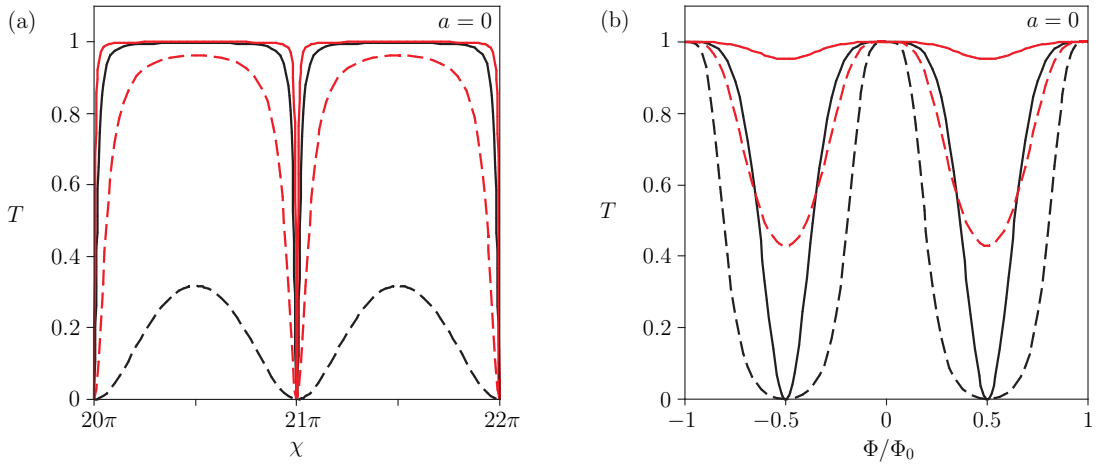

Figure 3.2: The effect of asymmetric injection on the transmission probability when no scatterers are present in the ring, and the coupling between the ring and the leads is assumed to be ideal, i.e., $a = 0$. Black and red curves correspond to symmetric injection (characterized by $\lambda = 1$) and asymmetric injection (characterized by $\lambda = 3$), respectively. (a) Transmission as a function of χ, for $\Phi/\Phi_0 = 0.1$ (solid curve) and $\Phi/\Phi_0 = 0.4$ (dashed curve). (b) Transmission as a function of the flux Φ (in units of Φ_0) for $\chi = 20.5\pi$ (solid curve) and $\chi = 21.06\pi$ (dashed curve).

Figure 3.2 shows the transmission probability given by Eq. (3.33), as a function of χ for two different values of the flux, and as a function of Φ/Φ_0 for two different values of χ. In both cases, we assume that the coupling between the leads and the ring is maximal, i.e., $a = 0$. This corresponds to the value $1/2$ of ϵ in the case presented in Section 2.2.2. The figure also shows the effect of asymmetric injection (red curves) with respect to the case when the arms of the ring are symmetric (black curves). We note that for $\lambda = 1$ the results coincide with those of Ref. [62]. It can be seen in Fig. 3.2(a) that the ring is completely opaque for integer values of π irrespective of the value of the flux, even if the coupling is maximal. Asymmetric injection increases the transmission for both values of the flux compared to the symmetric case, but is not able to remove the transmission minima. In Fig. 3.2(b), the transmission probability shows oscillations with period Φ_0, which is a manifestation of the Aharonov-Bohm effect. For $\lambda > 1$ the destructive interferences are not complete due to the fact that the electron enters one of the arms (in this case the upper one) with higher probability.

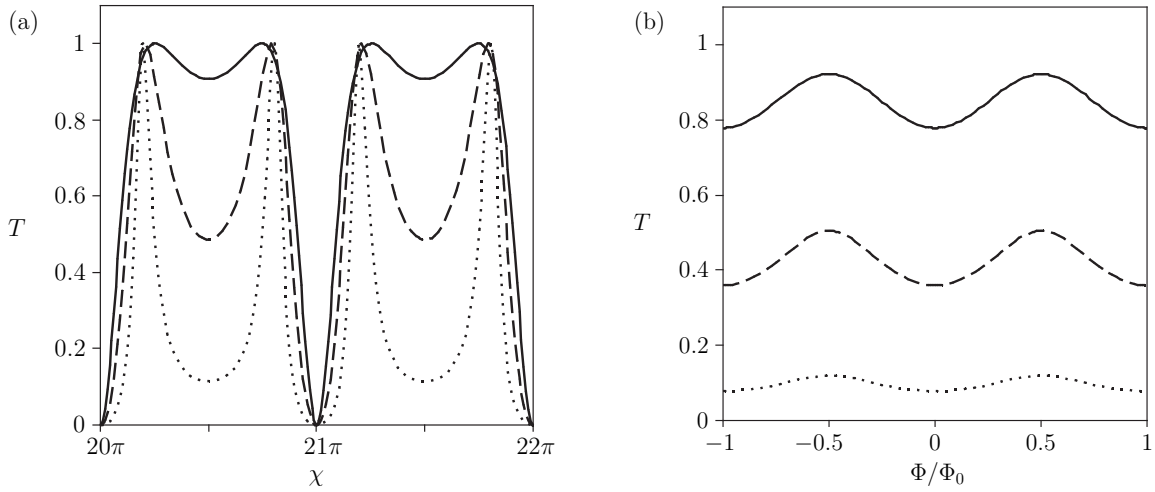

Figure 3.3: Transmission probability of the ring when an asymmetry characterized by $\lambda = 3$ is present between the two arms of the ring: (a) as a function of χ for $\Phi/\Phi_0 = 0.4$, and (b) as a function of the flux Φ (in units of Φ_0) for $\chi = 20.5\pi$, for different strength of the coupling between the ring and the leads. Solid, dashed and dotted curves correspond to $a = 0.25$, 0.5 and 0.75, respectively.

Figure 3.3 shows the dependence of the transmission probability on the coupling between the ring and the leads, characterized by the parameter a when no scatterer is present, and there is an asymmetry between the two arms of the ring, corresponding to $\lambda = 3$. In Fig. 3.3(a) the value of the flux is set to $\Phi/\Phi_0 = 0.4$. Even though the asymmetry increases the transmission compared to the symmetric case (see Fig. 3.2(a)), as the coupling between the ring and the leads gets weaker, the transmission probability decreases. However, there are certain values of χ, i.e. the energy (or wave number) for which the ring is still completely transmitting. These transmission peaks get narrower as a is increased. In the case of symmetric injection and weak coupling it has been pointed out in Ref. [62] that these resonances in the transmission can be related to the eigenenergies of the closed

ring. For such a ring with $\Phi/\Phi_0 = 0.4$, one obtains from the eigenvalue equation of the closed ring (2.11) that the transmission peaks are located at $\chi = (l \pm \Phi/\Phi_0)\,\pi$, where l is an integer. It can be seen that in our case, asymmetric injection shifts the positions of these peaks, and the eigenstates of the closed ring can not be directly related to the resonances. In Fig. 3.3(b), where χ is set to 20.5π, it can be seen that there is an overall decrease in the transmission probability. The amplitude of the oscillations pertaining to the non-resonant value of χ decreases as the coupling at the lead-ring junctions decreases. Additionally, the phase of the oscillations are shifted by π. The sinusoidal dependence of T on Φ/Φ_0 stems directly from the fact that the transmission probability is given by (3.33), and especially because of the numerator for $\lambda > 1$.

3.2.2 Scatterer in the arm

In this section we assume that there is a scatterer in one arm of the ring, e.g., in the upper arm. Then, the elements of the transfer matrices in the arms of the ring are determined by the following transmission and reflection amplitudes: $t_1 = \sqrt{T_\mathrm{s}}e^{\mathrm{i}(\chi+\delta\chi)}$, $t_2 = e^{\mathrm{i}\chi}$, $r_1 = r_1' = \sqrt{R_\mathrm{s}}e^{-\mathrm{i}\frac{\pi}{2}}e^{\mathrm{i}(\chi+\delta\chi)}$, $r_2 = r_2' = 0$, where χ is the geometrical phase and $\delta\chi$ is the phase difference between the two arms due to the presence of the scatterer. The phases resulting from the magnetic flux are $\theta_1 = \theta_2 = \pi\Phi/\Phi_0$.

In this case the transmission amplitude determined from Eq. (3.31) takes the form

$$\alpha_2' = \frac{2\mathrm{i}\left(1-a^2\right)\Lambda e^{\mathrm{i}\theta}\left[\sin\left(\chi+\delta\chi\right)+\lambda^2\sqrt{T_\mathrm{s}}e^{-2\mathrm{i}\theta}\sin\chi-\sqrt{R_\mathrm{s}}\right]}{\left(1+a\right)^2\Lambda_{\theta,\delta\chi}-\Lambda^2\left[F\left(\chi,a,\delta\chi\right)+2a\cos\delta\chi\right]-2\Lambda\sqrt{R_\mathrm{s}}G\left(\chi,a\right)+H\left(a,\delta\chi\right)}, \quad (3.34)$$

where

$$\begin{aligned}
\Lambda_{\theta,\delta\chi} &= \left(1+\lambda^4\right)\cos\delta\chi+2\lambda^2\sqrt{T_\mathrm{s}}\cos\left(2\theta\right), \\
F\left(\chi,a,\delta\chi\right) &= \left(1+a^2\right)\cos\left(2\chi+\delta\chi\right)-\mathrm{i}\left(1-a^2\right)\sin\left(2\chi+\delta\chi\right), \\
G\left(\chi,a\right) &= \left(1-2\lambda^2a+a^2\right)\sin\chi+\mathrm{i}\left(1-a^2\right)\cos\chi, \\
H\left(a,\delta\chi\right) &= \mathrm{i}\left(1-a^2\right)\left(1-\lambda^4\right)\sin\left(\Delta\chi\right).
\end{aligned} \quad (3.35)$$

In order to save space, we do not present here the explicit form of the transmission probability $T = |\alpha_2'|^2$, as it can be easily calculated from Eq. (3.34).

Figure 3.4 shows the transmission probability through the ring as a function of the flux when a weak scatterer ($T_\mathrm{s} = 0.95$) is present in the upper arm of the ring for $\chi = 20.3\pi$. We assume that the coupling between the ring and the leads is maximal ($a = 0$). Black and red curves correspond to $\lambda = 1$, and $\lambda = 1.6$, respectively. For clarity, we shifted the dashed and dashdotted curves by +1 and +2, respectively. Figure 3.4(a) shows how the oscillations of the transmission are affected by the phase difference caused by the scatterer, as $\delta\chi$ is changed from 0 to $\pi/3$, and $2\pi/3$, and in Fig. 3.4(b) from π to $4\pi/3$, and to $5\pi/3$.

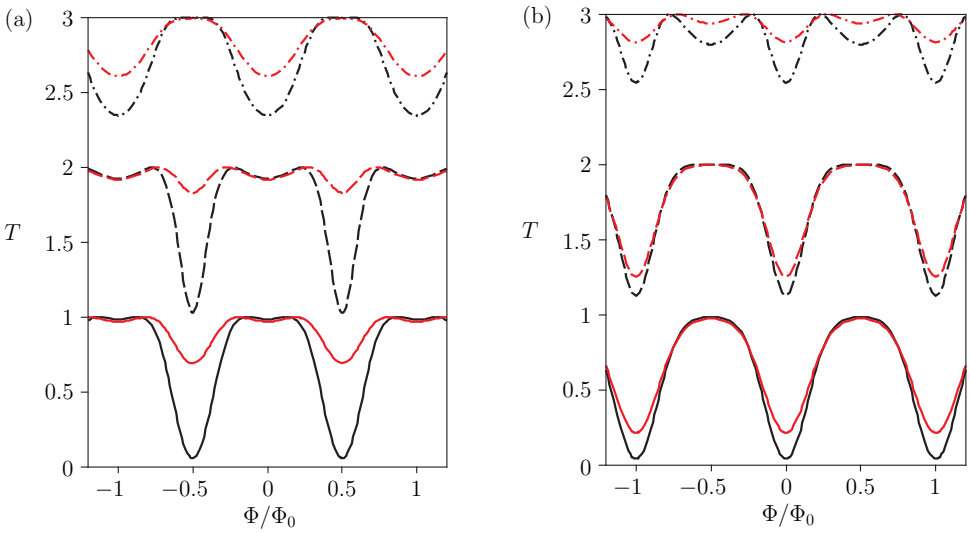

Figure 3.4: Transmission probability through the ring when a scatterer is present in the upper arm of the ring with strength $T_s = 0.95$ as a function of the flux Φ (in units of Φ_0) for $\chi = 20.3\pi$ and maximal coupling ($a = 0$). Black and red curves correspond to $\lambda = 1$, and $\lambda = 1.6$, respectively. Dashed and dashdotted curves are shifted by +1 and +2, respectively. Solid, dashed and dashdotted curves in (a) correspond to $\delta\chi = 0$, $\pi/3$, and $2\pi/3$, while in (b) to $\delta\chi = \pi$, $4\pi/3$, and $5\pi/3$, respectively.

It can be seen that as a result of the phase introduced by the scatterer, the phase of the oscillations are shifted when $\delta\chi$ is increased from 0 to $5\pi/3$. Destructive interference in the symmetric case is not complete as propagation in the lower arm is free, while in the upper arm, the scatterer has a probability $R_s = 0.05$ to reflect the electron. In the case characterized by $\lambda = 1.6$ (red curves), when asymmetry favors the upper arm of the ring, where the weak scatterer is located, the transmission minima shift to higher values. In this case, complete destructive interference does not take place as propagation through the upper arm has a higher probability. It can also be seen, that the phase difference $\delta\chi$ also changes the amplitude of the oscillations.

Figure 3.5 shows the transmission probability as a function of the flux for two values of the geometric phase χ, when a strong scatterer ($T_s = 0.25$) is present in the upper arm of the ring, and the coupling between the ring and the leads is maximal ($a = 0$). Black and red curves correspond to symmetric ($\lambda = 1$), and asymmetric injection (characterized by $\lambda = 2$), respectively. Solid, dashed, dashdotted, and dotted curves correspond to $\delta\chi = 0$, $\pi/3$, $2\pi/3$, and π, and are shifted by +1, +2, and +3, respectively. It can be seen that – contrary to the case of a weak scatterer – the difference between the phases acquired in the two arms of the ring ($\delta\chi$) here does not change the phase of the oscillations. However, similarly to the previous case, it may slightly modify their amplitude. When injection is symmetric, then, similarly to the case when a weak scatterer was present in the upper arm, transmission minima are not zero, as destructive interference is not complete, due to free propagation in the lower arm. The effect of asymmetric injection (red curves), which favors the arm in which the scatterer is located, is an overall decrease of the transmission probability. This may be expected from the fact that the electron is injected towards the

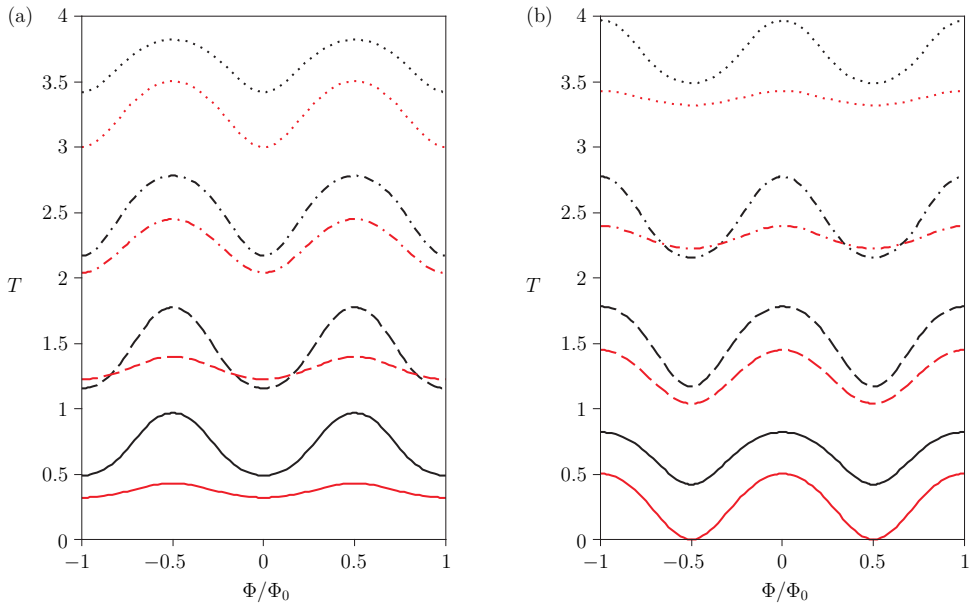

Figure 3.5: Transmission probability through the ring as a function of the flux when a scatterer is present in the upper arm with $T_s = 0.25$, (a) for $\chi = 20.4\pi$ and (b) for $\chi = 21.6\pi$. We assume perfect coupling ($a = 0$) between the ring and the leads. Black and red curves correspond to $\lambda = 1$, and $\lambda = 2$, respectively. Solid, dashed, dashdotted, and dotted curves correspond to $\delta\chi = 0$, $\pi/3$, $2\pi/3$, and π, respectively. Dashed, dashdotted, and dotted curves are shifted by $+1$, $+2$, and $+3$, respectively.

scatterer with a higher probability than into the other arm, and the scatterer transmits the electron with a small probability. It can also be seen that there are certain values of the phase difference $\delta\chi$, where asymmetric injection leads to complete destructive interference.

3.3 Conclusions

We determined the transmission through a one-dimensional ring, in the presence of an Aharonov-Bohm flux, using a scattering matrix in the junctions of the leads with the ring, in which the elements describing the probability of transmission from the lead into the two arms were different. We evaluated the transmission probability through the ring assuming no scatterers in the arms and showed that asymmetric injection increases the transmission probability as a function of the geometric phase acquired in the arms of the ring. We also showed that the asymmetry parameter affects the amplitude of the transmission oscillations as a function of the magnetic flux: the transmission minima shift to higher values due to incomplete destructive interference. We investigated the effect of the coupling between the leads and the ring when asymmerty was present between the two arms. We found that the probability of transmission is decreased except for certain values of the geometric phase, where the ring may still be completely transparent for the electrons. For other values of the geometric phase, an overall reduction of the transmission could be seen as a function of the magnetic flux. We also investigated the case when

a scatterer was present in the arm of the ring, which was also favored by asymmetric injection. We showed that in the case of a weak scatterer the phase of the oscillations is shifted as the phase introduced by the scatterer is changed. Furthermore, asymmetry leads to the increase of transmission minima. In the case of a strong scatterer, we showed that the phase of the oscillations of the transmission probability as a function of the flux is insensitive to the phase difference resulting from the presence of the scatterer. We showed that an asymmery, which favors the arm in which the strong scatterer is present, leads to an overall decrease of the transmission with respect to the symmetric case.

Chapter 4

Three-terminal quantum ring with spin-dependent propagation

The realization of spin-polarized transport is an important issue of spintronics. Several systems have been proposed for this purpose. A four-terminal mesoscopic device similar to the Mach-Zehnder interferometer with a local Rashba spin-orbit interaction in one arm and a global magnetic field was shown to be equivalent to the optical polarizing beam splitter [99]. An electron spin filter based on a branching geometry was proposed in Ref. [100] for generating spin-polarized currents via Rashba spin-orbit coupling without the use of spin-dependent interference. In Ref. [101] it was shown that in a narrow gap semiconductor quantum well or quantum wire, an observable electron spin current can be generated with a time-dependent gate which modifies the Rashba spin-orbit coupling constant. A device that achieves spin filtering by momentum-resolved tunneling between parallel electron waveguides due to Rashba spin-orbit coupling was proposed in Ref. [102]. In Ref. [103] the elastic scattering of unpolarized electrons by a nonuniform Rashba coupling strength in a two-dimensional electron system was shown to lead to almost full polarization around the forward-scattered beam. In Ref. [104] it was shown that highly polarized transport can be achieved in a two-dimensional electron gas that is periodically modulated by ferromagnetic and Schottky metal stripes.

In this chapter we investigate the possiblity of spin-polarization with quantum rings, which are attached to three current-carrying leads. Fisrt, in Section 4.1, we solve the scattering problem of such a ring with Rashba spin-orbit interaction and a perpendicular magnetic field for the most general boundary condition in the terminals [95]. Then, in Section 4.2, we show that a three-terminal ring with one terminal acting as an input and two terminals acting as outputs, can operate as a spin beam splitter: different polarizations can be achieved in the two output channels from a totally unpolarized incoming spin state [96, 97]. In Section 4.3, we investigate in detail the physical background of this polarizing effect, and show that it is a result of an appropriate interference of states that

carry oppositely directed currents [97]. Finally, in Section 4.4 we show that in a three-terminal ring the spatial degree of freedom, i.e., the presence of two different possible output channels, gets intertwined with the spin direction as a consequence of quantum interference and spin-orbit interaction [98].

4.1 Formal solution of the problem

In this section we solve the scattering problem of a three-terminal quantum ring in which Rashba-type spin-orbit interaction and a perpendicular magnetic field are present, using the model presented in Section 2.3. We assume that the magnetic field is weak enough to be treated as a perturbation. We determine the spinor-valued wavefunctions for the most general boundary condition, i.e., when there are incoming and outgoing waves in each terminal [95]. We note that although the results of the following sections of this chapter are obtained for a less general boundary condition (namely, having only one input) and zero magnetic field, we chose to start here from this most general case in order to derive results that are suitable for using in Chapter 5 as well.

Let us consider a quantum ring of radius ρ located in the $x-y$ plane in the presence of Rashba spin-orbit coupling [22] and a perpendicular magnetic field B. We have seen in Section 2.3.1, that the Hamiltonian of a single electron is then given by Eq. (2.31). If B is relatively weak, then the interaction between the electron spin and the field, i.e. the Zeeman term can be treated as a perturbation and the relevant dimensionless Hamiltonian reads [90, 92]

$$H = \left[\left(-\mathrm{i}\frac{\partial}{\partial\varphi} - \frac{\Phi}{\Phi_0} + \frac{\omega_{\mathrm{SO}}}{2\Omega}\sigma_r\right)^2 - \frac{\omega_{\mathrm{SO}}^2}{4\Omega^2}\right] + H_{\mathrm{p}}, \tag{4.1}$$

where φ is the azimuthal angle of a point on the ring, Φ denotes the magnetic flux encircled by the ring, $\Phi_0 = h/|e|$ is the flux quantum, and $\omega_{\mathrm{SO}} = \alpha/\hbar\rho$ is the frequency associated with the spin-orbit interaction. $\hbar\Omega = \hbar^2/2m^*\rho^2$ characterizes the kinetic energy with m^* being the effective mass of the electron, and the radial spin operator is given by $\sigma_r = \sigma_x\cos\varphi + \sigma_y\sin\varphi$. The perturbative Zeeman term H_{p} is given by [92]

$$H_{\mathrm{p}} = \frac{\omega_{\mathrm{B}}}{\Omega}\sigma_z, \tag{4.2}$$

where $\omega_{\mathrm{B}} = -2\mu B/\hbar = g^*eB/4m$ with g^* and m being the effective gyromagnetic ratio and the free electron mass, respectively.

The energy eigenvalues of the unperturbed Hamiltonian are the same as those of the case when only Rashba spin-orbit coupling is present, being given by Eq. (2.49) with κ

replaced by $(\kappa - \Phi/\Phi_0)$:

$$E_0^{(\mu)}(\kappa) = \left(\kappa - \frac{\Phi}{\Phi_0}\right)^2 + (-1)^\mu \left(\kappa - \frac{\Phi}{\Phi_0}\right) w + \frac{1}{4}, \quad (\mu = 1, 2)\,, \tag{4.3}$$

where

$$w = \sqrt{1 + \frac{\omega_{\mathrm{SO}}^2}{\Omega^2}}. \tag{4.4}$$

The corresponding eigenvectors in the $\{|\uparrow_z\rangle, |\downarrow_z\rangle\}$ eigenbasis of σ_z have the same form as the eigenspinors (2.45):

$$\psi^{(\mu)}(\kappa, \varphi) = e^{\mathrm{i}\kappa\varphi} \begin{pmatrix} e^{-\mathrm{i}\frac{\varphi}{2}} u^{(\mu)} \\ e^{\mathrm{i}\frac{\varphi}{2}} v^{(\mu)} \end{pmatrix}, \tag{4.5}$$

where

$$u^{(1)} = -v^{(2)} = \cos\frac{\theta}{2}, \tag{4.6}$$

$$u^{(2)} = v^{(1)} = \sin\frac{\theta}{2}, \tag{4.7}$$

and

$$\tan\frac{\theta}{2} = \frac{\Omega}{\omega_{\mathrm{SO}}}\,(1 - w)\,. \tag{4.8}$$

In order to treat the perturbation, we need to determine the matrix elements of H_{p} in the basis of these eigenstates

$$\left\langle \psi^{(\mu)} \right| H_{\mathrm{p}} \left| \psi^{(\mu)} \right\rangle = (-1)^{\mu+1} \frac{\omega_{\mathrm{B}}}{\Omega} \cos\theta = (-1)^{\mu+1} \frac{\omega_{\mathrm{B}}}{\Omega} \frac{1}{w}, \tag{4.9}$$

$$\left\langle \psi^{(1)} \right| H_{\mathrm{p}} \left| \psi^{(2)} \right\rangle = \frac{\omega_{\mathrm{B}}}{\Omega} \sin\theta. \tag{4.10}$$

In the first-order approximation one neglects the off-diagonal elements; this is reasonable if they are small, i.e., if $\omega_{\mathrm{B}}/\Omega \ll k^2\rho^2$, where k denotes the wave number of the incident electron, which, as we have mentioned in Section 2.3, is described as a plane wave. Within this approximation, the eigenspinors are not perturbed and their direction is still specified by the angle θ, given by Eq. (4.8). The energy eigenvalues including the first-order corrections are given by

$$E^{(\mu)}(\kappa) = E_0^{(\mu)}(\kappa) + (-1)^{\mu+1} \frac{\omega_{\mathrm{L}}}{\Omega} \frac{1}{w}. \tag{4.11}$$

As we have seen in Section 2.3, the energy of the incoming electron $E = \hbar^2 k^2/2m^*$ has to be conserved, therefore the condition $E/\hbar\Omega = k^2\rho^2 = E^{(\mu)}(\kappa)$ determines the possible

values of κ:

$$\kappa_j^{(\mu)} = (-1)^{\mu+1}\left[\frac{w}{2} + (-1)^j q^{(\mu)}\right] + \frac{\Phi}{\Phi_0}, \tag{4.12}$$

where $\mu, j = 1, 2$ and

$$q^{(\mu)} = \sqrt{q^2 + (-1)^\mu \frac{\omega_{\mathrm{L}}}{\Omega}\frac{1}{w}}, \tag{4.13}$$

with $q = \sqrt{(\omega_{\mathrm{SO}}/2\Omega)^2 + k^2\rho^2}$. To the four different $\kappa_j^{(\mu)}$ the following four eigenstates correspond ($j = 1, 2$):

$$\psi_j^{(1)}(\kappa_j^{(1)}, \varphi) = e^{\mathrm{i}\kappa_j^{(1)}\varphi}\begin{pmatrix} e^{-\mathrm{i}\frac{\varphi}{2}}\cos\frac{\theta}{2} \\ e^{\mathrm{i}\frac{\varphi}{2}}\sin\frac{\theta}{2}\end{pmatrix}, \tag{4.14}$$

$$\psi_j^{(2)}(\kappa_j^{(2)}, \varphi) = e^{\mathrm{i}\kappa_j^{(2)}\varphi}\begin{pmatrix} e^{-\mathrm{i}\frac{\varphi}{2}}\sin\frac{\theta}{2} \\ -e^{\mathrm{i}\frac{\varphi}{2}}\cos\frac{\theta}{2}\end{pmatrix}. \tag{4.15}$$

The wave function for a given energy E in the different sections of the ring is the linear combination of these states.

In the following we will show the detailed solution of the scattering problem for a ring with three terminals, shown in Fig. 4.1, where we assume that spin-orbit interaction is only present in the ring, but not in the leads. We consider the most general boundary condition, when there are incoming and outgoing waves on each terminal, i.e.:

$$\Psi_l(x_l) = \begin{pmatrix}(f_l)_\uparrow \\ (f_l)_\downarrow\end{pmatrix} e^{\mathrm{i}kx_l} + \begin{pmatrix}(r_l)_\uparrow \\ (r_l)_\downarrow\end{pmatrix} e^{-\mathrm{i}kx_l}, \qquad (l = \mathrm{I,II,III}). \tag{4.16}$$

The wave functions belonging to the same energy in the different sections of the ring are:

$$\Psi_i(\varphi) = \sum_{\mu,j} a_{i,j}^{(\mu)} e^{\mathrm{i}\kappa_j^{(\mu)}\varphi}\begin{pmatrix} e^{-\mathrm{i}\frac{\varphi}{2}}u^{(\mu)} \\ e^{\mathrm{i}\frac{\varphi}{2}}v^{(\mu)}\end{pmatrix}, \tag{4.17}$$

where $u^{(\mu)}$ and $v^{(\mu)}$ are given by Eqs. (4.6)-(4.7), and the subscript $i = 1, 2, 3$ denotes the sections of the ring in the counterclockwise direction, starting from the position of the incoming lead (see Fig. 4.1).

We have seen in Sec. 2.3.3 that at the three junctions the wave functions and the spin probability currents need to be fitted:

$$\begin{aligned}
\Psi_{\mathrm{I}}(0) &= \Psi_1(0) = \Psi_3(2\pi), \\
\Psi_{\mathrm{II}}(0) &= \Psi_1(\gamma_1) = \Psi_2(\gamma_1), \\
\Psi_{\mathrm{III}}(0) &= \Psi_2(\gamma_2) = \Psi_3(\gamma_2), \\
J_{\mathrm{I}}(0) - J_1(0) + J_3(2\pi) &= 0, \\
J_{\mathrm{II}}(0) + J_1(\gamma_1) - J_2(\gamma_1) &= 0, \\
J_{\mathrm{III}}(0) + J_2(\gamma_2) - J_3(\gamma_2) &= 0.
\end{aligned} \tag{4.18}$$

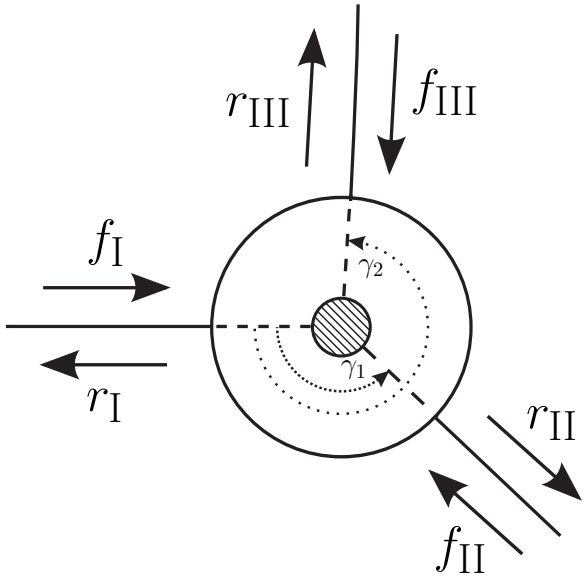

Figure 4.1: The notations used for the incoming and outgoing amplitudes in a three-terminal quantum ring. f_{I}, r_{I}, f_{II}, etc. denote two-component spinors.

By determining the continuity equation, the spin probability currents $J_i(\varphi)$ in the ring can be shown to be given by [95]:

$$J_i(\varphi) = 2\mathcal{R}e\left[\Psi_i^{\dagger}(\varphi)\left(-\mathrm{i}\frac{\partial}{\partial\varphi} + \frac{\omega_{\mathrm{SO}}}{2\Omega}\sigma_r(\varphi) - \frac{\Phi}{\Phi_0}\right)\Psi_i(\varphi)\right]. \tag{4.19}$$

The spin probability currents $J_{\mathrm{l}}(x_l)$ in the leads, where no spin-orbit interaction is present, are given by Eq. (2.54).

From Eqs. (4.18) we can determine the outgoing spinors (r_{I}, r_{II} and r_{III}) as a function of the incoming ones (f_{I}, f_{II} and f_{III}). This connection can be described by 2×2 reflection and transmission matrices, like the one given by Eq. (2.56), but now we have one reflection and two transmission matrices for each input:

$$r_{\mathrm{I}} = \hat{R}^{f_{\mathrm{I}}} f_{\mathrm{I}} + \hat{T}_2^{f_{\mathrm{II}}} f_{\mathrm{II}} + \hat{T}_1^{f_{\mathrm{III}}} f_{\mathrm{III}}, \tag{4.20a}$$

$$r_{\mathrm{II}} = \hat{T}_1^{f_{\mathrm{I}}} f_{\mathrm{I}} + \hat{R}^{f_{\mathrm{II}}} f_{\mathrm{II}} + \hat{T}_2^{f_{\mathrm{III}}} f_{\mathrm{III}}, \tag{4.20b}$$

$$r_{\mathrm{III}} = \hat{T}_2^{f_{\mathrm{I}}} f_{\mathrm{I}} + \hat{T}_1^{f_{\mathrm{II}}} f_{\mathrm{II}} + \hat{R}^{f_{\mathrm{III}}} f_{\mathrm{III}}. \tag{4.20c}$$

The $\hat{R}^{f_{\mathrm{I}}}$ matrix, which describes the reflected part of the input f_{I} into lead I is given by:

$$\begin{aligned}
\hat{R}_{\uparrow\uparrow}^{f_{\mathrm{I}}} &= \hat{\varrho}^{(1)}\cos^2\frac{\theta}{2} + \hat{\varrho}^{(2)}\sin^2\frac{\theta}{2} - 1, \\
\hat{R}_{\uparrow\downarrow}^{f_{\mathrm{I}}} &= (\hat{\varrho}^{(1)} - \hat{\varrho}^{(2)})\sin\frac{\theta}{2}\cos\frac{\theta}{2}, \\
\hat{R}_{\downarrow\uparrow}^{f_{\mathrm{I}}} &= \hat{R}_{\uparrow\downarrow}^{f_{\mathrm{I}}}, \\
\hat{R}_{\downarrow\downarrow}^{f_{\mathrm{I}}} &= \hat{\varrho}^{(1)}\sin^2\frac{\theta}{2} + \hat{\varrho}^{(2)}\cos^2\frac{\theta}{2} - 1,
\end{aligned} \tag{4.21}$$

where

$$\begin{aligned}\hat{\varrho}^{(\mu)} &= \frac{8k\rho}{\hat{y}^{(\mu)}}\left\{\mathrm{i}k^2\rho^2\sin\left(q^{(\mu)}\gamma_1\right)\sin\left(q^{(\mu)}(\gamma_2-\gamma_1)\right)\sin\left(q^{(\mu)}(2\pi-\gamma_2)\right)-\mathrm{i}(q^{(\mu)})^2\sin\left(2q^{(\mu)}\pi\right)\right.\\ &\left.-k\rho q^{(\mu)}\left[\sin\left(q^{(\mu)}\gamma_1\right)\sin\left(q^{(\mu)}(2\pi-\gamma_1)\right)+\sin\left(q^{(\mu)}\gamma_2\right)\sin\left(q^{(\mu)}(2\pi-\gamma_2)\right)\right]\right\}, \quad (4.22)\end{aligned}$$

$$\begin{aligned}\hat{y}^{(\mu)} &= 8(q^{(\mu)})^3\left\{\cos\left[\left((-1)^{\mu+1}w+2\phi\right)\pi\right]+\cos\left(2q^{(\mu)}\pi\right)\right\}-12\mathrm{i}k\rho(q^{(\mu)})^2\sin\left(2q^{(\mu)}\pi\right)\\ &-2k^2\rho^2q^{(\mu)}\left[\cos\left(2q^{(\mu)}(\pi-\gamma_2+\gamma_1)\right)+\cos\left(2q^{(\mu)}(\pi-\gamma_2)\right)+\cos\left(2q^{(\mu)}(\pi-\gamma_1)\right)\right.\\ &\left.-3\cos\left(2q^{(\mu)}\pi\right)\right]+\mathrm{i}k^3\rho^3\left[\sin\left(2q^{(\mu)}(\pi-\gamma_2+\gamma_1)\right)-\sin\left(2q^{(\mu)}(\pi-\gamma_2)\right)\right.\\ &\left.+\sin\left(2q^{(\mu)}(\pi-\gamma_1)\right)-\sin\left(2q^{(\mu)}\pi\right)\right]. \quad (4.23)\end{aligned}$$

The $\hat{T}_1^{f_{\mathrm{I}}}$ and $\hat{T}_2^{f_{\mathrm{I}}}$ matrices, which describe the transmitted part of the input f_{I} into lead II and III, respectively, are given by:

$$\begin{aligned}\left(\hat{T}_n^{f_{\mathrm{I}}}\right)_{\uparrow\uparrow} &= e^{-\mathrm{i}\frac{\gamma_n}{2}}\left(\hat{\tau}_n^{(1)}\cos^2\frac{\theta}{2}+\hat{\tau}_n^{(2)}\sin^2\frac{\theta}{2}\right),\\ \left(\hat{T}_n^{f_{\mathrm{I}}}\right)_{\uparrow\downarrow} &= e^{-\mathrm{i}\frac{\gamma_n}{2}}\left(\hat{\tau}_n^{(1)}-\hat{\tau}_n^{(2)}\right)\sin\frac{\theta}{2}\cos\frac{\theta}{2},\\ \left(\hat{T}_n^{f_{\mathrm{I}}}\right)_{\downarrow\uparrow} &= e^{\mathrm{i}\frac{\gamma_n}{2}}\left(\hat{\tau}_n^{(1)}-\hat{\tau}_n^{(2)}\right)\sin\frac{\theta}{2}\cos\frac{\theta}{2},\\ \left(\hat{T}_n^{f_{\mathrm{I}}}\right)_{\downarrow\downarrow} &= e^{\mathrm{i}\frac{\gamma_n}{2}}\left(\hat{\tau}_n^{(1)}\sin^2\frac{\theta}{2}+\hat{\tau}_n^{(2)}\cos^2\frac{\theta}{2}\right),\end{aligned} \quad (4.24)$$

where $n=1,2$, indicating the two possible output channels, and

$$\begin{aligned}\hat{\tau}_1^{(\mu)} &= \frac{8k\rho q^{(\mu)}}{\hat{y}^{(\mu)}}e^{\mathrm{i}\frac{\gamma_1}{2}\left((-1)^{\mu+1}w+2\phi\right)}\left\{-k\rho\sin\left(q^{(\mu)}(\gamma_2-\gamma_1)\right)\sin\left(q^{(\mu)}(2\pi-\gamma_2)\right)\right.\\ &\left.+\mathrm{i}q^{(\mu)}\left[e^{-\mathrm{i}\pi\left((-1)^{\mu+1}w+2\phi\right)}\sin\left(q^{(\mu)}\gamma_1\right)-\sin\left(q^{(\mu)}(2\pi-\gamma_1)\right)\right]\right\}, \quad (4.25)\\ \hat{\tau}_2^{(\mu)} &= \frac{8k\rho q^{(\mu)}}{\hat{y}^{(\mu)}}e^{\mathrm{i}\frac{\gamma_2}{2}\left((-1)^{\mu+1}w+2\phi\right)}\left\{k\rho e^{-\mathrm{i}\pi\left((-1)^{\mu+1}w+2\phi\right)}\sin\left(q^{(\mu)}\gamma_1\right)\sin\left(q^{(\mu)}(\gamma_2-\gamma_1)\right)\right.\\ &\left.+\mathrm{i}q^{(\mu)}\left[e^{-\mathrm{i}\pi\left((-1)^{\mu+1}w+2\phi\right)}\sin\left(q^{(\mu)}\gamma_2\right)-\sin\left(q^{(\mu)}(2\pi-\gamma_2)\right)\right]\right\}. \quad (4.26)\end{aligned}$$

It can be shown that the $\hat{R}^{f_{\mathrm{II}}}$ ($\hat{R}^{f_{\mathrm{III}}}$) matrix, which describes the reflected part of the input f_{II} (f_{III}) into lead II (III), and the $\hat{T}_n^{f_{\mathrm{II}}}$ ($\hat{T}_n^{f_{\mathrm{III}}}$) matrices, which describe the transmitted part of the spinor f_{II} (f_{III}) into leads III and I (I and II), can be given by transforming the $\hat{R}^{f_{\mathrm{I}}}$ and $\hat{T}^{f_{\mathrm{I}}}$ matrices in the following manner

$$M^{f_{\mathrm{II}}} = U_{\gamma_1}M^{f_{\mathrm{I}}}_{\substack{\gamma_1\leftrightarrow\gamma_2-\gamma_1\\ \gamma_2\leftrightarrow 2\pi-\gamma_1}}U_{\gamma_1}^{-1}, \quad (4.27)$$

$$M^{f_{\mathrm{III}}} = U_{\gamma_2}M^{f_{\mathrm{I}}}_{\substack{\gamma_1\leftrightarrow 2\pi-\gamma_2\\ \gamma_2\leftrightarrow 2\pi-\gamma_2+\gamma_1}}U_{\gamma_2}^{-1}, \quad (4.28)$$

where $M = \hat{R}, \hat{T}_1, \hat{T}_2$ and

$$U_{\gamma_n} = \begin{pmatrix} e^{-\mathrm{i}\frac{\gamma_n}{2}} & 0 \\ 0 & e^{\mathrm{i}\frac{\gamma_n}{2}} \end{pmatrix}, \quad n = 1, 2. \tag{4.29}$$

This is due to the fact that the matrices corresponding to a given input should also be able to describe any other input if the angles are changed accordingly. For example, for the input f_{I} the angles of the outputs II and III are measured from lead I, thus, when we want to determine the matrices for the input f_{II}, the angles of the output leads III and I need to be measured from lead II. However, the matrices obtained in this way will give the reflected and transmitted part of the given input in its own reference frame. In order to determine the contributions of each input in the same reference frame (here we chose that of f_{I}) the similarity transformations, given by Eqs. (4.27) and (4.28) need to be applied.

4.2 The three-terminal quantum ring as an electron spin beam splitter

In this section we show that due to quantum interference and spin-orbit interaction in a three-terminal ring with one input and two output leads, different polarizations can be achieved in the two outputs from an originally totally spin-unpolarized incoming state [96]. First, we present the transmission matrices of a three-terminal ring with one input and two outputs in which only Rashba spin-orbit interaction is present [97]. Then, we determine the condition for spin-polarization and show, that it can be satisfied for both symmetric and asymmetric configurations of the leads [96, 97].

4.2.1 One input, two outputs

Let us consider the three-terminal quantum ring for which we solved the scattering problem in the previous section, but let us assume, that the magnetic field is zero, and there is only one input lead, i.e. $f_{\mathrm{II}}, f_{\mathrm{III}} = 0$, using the notations of Fig. 4.1. Then, Eqs. (4.13) and (4.23) lead to

$$q^{(1)} = q^{(2)} = q, \tag{4.30}$$

$$\hat{y}^{(1)} = \hat{y}^{(2)} = \hat{y}, \tag{4.31}$$

where

$$\begin{aligned}\hat{y} &= 8q^3\left[\cos\left(w\pi\right)+\cos\left(2q\pi\right)\right]-12\mathrm{i}k\rho q^2\sin\left(2q\pi\right)+4k^2\rho^2 q\cos\left(2q\pi\right) \\ &-2k^2\rho^2 q\left[\cos\left(2q\left(\pi-\gamma_2+\gamma_1\right)\right)-\cos\left(2q\pi\right)+\cos\left(2q\left(\pi-\gamma_1\right)\right)+\cos\left(2q\left(\pi-\gamma_2\right)\right)\right] \\ &+\mathrm{i}k^3\rho^3\left[\sin\left(2q\left(\pi-\gamma_2+\gamma_1\right)\right)-\sin\left(2q\pi\right)+\sin\left(2q\left(\pi-\gamma_1\right)\right)-\sin\left(2q\left(\pi-\gamma_2\right)\right)\right].\end{aligned} \tag{4.32}$$

Consequently, equations (4.25) and (4.26) simplify to

$$\hat{\tau}_1^{(\mu)} = \frac{8k\rho q}{\hat{y}}\left[h_1^{(\mu)}+g_1^{(\mu)}\right], \tag{4.33a}$$

$$\hat{\tau}_2^{(\mu)} = \frac{8k\rho q}{\hat{y}}\left[h_2^{(\mu)}+g_2^{(\mu)}\right], \tag{4.33b}$$

where $h_n^{(\mu)}$ and $g_n^{(\mu)}$ are given by

$$\begin{aligned}h_1^{(\mu)} &= -k\rho e^{\mathrm{i}\frac{\gamma_1}{2}(-1)^{\mu+1}w}\sin(q(\gamma_2-\gamma_1))\sin(q(2\pi-\gamma_2)), \\ h_2^{(\mu)} &= k\rho e^{\mathrm{i}\frac{\gamma_2}{2}(-1)^{\mu+1}w}e^{-\mathrm{i}\pi(-1)^{\mu+1}w}\sin(q(\gamma_2-\gamma_1))\sin(q\gamma_1), \\ g_1^{(\mu)} &= \mathrm{i}qe^{\mathrm{i}\frac{\gamma_1}{2}(-1)^{\mu+1}w}\left[e^{-\mathrm{i}\pi(-1)^{\mu+1}w}\sin(q\gamma_1)-\sin(q(2\pi-\gamma_1))\right], \\ g_2^{(\mu)} &= \mathrm{i}qe^{\mathrm{i}\frac{\gamma_2}{2}(-1)^{\mu+1}w}\left[e^{-\mathrm{i}\pi(-1)^{\mu+1}w}\sin(q\gamma_2)-\sin(q(2\pi-\gamma_2))\right].\end{aligned} \tag{4.34}$$

Notice that $h_n^{(2)}=\left(h_n^{(1)}\right)^*$ and $g_n^{(2)}=-\left(g_n^{(1)}\right)^*$.

Using the notations $h_n^{(1)}=h_n$ and $g_n^{(1)}=g_n$, and substituting Eqs. (4.33) into Eqs. (4.24), the transmission matrices of the two outgoing leads read [97]

$$\begin{aligned}\left(\hat{T}_n\right)_{\uparrow\uparrow} &= \left(\hat{T}_n^{f_\mathrm{I}}\right)_{\uparrow\uparrow}=\frac{8k\rho q}{\hat{y}}e^{-\mathrm{i}\frac{\gamma_n}{2}}\left[\left(h_n+g_n\right)\cos^2\frac{\theta}{2}+\left(h_n-g_n\right)^*\sin^2\frac{\theta}{2}\right], \\ \left(\hat{T}_n\right)_{\uparrow\downarrow} &= \left(\hat{T}_n^{f_\mathrm{I}}\right)_{\uparrow\downarrow}=\frac{8k\rho q}{\hat{y}}e^{-\mathrm{i}\frac{\gamma_n}{2}}\left[\left(h_n+g_n\right)+\left(h_n-g_n\right)^*\right]\sin\frac{\theta}{2}\cos\frac{\theta}{2}, \\ \left(\hat{T}_n\right)_{\downarrow\uparrow} &= \left(\hat{T}_n^{f_\mathrm{I}}\right)_{\downarrow\uparrow}=\frac{8k\rho q}{\hat{y}}e^{\mathrm{i}\frac{\gamma_n}{2}}\left[\left(h_n+g_n\right)+\left(h_n-g_n\right)^*\right]\sin\frac{\theta}{2}\cos\frac{\theta}{2}, \\ \left(\hat{T}_n\right)_{\downarrow\downarrow} &= \left(\hat{T}_n^{f_\mathrm{I}}\right)_{\downarrow\downarrow}=\frac{8k\rho q}{\hat{y}}e^{\mathrm{i}\frac{\gamma_n}{2}}\left[\left(h_n+g_n\right)\sin^2\frac{\theta}{2}+\left(h_n-g_n\right)^*\cos^2\frac{\theta}{2}\right].\end{aligned} \tag{4.35}$$

(Note that since in this case there is only one input f_I, for the sake of simplicity, we have omitted the superscript f_I from the notations: $\hat{T}_n=\hat{T}_n^{f_\mathrm{I}}$.)

Let us note here that for a ring that is symmetric with respect to the incoming lead, i.e., $\gamma_1=2\pi-\gamma_2$, it can easily be seen that the two transmission matrices possess the

following symmetry property [96]

$$\begin{aligned} \left(\hat{T}_1\right)_{\uparrow\uparrow} &= \left(\hat{T}_2\right)_{\downarrow\downarrow}, \qquad \left(\hat{T}_1\right)_{\uparrow\downarrow} = -\left(\hat{T}_2\right)_{\downarrow\uparrow}, \\ \left(\hat{T}_1\right)_{\downarrow\uparrow} &= -\left(\hat{T}_2\right)_{\uparrow\downarrow}, \quad \left(\hat{T}_1\right)_{\downarrow\downarrow} = \left(\hat{T}_2\right)_{\uparrow\uparrow}. \end{aligned} \tag{4.36}$$

This is due to the fact that for a symmetric configuration of the leads, a rotation of the ring together with the external field generating the Rashba coupling around the axis of the incoming lead by an angle of π, requires the transmission properties to remain unchanged. For a ring which is not symmetric with respect to the direction of the incoming lead, the transmission matrices (4.35) do not have this symmetry.

4.2.2 The condition for spin polarization

When the incoming electron is not perfectly spin-polarized, i.e. its spin state is a mixture, which – instead of a two-component spinor – should be described by a 2×2 density matrix ϱ_{in}, then we can easily generalize Eq. (4.35) to obtain the output density matrices ϱ_1 and ϱ_2 by

$$\varrho_n = \hat{T}_n \varrho_{\text{in}} \hat{T}_n^\dagger. \tag{4.37}$$

Considering a completely unpolarized input, i.e. ϱ_{in} being proportional to the 2×2 identity matrix

$$\varrho_{\text{in}} = \frac{1}{2}\begin{pmatrix} 1 & 0 \\ 0 & 1 \end{pmatrix}, \tag{4.38}$$

then, in order to get polarized outputs, the output density operators (4.37) should be projectors (apart from the possible reflective losses):

$$\varrho_n = \frac{1}{2}\hat{T}_n \hat{T}_n^\dagger = \eta_n \left|\phi_n\right\rangle \left\langle\phi_n\right|. \tag{4.39}$$

The non-negative numbers η_1 and η_2 measure the efficiency of the polarizing device, i.e. $\eta_1 + \eta_2 = 1$ means a reflectionless process.

Equation (4.39) is equivalent to requiring the determinants of $\hat{T}_n \hat{T}_n^\dagger$ to vanish. According to Eqs. (4.35), there are two different conditions for each transmission matrix to satisfy this requirement:

$$h_n \pm g_n = 0, \quad (n = 1, 2).$$

However, only the following two cases lead to nonzero transmission at **both** outputs:

$$h_1 + g_1 = 0, \quad \text{and} \quad h_2 - g_2 = 0, \tag{4.40a}$$

or

$$h_1 - g_1 = 0, \quad \text{and} \quad h_2 + g_2 = 0. \tag{4.40b}$$

Using Eqs. (4.35) these conditions can be formulated as

$$\sin(w\pi) = \pm\frac{k\rho}{q}\frac{\sin(q\,(2\pi-\gamma_2))\sin(q\,(\gamma_2-\gamma_1))}{\sin(q\gamma_1)} = \pm\frac{k\rho}{q}\frac{\sin(q\gamma_1)\sin(q\,(\gamma_2-\gamma_1))}{\sin(q\,(2\pi-\gamma_2))} \tag{4.41a}$$

$$\cos(w\pi) = \frac{\sin(q\,(2\pi-\gamma_1))}{\sin(q\gamma_1)} = \frac{\sin(q\gamma_2)}{\sin(q\,(2\pi-\gamma_2))} \tag{4.41b}$$

where Eq. (4.41a) with the plus sign together with Eq. (4.41b) correspond to the first case, given by Eq. (4.40a), while Eq. (4.41a) with the minus sign together with Eq. (4.41b) correspond to the second case, given by Eq. (4.40b).

From the second equation of (4.41b) and (4.41a) we can find

$$\sin(q\gamma_1) = \pm\sin(q\,(2\pi-\gamma_2)), \tag{4.42}$$

$$\sin(q\gamma_2) = \pm\sin(q\,(2\pi-\gamma_1)), \tag{4.43}$$

which lead to the following relation between the possible positions of the outgoing leads:

$$\gamma_1 = 2\pi - \gamma_2 \pm m\pi/q, \tag{4.44}$$

where m is a nonnegative integer, which ensures $0 < \gamma_1 < \gamma_2 < 2\pi$. Then, we may consider either γ_1 or γ_2 as the free parameter together with $k\rho$ and $\omega_{\mathrm{SO}}/\Omega$ to find the solutions of Eqs. (4.41). In either case, Eq. (4.44) will give the possible positions of the other output lead.

4.2.3 Polarization in a symmetric ring

The $m = 0$ case in Eq. (4.44) corresponds to a symmetric configuration of the outgoing leads with respect to the incoming lead [96]. Taking γ_2 as the free parameter (i.e. $\gamma_1 = 2\pi - \gamma_2$), we find that

$$h_2 = -h_1^*, \tag{4.45}$$

$$g_2 = g_1^*, \tag{4.46}$$

thus the conditions given by Eq. (4.40a) and (4.40b) can be written as

$$h_1 + g_1 = 0, \tag{4.47a}$$

$$h_1 - g_1 = 0, \tag{4.47b}$$

respectively. Furthermore, (4.41a) and (4.41b) simplify to

$$\sin(w\pi) = \mp\frac{k\rho}{q}\sin\left(2q\left(\pi-\gamma_2\right)\right), \tag{4.48a}$$

$$\cos(w\pi) = \frac{\sin(q\gamma_2)}{\sin\left(q\left(2\pi-\gamma_2\right)\right)}. \tag{4.48b}$$

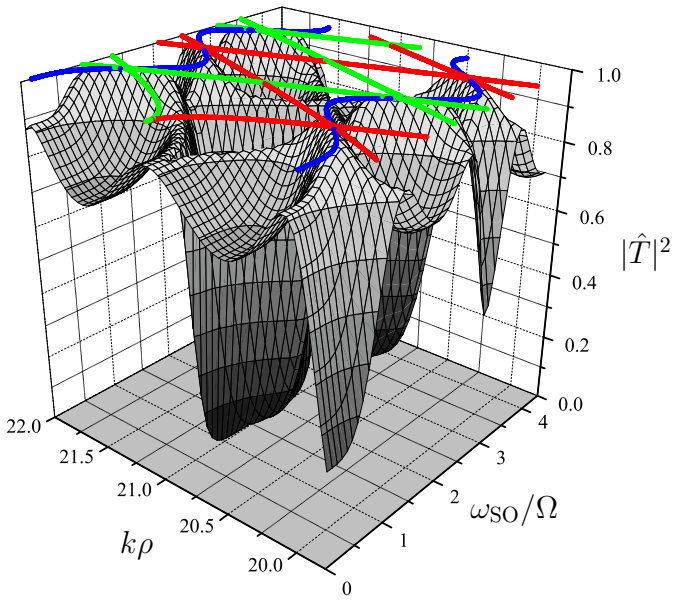

Figure 4.2: Transmission probability through the outputs of a symmetric three-terminal ring ($\gamma_1 = 2\pi/3$, $\gamma_2 = 4\pi/3$) and the determination of the parameter values corresponding to spin-polarization: Equation (4.48a) with the plus and minus sign are satisfied along the red and green curves, respectively, while Eq. (4.48b) is satisfied along the blue curves. At each intersection of a red or a green curve with the blue one, the ring acts as a spin-polarizing device.

Each of these conditions leads to a $k\rho - \omega_{SO}$ relation as depicted in Fig. 4.2 for a representative example corresponding to $\gamma_2 = 4\pi/3$ ($\gamma_1 = 2\pi/3$). The parameters corresponding to the crossing points of the red and green curves [solutions of Eq. (4.48a)] with the blue curve [solution of Eq. (4.48b)], ensure the formation of polarized outputs. We note that similar curves can be drawn for arbitrary (symmetric) geometry. This implies that there are lines in the three-dimensional $\{\gamma_2, \omega_{SO}/\Omega, k\rho\}$ space along which the ring polarizes a completely unpolarized input. The figure also shows the transmission probability $|\hat{T}|^2 = Tr(\hat{T}_1\hat{T}_1^\dagger) = Tr(\hat{T}_2\hat{T}_2^\dagger)$ through the outputs of the ring. It can be seen that there are parameter values where perfect spin-polarization is expected, i.e., where the transmission probability is practically unity. This property can also be seen in Fig. 4.3, which shows that along a line defined by $h_1 + g_1 = 0$ in the space $\{\gamma_2, \omega_{SO}/\Omega, k\rho\}$, the efficiency η of the transmission is a quasiperiodic function of γ_2. (A similar figure can be drawn for the condition $h_1 - g_1 = 0$.) As can be seen, there are certain points (that is, parameter combinations), where η is unity. Thus, the results of this simple model suggest

that it is possible to obtain 100% spinpolarized outputs from a perfectly unpolarized input, even without reflective losses.

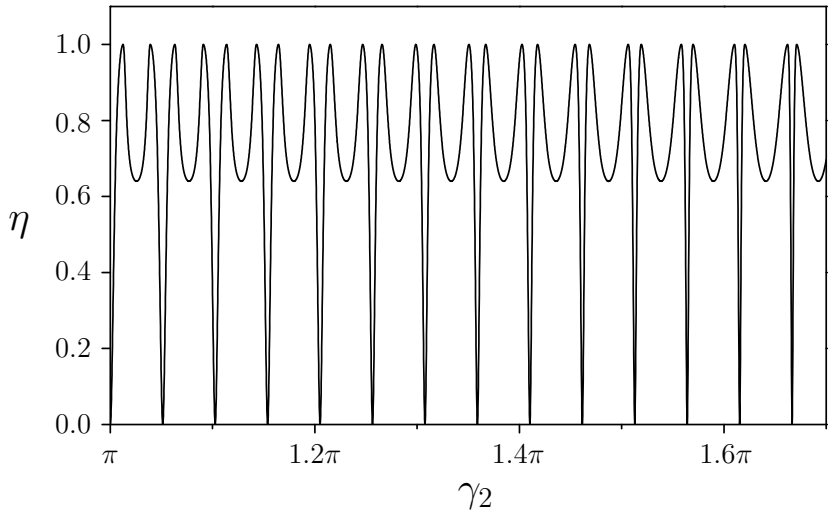

Figure 4.3: Transmission probability of a spin-polarizing ring as a function of γ_2. The parameter $k\rho$ changes in the range of [19.0, 21.0], while $0 < \omega_{\mathrm{SO}}/\Omega < 5$, and the plot corresponds to the condition $h_1 + g_1 = 0$.

Now we turn to the investigation of the outgoing spinors which arise as a consequence of the polarizing property of the ring. Clearly, these are the eigenstates $|\phi_n\rangle$ of the transmitted density matrices corresponding to the nonzero eigenvalues which are given by

$$\eta_1 = \eta_2 = \frac{128 q^2 k^2 \rho^2 \left|h_1\right|^2}{\left|\hat{y}\right|^2}. \tag{4.49}$$

Note that the quasiperiodic behavior of the transmission probability $\eta = \eta_1 + \eta_2$ seen in Fig. 4.3 is related to the sine and cosine functions in h_1 and $\hat{y}$. Focusing on the case of $h_1 + g_1 = 0$, the eigenstates of the respective transmitted density matrices corresponding to the nonzero eigenvalues η_1 and η_2 read

$$|\phi_1\rangle_+ = \begin{pmatrix} \sin\frac{\theta}{2} \\ -e^{-\mathrm{i}\gamma_2}\cos\frac{\theta}{2} \end{pmatrix}, \quad |\phi_2\rangle_+ = \begin{pmatrix} e^{-\mathrm{i}\gamma_2}\cos\frac{\theta}{2} \\ \sin\frac{\theta}{2} \end{pmatrix}. \tag{4.50}$$

These results describe the connection between the strength of the spin-orbit coupling (encoded in θ), the geometry of the device, and its polarizing directions. We note that these polarizing directions are, in general, not orthogonal, their overlap is given by ${}_+\langle\phi_2|\,\phi_1\rangle_+ = \mathrm{i}\sin\theta\sin\gamma_2$. Similarly, for $h_1 - g_1 = 0$, we have

$$|\phi_1\rangle_- = \begin{pmatrix} e^{\mathrm{i}\gamma_2}\cos\frac{\theta}{2} \\ \sin\frac{\theta}{2} \end{pmatrix}, \quad |\phi_2\rangle_- = \begin{pmatrix} \sin\frac{\theta}{2} \\ -e^{\mathrm{i}\gamma_2}\cos\frac{\theta}{2} \end{pmatrix}. \tag{4.51}$$

Considering the transmission matrices (4.35) themselves, it is clear that under the conditions given by Eqs. (4.48a) and (4.48b), their determinants also vanish. That is, each $\hat{T}_n$ has a zero eigenvalue, but – due to the nonhermiticity – its eigenspinors are not orthogonal. It can be verified that the eigenstates corresponding to the nonzero eigenvalue of the transmission matrices coincide with $|\phi_n\rangle_+$ and $|\phi_n\rangle_-$, while the spinors annulled by the transmission matrices $\hat{T}_n |\phi_n^0\rangle = 0$ have the following components:

$$\left|\phi_1^0\right\rangle_+ = \left|\phi_2^0\right\rangle_- = \begin{pmatrix} \cos\frac{\theta}{2} \\ \sin\frac{\theta}{2} \end{pmatrix}, \quad \left|\phi_2^0\right\rangle_+ = \left|\phi_1^0\right\rangle_- = \begin{pmatrix} -\sin\frac{\theta}{2} \\ \cos\frac{\theta}{2} \end{pmatrix}. \tag{4.52}$$

where the subscript $+$ and $-$ corresponds to the condition $h_1 + g_1 = 0$ and $h_1 - g_1 = 0$, respectively.

These results show that if the conditions given by Eqs. (4.48a) and (4.48b) are satisfied, the device acts similar to a Stern-Gerlach apparatus in the sense that (1) for an unpolarized input, we have two different spin directions (4.50) in the outputs, (2) if we consider one of the eigenstates (4.50) as the input, its spin direction will not change in the appropriate output, and (3) there are spinors given by Eq. (4.52), for which the transmission probability into a given output lead is zero. The analogy is not perfect though; the polarized spinors (4.50) are not orthogonal and the spinor which has zero probability to be transmitted through a given lead is not equal to the eigenstate corresponding to the nonzero eigenvalue of the other lead: $|\phi_n\rangle \neq \left|\phi_{n'}^0\right\rangle$ for $n \neq n'$. From this point of view, an optical polarizing beam splitter [105,106] with nonorthogonal polarizing directions can be the closest analog of our device.

4.2.4 Polarization with asymmetric configurations

We have seen in Sec. 4.2, that the polarizing condition is not restricted to symmetric geometries: there are asymmetric configurations as well, as can be seen from Eq. (4.44). These positions differ by $\pm m\pi/q$ from the symmetric ones. In the previous section (see Fig. 4.2) we demonstrated that for a given symmetric geometry, with proper combinations of the parameters $\omega_{\mathrm{SO}}/\Omega$ and $k\rho$ the conditions (4.48a) and (4.48b) can be satisfied. This means that an asymmetric ring, the geometry of which is determined from the symmetric configuration by Eq. (4.44), is then also able to produce polarized outputs. This is an important generalization of the previous results: There are several appropriate positions for the output leads, the symmetric case is just one of them.

When the requirement (4.39) for polarization is satisfied, we have seen in the previous section, that the output spinors are the eigenstates $|\phi_n\rangle$ of the transmitted density matrices, which correspond to the nonzero eigenvalues. For an asymmetric configuration,

these eigenstates in the two cases (4.40a) and (4.40b) are given by

$$|\phi_1\rangle_a = \begin{pmatrix} e^{-\mathrm{i}\frac{\gamma_1}{2}} \sin\frac{\theta}{2} \\ -e^{\mathrm{i}\frac{\gamma_1}{2}} \cos\frac{\theta}{2} \end{pmatrix}, \quad |\phi_2\rangle_a = \begin{pmatrix} e^{-\mathrm{i}\frac{\gamma_2}{2}} \cos\frac{\theta}{2} \\ e^{\mathrm{i}\frac{\gamma_2}{2}} \sin\frac{\theta}{2} \end{pmatrix}, \tag{4.53a}$$

$$|\phi_1\rangle_b = \begin{pmatrix} e^{-\mathrm{i}\frac{\gamma_1}{2}} \cos\frac{\theta}{2} \\ e^{\mathrm{i}\frac{\gamma_1}{2}} \sin\frac{\theta}{2} \end{pmatrix}, \quad |\phi_2\rangle_b = \begin{pmatrix} e^{-\mathrm{i}\frac{\gamma_2}{2}} \sin\frac{\theta}{2} \\ -e^{\mathrm{i}\frac{\gamma_2}{2}} \cos\frac{\theta}{2} \end{pmatrix}, \tag{4.53b}$$

respectively. The output spin states in both cases are the two types of eigenspinors of the Hamiltonian taken at the positions of the output junctions. For a given output lead, the two eigenspinors are interchanged in the two cases (corresponding to Eqs. (4.40a) and (4.40b)). Note that the output spinors are still nonorthogonal, their overlap is given by ${}_\beta\langle\phi_2|\,\phi_1\rangle_\beta = \mathrm{i}\sin(\gamma_2-\gamma_1)/2$, for both $\beta = a, b$.

4.2.5 Conclusions

We showed that a quantum ring with one input and two output leads in the presence of Rashba-type spin-orbit interaction has remarkable similarities with the Stern-Gerlach apparatus. Parameter values, within the experimentally feasible range were identified when the three-terminal ring delivers perfectly polarized output beams of electrons without reflective losses. We found that appropriate spin-polarized input states are transmitted without modification, but it is also possible to prepare inputs, for which the transmission into a given lead is forbidden.

4.3 The physical background of spin polarization: spatial interference

We have shown in the previous section, that a one-dimensional three-terminal quantum ring in the presence of Rashba spin-orbit interaction can act as an electron spin beam splitter. In this section we analyze the physical origin of this polarizing effect, and show that it is a result of an appropriate interference of states that carry oppositely directed currents. We visualize the stationary spin directions along the ring for an originally totally spin-unpolarized electron, revealing the formation of the pure spin states on the outputs [97].

4.3.1 Spin probability currents in the ring

The mathematical treatment used in the previous section demonstrated the interesting fact that a three-terminal ring can spin-polarize electrons which are originally unpolarized. Unfortunately however, it is unable to provide a clear insight into the underlying physics.

In order to show how polarized spin states are formed on the outputs, let us consider again a completely unpolarized input, now taken as the following equal weight sum of *pure* state orthogonal projectors

$$\varrho_{\text{in}} = \frac{1}{2}\left(\left|\psi_{\text{in}}^{(1)}\right\rangle\left\langle\psi_{\text{in}}^{(1)}\right| + \left|\psi_{\text{in}}^{(2)}\right\rangle\left\langle\psi_{\text{in}}^{(2)}\right|\right). \tag{4.54}$$

Here $\psi_{\text{in}}^{(\mu)} = \psi_1^{(\mu)}(0) = \psi_2^{(\mu)}(0)$ ($\mu = 1,2$), given by Eqs. (4.14) and (4.15), are the eigenspinors of the Hamiltonian at the position of the incoming lead. The density operator in the different sections (i = I,II,III) of the ring is then

$$\varrho_i(\varphi) = \frac{1}{2}\left(\left|\Psi_i^{(1)}(\varphi)\right\rangle\left\langle\Psi_i^{(1)}(\varphi)\right| + \left|\Psi_i^{(2)}(\varphi)\right\rangle\left\langle\Psi_i^{(2)}(\varphi)\right|\right), \tag{4.55}$$

where

$$\begin{aligned}
\Psi_i^{(1)}(\varphi) &= \sum_{j=1,2}\Psi_{i,j}^{(1)}(\varphi) = N_i^{(1)}(\varphi)\begin{pmatrix} e^{-\mathrm{i}\frac{\varphi}{2}}\cos\frac{\theta}{2} \\ e^{\mathrm{i}\frac{\varphi}{2}}\sin\frac{\theta}{2}\end{pmatrix}, \\
\Psi_i^{(2)}(\varphi) &= \sum_{j=1,2}\Psi_{i,j}^{(2)}(\varphi) = N_i^{(2)}(\varphi)\begin{pmatrix} e^{-\mathrm{i}\frac{\varphi}{2}}\sin\frac{\theta}{2} \\ -e^{\mathrm{i}\frac{\varphi}{2}}\cos\frac{\theta}{2}\end{pmatrix},
\end{aligned} \tag{4.56}$$

are the spinor valued wave functions of the electron in the different domains of the ring for the pure inputs $\psi_{\text{in}}^{(1)}$ and $\psi_{\text{in}}^{(2)}$, respectively, with

$$N_i^{(\mu)}(\varphi) = \sum_{j=1,2} a_{i,j}^{(\mu)} e^{i\kappa_j^{(\mu)}\varphi}, \quad \mu = 1,2.$$

$\Psi_i^{(\mu)}(\varphi)$ consists of two of the four eigenstates of the Hamiltonian, those which have the same spinor part, but different κ.

By examining the spin probability current corresponding to the $\Psi_{ij}^{(\mu)}(\varphi)$ states appearing in (4.56)

$$J_{ij}^{(\mu)} = \left|a_{ij}^{(\mu)}\right|^2\left[2\kappa_j^{(\mu)} + (-1)^\mu\left(\cos\theta - \frac{\omega_{\text{SO}}}{\Omega}\sin\theta\right)\right] = (-1)^{\mu+j+1}\,2q\left|a_{ij}^{(\mu)}\right|^2, \tag{4.57}$$

it can be seen that $\Psi_{i1}^{(\mu)}(\varphi)$ and $\Psi_{i2}^{(\mu)}(\varphi)$ represent oppositely directed (clockwise and anticlockwise) spin currents in each section (identified by the index i) of the ring, since the signs of $J_{i1}^{(\mu)}$ and $J_{i2}^{(\mu)}$ are opposite. The overall spin current densities which correspond to the input $\psi_{\text{in}}^{(\mu)}$ are

$$\begin{aligned}
J_i^{(\mu)} &= 2\mathcal{R}e\left\{a_{i1}^{(\mu)}\left(a_{i2}^{(\mu)}\right)^* e^{\mathrm{i}\left(\kappa_1^{(\mu)}-\kappa_2^{(\mu)}\right)\varphi}\right\}\left[\kappa_1^{(\mu)} + \kappa_2^{(\mu)} + (-1)^\mu\left(\cos\theta - \frac{\omega_{\text{SO}}}{\Omega}\sin\theta\right)\right] \\
&+ 2q(-1)^\mu\left(\left|a_{i1}^{(\mu)}\right|^2 - \left|a_{i2}^{(\mu)}\right|^2\right) = 2q(-1)^\mu\left(\left|a_{i1}^{(\mu)}\right|^2 - \left|a_{i2}^{(\mu)}\right|^2\right) = J_{i1}^{(\mu)} + J_{i2}^{(\mu)},
\end{aligned} \tag{4.58}$$

that is, the sum of the clockwise and anticlockwise directed currents given by Eq. (4.57). We note that the cross terms in Eq. (4.58) disappear as a result of the fact that $\tan\theta = -\omega_{\mathrm{SO}}/\Omega$.

The output spinors (4.53a) and (4.53b) suggest, that in order to obtain a polarized (pure) state at a given output, one of the projectors of (4.55) should vanish, and the other one should remain nonzero at that point of the ring. In order to have different polarized spin states in both outputs, the two projectors need to vanish at different output junctions. One of the possible ways to achieve this is to have $\Psi_1^{(1)}(\gamma_1)$ and $\Psi_2^{(2)}(\gamma_2)$ zero, which happens only if the spatial parts of these wave functions are zero (see Eqs. (4.56)):

$$N_{\mathrm{I}}^{(1)}(\gamma_1) = 0, \qquad N_{\mathrm{II}}^{(2)}(\gamma_2) = 0, \tag{4.59}$$

indicating destructive interference at the given output. By exchanging $\mu = 1$ and $\mu = 2$, the other case of polarization can be described. From condition (4.59) follows that

$$\left|a_{\mathrm{I},1}^{(1)}\right| = \left|a_{\mathrm{I},2}^{(1)}\right|, \qquad \left|a_{\mathrm{II},1}^{(2)}\right| = \left|a_{\mathrm{II},2}^{(2)}\right|, \tag{4.60}$$

which can be shown to be equivalent to Eqs. (4.40a). (Exchanging $\mu = 1$ and $\mu = 2$ in (4.59) leads to (4.40b)). Equation (4.60) implies that the spin currents $J_{\mathrm{I}}^{(1)}$ and $J_{\mathrm{II}}^{(2)}$ given by Eq. (4.58) vanish as a consequence of the interference of the oppositely directed currents corresponding to the states of the same spinor parts, given by Eq. (4.57). The requirement for spin-polarization, given by Eq. (4.39), thus has a very clear physical interpretation in terms of destructive interference and vanishing spin currents.

4.3.2 Visualization of the effect

Fig. 4.4 shows how pure spin states at the outputs (denoted by II and III) of a symmetric three-terminal ring are formed when the input is completely unpolarized, decomposed as (4.54). Here, the polarization condition (4.40a) is satisfied with the parameters $\omega_{\mathrm{SO}}/\Omega = 3.05$ and $k\rho = 1.38$. (We note that in semiconductor rings, the actual value of $k\rho$ is usually an order of magnitude larger. The values used here are intended to provide a better visualization of the phenomenon.) In the left panel we show the probability density of the electron at the given azimuthal angle φ on the ring. The colors of the curves correspond to the two spin components of the input shown with the same color in the right panel. The dotted lines mark the positions of the outgoing leads, where one of the two probability densities becomes zero, resulting in the output of the other spinor at that point as a pure state. In the right panel the stationary spin directions of the electron are depicted along the ring. Red and blue arrows correspond to ψ_{in}^1 and ψ_{in}^2, respectively. The lengths of the arrows are proportional to the probability densities shown in the left panel. The two outputs in this case are given by Eqs. (4.53a). As it can also be seen

from the figure, spin transformation in this case is a rotation around the z-axis by an angle pertaining to the given point on the ring, as can already be seen in case of a closed ring [36].

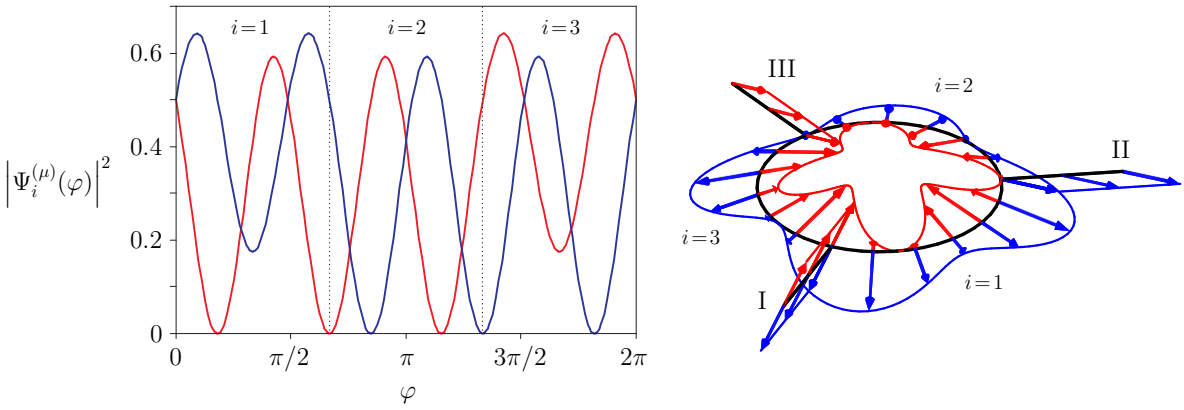

Figure 4.4: Formation of pure spin states at the outputs (II and III) of a symmetric three-terminal ring ($\gamma_1 = 2\pi/3$, $\gamma_2 = 4\pi/3$) for a completely unpolarized input decomposed as (4.54) when the parameters $\omega_{\mathrm{SO}}/\Omega = 3.05$ and $k\rho = 1.38$ ensure perfect polarization in the case given by equation (4.40a). Left panel: The probability densities of the electron at the given point on the ring for the spin component shown with the same color in the right panel. The dotted lines in the graph mark the positions of the outgoing leads, where one of the two probability densities becomes zero, resulting in the output of the other spinor at that point as a pure state. Right panel: The stationary spin directions of the electron along the ring. Red and blue arrows correspond to ψ^1_{in} and ψ^2_{in}, respectively. The lengths of the arrows are proportional to the probability densities at the given point on the ring, shown in the left panel. The two outputs in this case are given by Eqs. (4.53a).

It is also interesting to see how polarization is produced if we decompose the incoming perfect mixture as an equal weight sum of the eigenstates of S_z

$$\varrho_{\mathrm{in}} = \frac{1}{2}\left(|\uparrow_z\rangle\langle\uparrow_z| + |\downarrow_z\rangle\langle\downarrow_z|\right). \tag{4.61}$$

Figure 4.5 shows how pure spin states at the outputs (II and III) are formed in the same symmetric ring as in Fig. 4.4, for a completely unpolarized input decomposed as (4.61). In the left panel the trace of the square of the total spin density matrix $\varrho_i(\varphi)$ at the given azimuthal angle φ is shown. $Tr\left[\varrho_i(\varphi)\right]^2 = 1$ and 0.5 correspond to the spin state being pure and maximally mixed, respectively. The dotted lines in the graph mark the positions of the outgoing leads, where – as it can be seen – the total spin state is pure. In the right panel the stationary spin directions are shown along the ring. Green and purple arrows correspond to inputs $|\uparrow_z\rangle$ and $|\downarrow_z\rangle$, respectively. We can see that for this decomposition of the completely unpolarized input, polarization is due to the fact that the spin states $|\uparrow_z\rangle$ and $|\downarrow_z\rangle$ are rotated into the same direction at the position of the output leads. Note that since we only took a different decomposition of the same input, the resulting polarized states (red and blue arrows) are obviously the same ones as in Fig. 4.4.

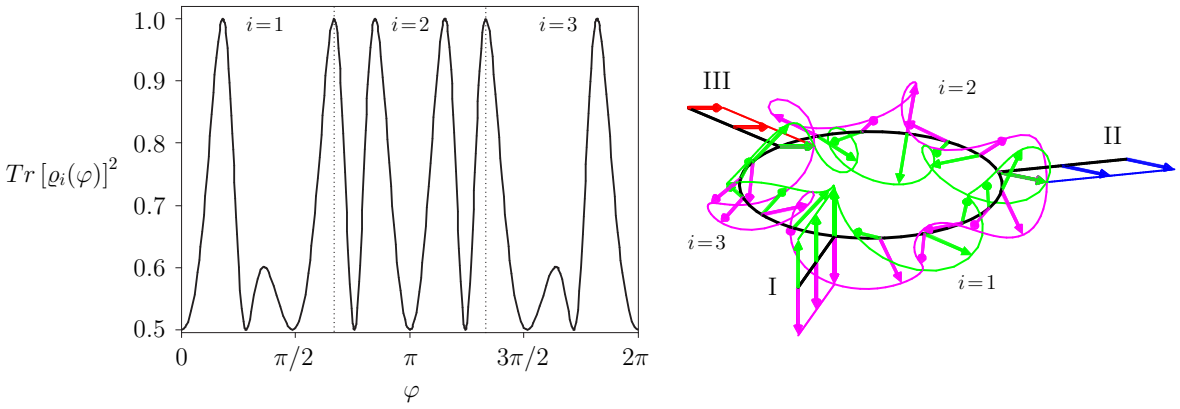

Figure 4.5: Formation of pure spin states at the outputs (II and III) of the same symmetric ring as in Fig. 4.4, for a completely unpolarized input decomposed as (4.61). Left panel: The trace of the square of the total spin density matrix $\varrho_i(\varphi)$ at the given point on the ring, $Tr\,[\varrho_i(\varphi)]^2 = 1$ and 0.5 corresponding to the spin state being pure and maximally mixed, respectively. The dotted lines in the graph mark the positions of the outgoing leads, where the total spin state is pure. Right panel: The stationary spin directions along the ring. Green and purple arrows correspond to inputs $|\uparrow_z\rangle$ and $|\downarrow_z\rangle$, respectively. These input spin states are rotated into the same direction at the output leads, resulting in the polarized states (red and blue arrows) seen in Fig. 4.4.

Figures 4.4 and 4.5 also show additional, asymmetrically situated points on both branches of the ring where the state of the electron is pure. These points are clearly those that can be determined from Eqs. (4.44), which give the appropriate ring configurations for spin polarization. If the output leads are placed into these positions, the outcoming spin states are the pure ones given by (4.53a) corresponding to these new positions.

4.3.3 Conclusions

We studied a three-terminal quantum ring with one input and two output leads, which – for appropriate parameter values – acts as a spin polarizer. We provided an instructive physical interpretation of the polarization process: for both symmetric and nonsymmetric geometries, polarization is due to spatial interference. At a given junction this interference is destructive for a certain spin direction, while constructive for its orthogonal counterpart which, consequently, is transmitted into the output lead.

4.4 Spatial-spin correlations: intertwining

In this section we investigate what kind of correlations can be present between the spatial and spin degrees of freedom of the electron at the output of a three-terminal quantum ring in which Rashba spin-orbit coupling is present. We show that these correlations can be classical when the possibility of quantum mechanical interference does not play a role, or that there can be intertwining [107] between the different degrees of freedom, which is similar to entanglement but in this case we have a single particle [98].

4.4.1 Mathematical formulation of the problem

Let us consider again a quantum ring, shown in Fig. 4.6 with one input and two output leads, which is symmetric with respect to the direction of the input lead, i.e., $\gamma_1 = 2\pi - \gamma_2$. We note that in all of the following discussions, we will focus on the spinor part of the wave function and ignore the plane wave part.

The quantum mechanical state of an electron (not necessarily pure) after the ring can be described by a single-particle density operator, which is defined on the tensorial product of two two-dimensional Hilbert spaces. The spin degree of freedom can be described on a Hilbert space spanned by the $\{|\uparrow_z\rangle, |\downarrow_z\rangle\}$ eigenstates of S_z, while a suitable basis in the other Hilbert space is provided by the states $\{|1\rangle, |2\rangle\}$ corresponding to the different leads, where the electron can leave the ring. Clearly, there can be correlations between these degrees of freedom: in the polarizing case described in Sec. 4.2, knowing the path along which the electron left the ring, we also know the direction of its spin.

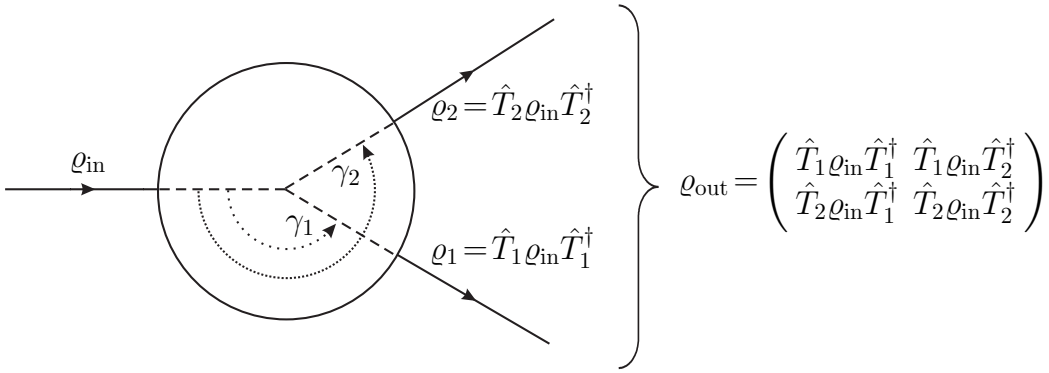

Figure 4.6: The geometry of the device and the relevant spinor density operators in the different leads.

In order to investigate the nature of these correlations, we need the "total" 4×4 output density matrix, which, in the $\{|1,\uparrow\rangle, |1,\downarrow\rangle, |2,\uparrow\rangle, |2,\downarrow\rangle\}$ basis reads

$$\varrho_{\text{out}} = \begin{pmatrix} \hat{T}_1 \varrho_{\text{in}} \hat{T}_1^\dagger & \hat{T}_1 \varrho_{\text{in}} \hat{T}_2^\dagger \\ \hat{T}_2 \varrho_{\text{in}} \hat{T}_1^\dagger & \hat{T}_2 \varrho_{\text{in}} \hat{T}_2^\dagger \end{pmatrix}, \tag{4.62}$$

where the 2×2 density matrices ϱ_1 and ϱ_2 appear in the diagonal (see Fig. 4.6). Note that (4.62) is a straightforward generalization of the case when the input spin is a pure state $|\Psi_{\text{in}}\rangle$ which is transformed into

$$|\Psi_{\text{out}}\rangle = |1\rangle \otimes \left(\hat{T}_1 |\Psi_{\text{in}}\rangle\right) + |2\rangle \otimes \left(\hat{T}_2 |\Psi_{\text{in}}\rangle\right) \tag{4.63}$$

and can be represented by a projector having the form of (4.62).

4.4.2 The nature of spatial-spin correlations

In this section we investigate what kind of spatial-spin correlations can build up as a consequence of quantum interference and spin-orbit interaction in the ring.

If the incoming state is a complete mixture, and the conditions given by (4.48a) and (4.48b) are satisfied, it can easily be shown that ϱ_{out} is block-diagonal. Thus, in this case we can write

$$\varrho_{\text{out}} = \eta \left(|1, \phi_1\rangle \langle 1, \phi_1| + |2, \phi_2\rangle \langle 2, \phi_2| \right) = |1\rangle \langle 1| \otimes \varrho_1 + |2\rangle \langle 2| \otimes \varrho_2, \tag{4.64}$$

where the states $|\phi_n\rangle, (n = 1, 2)$ in the projectors can be either $|\phi_n\rangle_+$ (4.50) or $|\phi_n\rangle_-$ (4.51), and the parameter η takes the reflective losses into account. It can be seen that although the output density matrices ϱ_1 and ϱ_2 represent pure states, globally we have a mixture and the correlation between the spatial and spin degrees of freedom is purely classical.

We note that by calculating the partial trace of ϱ_{out}, given by (4.64), with respect to the spin degree of freedom, the result is proportional to the identity matrix: not taking into account the spin degree of freedom, the electron, if transmitted at all, has the same probability to leave the ring along either lead.

On the other hand, if the incoming state is pure, then according to Eq. (4.63), the global outgoing state

$$\varrho_{\text{in}} = |\Psi_{\text{in}}\rangle \langle \Psi_{\text{in}}| \longrightarrow \varrho_{\text{out}} = \eta \, |\Psi_{\text{out}}\rangle \langle \Psi_{\text{out}}| ,$$

as well as the individual output states

$$\begin{aligned} \varrho_1 &= \hat{T}_1 \, |\Psi_{\text{in}}\rangle \langle \Psi_{\text{in}}| \, \hat{T}_1^\dagger, \\ \varrho_2 &= \hat{T}_2 \, |\Psi_{\text{in}}\rangle \langle \Psi_{\text{in}}| \, \hat{T}_2^\dagger, \end{aligned}$$

will be pure. In order to quantify the possible entanglement of the two different degrees of freedom contained in ϱ_{out} we calculate the entanglement of formation [108, 109]

$$\mathcal{E} = -\frac{1+\sqrt{1-C^2}}{2} \log_2 \left(\frac{1+\sqrt{1-C^2}}{2} \right) - \frac{1-\sqrt{1-C^2}}{2} \log_2 \left(\frac{1-\sqrt{1-C^2}}{2} \right), \tag{4.65}$$

where C is the so-called concurrence

$$C(\varrho) = \max \{0, \lambda_1 - \lambda_2 - \lambda_3 - \lambda_4\} . \tag{4.66}$$

The λ_i's are the eigenvalues (in decreasing order) of the Hermitian matrix

$$R = \sqrt{\sqrt{\tilde{\varrho}_{\rm out}}\,\hat{\varrho}_{\rm out}\sqrt{\tilde{\varrho}_{\rm out}}}, \tag{4.67}$$

where

$$\hat{\varrho}_{\rm out} = (\sigma_y \otimes \sigma_y)\,\tilde{\varrho}^*_{\rm out}\,(\sigma_y \otimes \sigma_y)\,, \tag{4.68}$$

and $\tilde{\varrho}^*_{\rm out}$ is the complex conjugate of the normalized total outgoing density matrix.

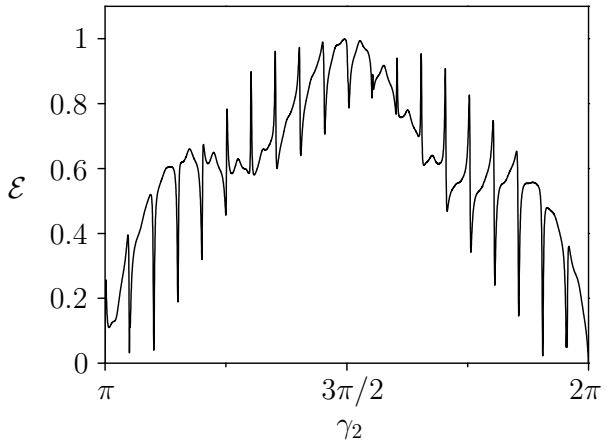

Figure 4.7: The entanglement of formation given by Eq. (4.65) of the output density matrix $\varrho_{\rm out}$ as a function of the geometrical angle γ_2 for $k\rho = 19.8$ and $\omega_{\rm SO}/\Omega = 3.7$.

Clearly, for the polarized output, given by Eq. (4.64), $\mathcal{E}$ vanishes, but generally it is nonzero and strongly depends on the parameters γ_2, $\omega_{\rm SO}/\Omega$, and ka. (Note that we consider symmetric geometry, i.e., $\gamma_1 = 2\pi - \gamma_2$). Figure 4.7 shows $\mathcal{E}$ as a function of γ_2 for the input spinor $|\Psi_{\rm in}\rangle = (|\uparrow_z\rangle + |\downarrow_z\rangle)/\sqrt{2} = |\uparrow_x\rangle$, i.e., one of the eigenspinors of S_x. The oscillations seen in this figure are due to the spatial interference inside the ring: the oppositely traveling electron waves form standing waves the periodicity of which modulates the behaviour of $\mathcal{E}$.

The entanglement of formation $\mathcal{E}$, shown in Fig. 4.7 is practically unity around $\gamma_2 = 3\pi/2$. This means that for the parameter values given in the caption of the figure, the intertwining between the spatial and spin degrees of freedom is maximal. Interestingly, in this case the output spinors are (to a very good approximation) eigenstates of S_y:

$$|\uparrow_x\rangle \to |\Psi_{\rm out}\rangle = \frac{1}{\sqrt{2}}\left(|1,\uparrow_y\rangle + {\rm i}\,|2,\downarrow_y\rangle\right). \tag{4.69}$$

We note that with the same parameters we also have

$$|\downarrow_x\rangle \to |\Psi_{\rm out}\rangle = \frac{1}{\sqrt{2}}\left(|1,\downarrow_y\rangle + {\rm i}\,|2,\uparrow_y\rangle\right), \tag{4.70}$$

and for both processes given by (4.69) and (4.70) the output spinors are orthogonal.

4.4.3 Conclusions

We investigated a three-terminal quantum ring, where one of the terminals served as input for the electrons, while the other two terminals were used as outputs. We focused on the nature of the correlation between the output electron spin and its spatial degree of freedom. We showed that in the case when quantum interference and spin-orbit coupling results in perfectly polarized outputs from a complete mixture input, this correlation is purely classical. On the other hand, when the spin state of the input electron is pure, we found that entanglement between the spin direction and the output path can be present.

Chapter 5

Two-dimensional quantum ring arrays

In this chapter we calculate the conductance and the spin transport properties of two-dimensional rectangular arrays consisting of quantum rings, in which Rashba-type spin-orbit interaction and a perpendicular magnetic field are present. Such arrays have already been fabricated in the heterojunction of InAlAs/InGaAs and studied in a recent experiment [32]. We describe the problem by using an analytically solvable one-dimensional ballistic model of single rings, which we use as building blocks of the array. By solving the scattering problem of ring arrays, our aim is to give a general survey of the magneto-conductance properties of such devices. In Section 5.1 we sketch the analytical solution of the scattering problem for single rings (given in detail in the Appendix), used as building blocks of the arrays. Then, in Section 5.2 we describe the building-block method, which we use to calculate the conductance of such arrays. We present the properties of the conductance of 3×3, 4×4, and 5×5 rectangular arrays as a function of the magnetic field, the Rashba spin-orbit coupling strength, and the wave vector. In Section 5.3 we study the spin-resolved transmission probabilities of the same array geometry with only one input channel. Finally, in Section 5.4 we investigate to what extent the conductance properties are modified by the presence of point-like random scattering centers between the rings.

5.1 Building blocks

The rectangular arrays we investigate are closed in the vertical and open in the horizontal direction, as shown in Fig. 5.1. We consider $N \times N$ arrays with N inputs (shown by the solid and dashed lines), and one input (shown by the solid line only). These consist of two-, three- and four-terminal rings, where the two- and three-terminal ones are situated on the boundary of the arrays (see Fig. 5.1). In what follows, we will consider these single rings as the building blocks of the arrays: first, we solve the scattering problem for the

different types of rings (we note that we have already done so for the three-terminal ring in Section 4.1), and then fit the wave functions and their derivatives in the points where neighboring rings touch each other. Thereby, we obtain a linear set of equations from which the (spin-dependent) transmission amplitudes can be determined, which can be used to calculate the conductance of the arrays with the Landauer formula.

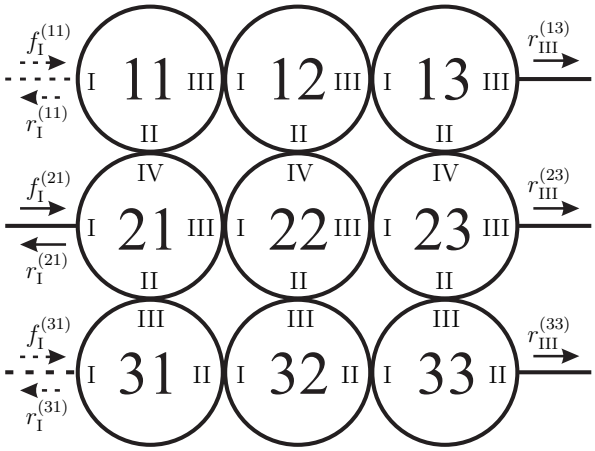

Figure 5.1: The geometry of the device in the simplest case of a 3×3 array with three or one (without leads displayed with dashed lines) input terminals. The notations can easily be generalized to larger arrays.

In order to be able to take into account every possible transmission and reflection inside the array, we need to solve the scattering problem of the individual rings for the most general boundary condition, i.e., when there are both incoming and outgoing spinor valued wave functions in each terminal: $\Psi_i = f_i e^{\mathrm{i}kx_i} + r_i e^{-\mathrm{i}kx_i}$ (i = I,II,III, IV), where x_i denotes the local coordinate in terminal i, as shown in Fig. 5.2. Note that the amplitudes $f_{\mathrm{I}}, r_{\mathrm{I}}, f_{\mathrm{II}}, ...$ refer to two-component spinors. For the case of a general three-terminal ring with Rashba spin-orbit interaction and a perpendicular magnetic field (Fig. 4.1), we have seen in Chapter 4 that the scattering problem can be solved analytically. The case of a ring with two or four terminals can be treated analogously. Here we do not detail these calculations as they can be carried out in a straightforward manner following the lines of Sec. 4. We note that these results are presented in the Appendix.

In a general two-terminal ring (see Fig. 5.2 without terminals III and IV) – where there are two incoming spinors (f_{I} and f_{II}) – the outgoing spin states can be given as the superposition of the reflected part of the input in the same lead and the transmitted part of the input in the other lead:

$$r_{\mathrm{I}} = R^{f_{\mathrm{I}}} f_{\mathrm{I}} + T^{f_{\mathrm{II}}} f_{\mathrm{II}}, \tag{5.1a}$$

$$r_{\mathrm{II}} = R^{f_{\mathrm{II}}} f_{\mathrm{II}} + T^{f_{\mathrm{I}}} f_{\mathrm{I}}. \tag{5.1b}$$

Here R^{f_i} and T^{f_i} (i = I,II) are 2×2 matrices, which can be determined by applying

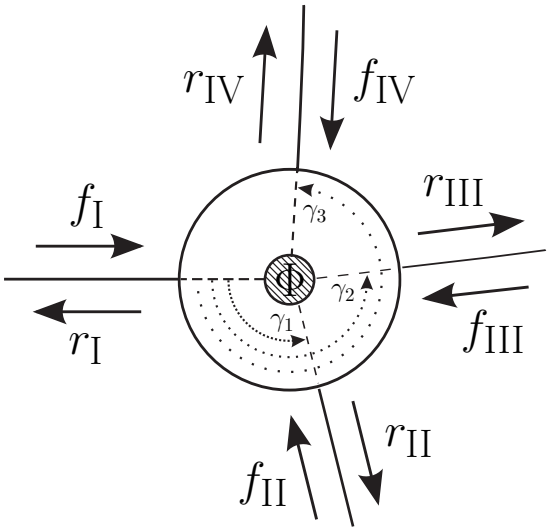

Figure 5.2: The notations used for the spinor part of the wave functions in the case of a four-terminal ring.

Griffith's boundary conditions at the junctions of the leads with the ring (see Section 2.3). As we have seen in the case of the three-terminal ring in Section 4.1, it is sufficient to determine the reflection and transmission matrices corresponding to the boundary condition of having only the input f_{I}, as the $R^{f_{\mathrm{II}}}$ and $T^{f_{\mathrm{II}}}$ matrices, which describe the reflected and transmitted part of the input f_{II}, can be given by:

$$M^{f_{\mathrm{II}}} = U_{\gamma_1} M^{f_{\mathrm{I}}}_{\gamma_1 \leftrightarrow 2\pi-\gamma_1} U^{-1}_{\gamma_1}, \tag{5.2}$$

where $M = R, T$, and U_{γ_1} is given by Eq. (4.29). The form of the matrices $\hat{R}^{f_{\mathrm{I}}}$ and $\hat{T}^{f_{\mathrm{I}}}$ is given in the Appendix.

In the case of a four-terminal ring, the outgoing spinors are also given as the superposition of the reflected part of the input in the respective lead and the transmitted part of the other inputs:

$$r_{\mathrm{I}} = \tilde{R}^{f_{\mathrm{I}}} f_{\mathrm{I}} + \tilde{T}_1^{f_{\mathrm{II}}} f_{\mathrm{II}} + \tilde{T}_2^{f_{\mathrm{III}}} f_{\mathrm{III}} + \tilde{T}_3^{f_{\mathrm{IV}}} f_{\mathrm{IV}}, \tag{5.3a}$$

$$r_{\mathrm{II}} = \tilde{R}^{f_{\mathrm{II}}} f_{\mathrm{II}} + \tilde{T}_1^{f_{\mathrm{III}}} f_{\mathrm{III}} + \tilde{T}_2^{f_{\mathrm{IV}}} f_{\mathrm{IV}} + \tilde{T}_3^{f_{\mathrm{I}}} f_{\mathrm{I}}, \tag{5.3b}$$

$$r_{\mathrm{III}} = \tilde{R}^{f_{\mathrm{III}}} f_{\mathrm{III}} + \tilde{T}_1^{f_{\mathrm{IV}}} f_{\mathrm{IV}} + \tilde{T}_2^{f_{\mathrm{I}}} f_{\mathrm{I}} + \tilde{T}_3^{f_{\mathrm{II}}} f_{\mathrm{II}}, \tag{5.3c}$$

$$r_{\mathrm{IV}} = \tilde{R}^{f_{\mathrm{IV}}} f_{\mathrm{IV}} + \tilde{T}_1^{f_{\mathrm{I}}} f_{\mathrm{I}} + \tilde{T}_2^{f_{\mathrm{II}}} f_{\mathrm{II}} + \tilde{T}_3^{f_{\mathrm{III}}} f_{\mathrm{III}}. \tag{5.3d}$$

Analogously to the case of the three-terminal ring (Section 4.1) and the two-terminal one presented above, the reflection and transmission matrices corresponding to the inputs f_{II}, f_{III} and f_{IV}, can be given by transforming the respective matrices corresponding to the input f_{I}:

$$M^{f_{\mathrm{II}}} = U_{\gamma_1} M^{f_{\mathrm{I}}}_{\substack{\gamma_1 \leftrightarrow \gamma_2 - \gamma_1 \\ \gamma_2 \leftrightarrow \gamma_3 - \gamma_2 \\ \gamma_3 \leftrightarrow 2\pi - \gamma_1}} U^{-1}_{\gamma_1}, \tag{5.4}$$

$$M^{f_{\rm III}} = U_{\gamma_2} M^{f_{\rm I}}_{\substack{\gamma_1\leftrightarrow\gamma_3-\gamma_2\\ \gamma_2\leftrightarrow 2\pi-\gamma_2\\ \gamma_3\leftrightarrow 2\pi-\gamma_2+\gamma_1}} U^{-1}_{\gamma_2}, \tag{5.5}$$

$$M^{f_{\rm IV}} = U_{\gamma_3} M^{f_{\rm I}}_{\substack{\gamma_1\leftrightarrow 2\pi-\gamma_3\\ \gamma_2\leftrightarrow 2\pi-\gamma_3+\gamma_1\\ \gamma_3\leftrightarrow 2\pi-\gamma_3+\gamma_1+\gamma_2}} U^{-1}_{\gamma_3}, \tag{5.6}$$

where $M = \tilde{R}, \tilde{T}_n$ $(n = 1, 2, 3)$ and U_{γ_n} is given by Eq. (4.29). For the detailed form of the matrices $\tilde{R}^{f_{\rm I}}$ and $\tilde{T}_n^{f_{\rm I}}$, we refer to the Appendix.

Using Eqs. (5.1), (4.20), and (5.3) the wave functions can be given in each terminal of the single two-, three- and four-terminal rings. By fitting the wave functions and their derivatives corresponding to the adjacent outputs of neighboring rings, these building blocks can be attached to each other to form arrays of arbitrary size. (We note that our method of using single rings as building blocks can easily be used to determine the conductance of arrays of arbitrary – not necessarily rectangular – configuration as well.) For the sake of simplicity, we restrict ourselves to $N \times N$ arrays, with $N = 3$, 4 and 5.

5.2 Properties of the conductance

Based on the analytic results presented in Section 4.1, 5.1 and in the Appendix, here we build two-dimensional rectangular arrays of 3×3, 4×4, and 5×5 quantum rings, where both Rashba spin-orbit interaction and a perpendicular magnetic field are present, so that the strength of the former one can be changed by an external gate voltage [23]. We assume that neighboring rings touch each other, and as we have mentioned in Section 5.1, we limit ourselves to arrays that are closed in the vertical and open in the horizontal direction, as shown in Fig. 5.1.

We derive the conductance from the linear set of equations resulting from the fit of the wave functions $\Psi_i^{(kl)}$ and their derivatives $\partial_{x_i^{(kl)}}\Psi_i^{kl}$ ($i =$ I,II,III,IV and $k, l = 1, ..., N$, where N is the number of rings along one direction in the array) in the points, where the rings touch each other. In the junction of ring {11} with ring {12} for example:

$$\begin{aligned} \Psi^{(11)}_{\rm III}\Big|_{x^{(11)}_{\rm III}=0} &= \Psi^{(12)}_{\rm I}\Big|_{x^{(12)}_{\rm I}=0}, \\ \partial_{x^{(11)}_{\rm III}}\Psi^{(11)}_{\rm III}\Big|_{x^{(11)}_{\rm III}=0} &= -\partial_{x^{(12)}_{\rm I}}\Psi^{(12)}_{\rm I}\Big|_{x^{(12)}_{\rm I}=0}. \end{aligned} \tag{5.7}$$

Note that the negative sign in Eq. (5.7) is a consequence of the opposite direction of the local coordinates in leads III of ring {11} and I of ring {12}. Equation (5.7) leads to

$$\begin{aligned} f^{(11)}_{\rm III} + r^{(11)}_{\rm III} &= f^{(12)}_{\rm I} + r^{(12)}_{\rm I}, \\ f^{(11)}_{\rm III} - r^{(11)}_{\rm III} &= -f^{(12)}_{\rm I} + r^{(12)}_{\rm I}, \end{aligned}$$

from which follows that

$$\begin{aligned} f_{\mathrm{III}}^{(11)} &= r_{\mathrm{I}}^{(12)}, \\ r_{\mathrm{III}}^{(11)} &= f_{\mathrm{I}}^{(12)}, \end{aligned} \tag{5.8}$$

i.e., the spinor entering (exiting) ring {11} on terminal III is equal to the spinor exiting (entering) ring {12} on terminal I. The spinors $r_{\mathrm{III}}^{(11)}$ and $r_{\mathrm{I}}^{(12)}$ can be given with the help of the reflection and transmission matrices of a three-terminal ring presented in Sec. 4.1 according to Eqs. (4.20).

For a small number of rings the resulting set of equations can be solved analytically; however already for an array of 3×3 rings shown in Fig. 5.1, it consists of 60 equations, which is preferably solved by numerical means, although analytic solutions exist in principle. (For larger arrays the number of equations scales practically with the number of rings.) After having determined the output spinor valued wave functions $r_{\mathrm{III}}^{(1N)}, r_{\mathrm{III}}^{(2N)}, ..., r_{\mathrm{II}}^{(NN)}$, we use the Landauer [1] formula

$$G = G_{\uparrow} + G_{\downarrow},$$

where

$$\begin{aligned} G_{\uparrow} &= \frac{e^2}{h}\left(\left|(r_{\mathrm{III}}^{(1N)})_{\uparrow}\right|^2 + \left|(r_{\mathrm{III}}^{(2N)})_{\uparrow}\right|^2 + ... + \left|(r_{\mathrm{II}}^{(NN)})_{\uparrow}\right|^2\right), \\ G_{\downarrow} &= \frac{e^2}{h}\left(\left|(r_{\mathrm{III}}^{(1N)})_{\downarrow}\right|^2 + \left|(r_{\mathrm{III}}^{(2N)})_{\downarrow}\right|^2 + ... + \left|(r_{\mathrm{II}}^{(NN)})_{\downarrow}\right|^2\right), \end{aligned}$$

averaged over the two σ_z eigenspinor inputs (see also Sec. 1.28) to calculate the conductance of the arrays.

The left panel of Fig. 5.3 shows a contour plot of the conductance (in units of e^2/h) of rectangular arrays of 3×3, 4×4 and 5×5 quantum rings, for zero magnetic flux as a function of the Rashba-coupling strength $\omega_{\mathrm{SO}}/\Omega$ and $k\rho$. The values of $k\rho$ are varied around $k_F\rho = 20.4$, corresponding to a Fermi energy of 11.13 meV in case of an effective mass $m^* = 0.023m$ of InGaAs and rings of radius $\rho = 0.25$ μm. The different arrays show similar behavior for larger values of the spin-orbit interaction strength: there are slightly downwards bending stripes (initially around even values of $k\rho$), where the devices are completely opaque for the electrons, and also conducting regions, which are initially around odd values of $k\rho$ and have complex internal structure. The bending of the stripes may be related to the effect of $q = \sqrt{k^2\rho 2 + (\omega_{\mathrm{SO}}/2\Omega)^2}$ on the transmission probability of the rings constituting the array, which can be directly seen in the case of a sinlge, diametric, two-terminal ring from Eq. (A-1). In the range of the values of $k\rho$ used, the increasing values of $\omega_{\mathrm{SO}}/\Omega$ decrease the dominance of $k\rho$ in q. Further comparing our

results to the case of a single ring with diametrically coupled leads (Fig. 2.8), it can be seen that the overall periodicity as a function of $k\rho$ is determined by single-ring interferences. The increasing number of the rings causes modulations superimposing on the single-ring behavior. This is probably the most apparent if we recall [92] that zero conductance areas are simply lines on the $k\rho - \omega_{\mathrm{SO}}/\Omega$ plane for a single two-terminal ring, while in our case there are stripes, the width of which is slightly increasing with the size of the array. This effect is related to the increasing number of consecutive partially destructive interferences that finally lead to essentially zero currents at the outputs. Additionally, if we considered an infinite array, the periodic boundary conditions would allow only discrete values of $k\rho$ for a given spin-orbit interaction strength with nonzero conductance. Thus the results presented in Figs. 5.3(a), (b) and (c) demonstrate a transition between the conductance properties of a single ring and that of an infinite array.

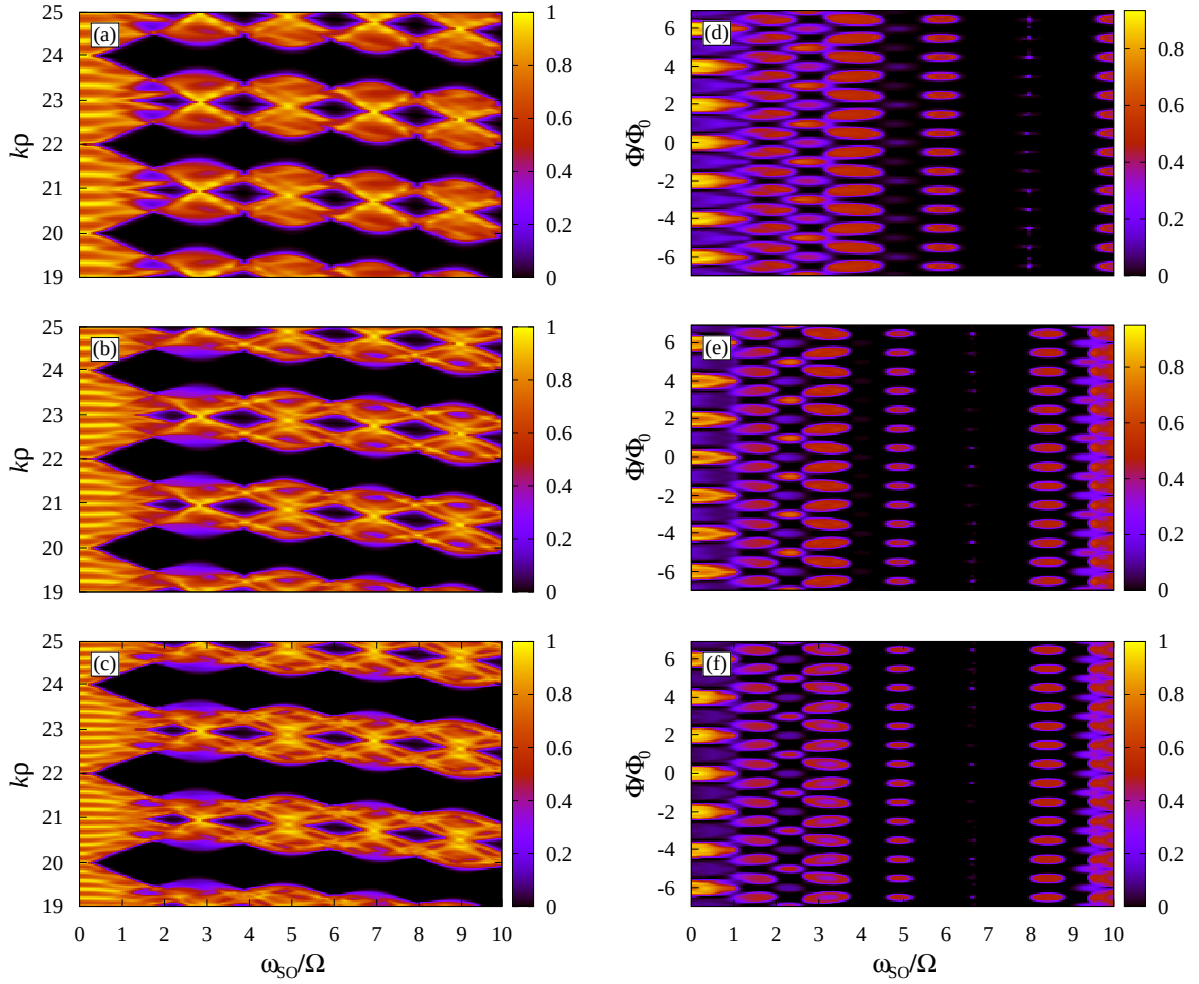

Figure 5.3: The conductance G/G_0 ($G_0 = e^2/h$) of rectangular arrays of different sizes. Left panel: The conductance as a function of the spin-orbit coupling strength $\omega_{\mathrm{SO}}/\Omega$ and $k\rho$ for zero magnetic flux of a (a) 3×3, (b) 4×4 and (c) 5×5 rectangular array with 3, 4, and 5 input terminals, respectively. Right panel: The conductance as a function of the spin-orbit coupling strength $\omega_{\mathrm{SO}}/\Omega$ and the magnetic flux Φ (in units of Φ_0) for $ka = 19.6$ of a (d) 3×3, (e) 4×4, and (f) 5×5 array with 3, 4,and 5 input terminals, respectively.

For small values of $\omega_{\mathrm{SO}}/\Omega$, Figs. 5.3(a)-(c) show that the width of the non-conducting regions narrow until they eventually disappear when no spin-orbit coupling is present. Here the conductance still depends on $k\rho$, but its minimal values are not zeros (similarly to the transmission probability of a single diametric ring for zero flux and zero spin-orbit coupling, shown by the dotted curve in Fig. 2.8) and a periodic behavior can be seen: for an array of $N \times N$ rings, there are N minima as the value of $k\rho$ is increased by 1. This size-dependent modulation is related to the horizontal extent of the device: If we compare the conductance of the arrays to that of rings of the same size and number without vertical connections, the same periodic behavior can be seen around zero Rashba coupling [110].

The right panel of Fig. 5.3 shows the normalized conductance of arrays of 3×3, 4×4 and 5×5 quantum rings for $k\rho = 19.6$ as a function of the spin-orbit interaction strength $\omega_{\mathrm{SO}}/\Omega$ and the magnetic flux Φ (measured in units of Φ_0). The conductuance oscillates as a function of both parameters. The oscillations as a function of the magnetic flux Φ are manifestations of the Aharonov-Bohm effect [5] (Sec. 2.1.2). The oscillations as a function of the Rashba coupling strength $\omega_{\mathrm{SO}}/\Omega$ are due to spin-dependent quantum interferences. The actual value of the transmission in a single ring is determined by the interference resulting from the interplay between the phases acquired due to the magnetic field and the Rashba spin-orbit interaction. Therefore, as $\omega_{\mathrm{SO}}/\Omega$ is increased, the spin-dependent phase changes periodically, which leads to the change in phase of the oscillations as a function of the flux. This can also be seen in the case of arrays, although the interference in consecutive rings slightly changes the periodicity of the oscillations. As the figures in the right panel of Fig. 5.3 were plotted at a fixed value of $k\rho$, the effect of the bending non-conducting stripes shown in the left panel can also be seen as the decrease of the conductance when such a stripe is reached due to the change of the spin-orbit interaction strength, and its increase again, when the stripe is left. We note that – as we have mentioned above – for larger values of $k\rho$ this bending effect is less pronounced, as $k\rho$ remains dominant over $\omega_{\mathrm{SO}}/\Omega$ in q.

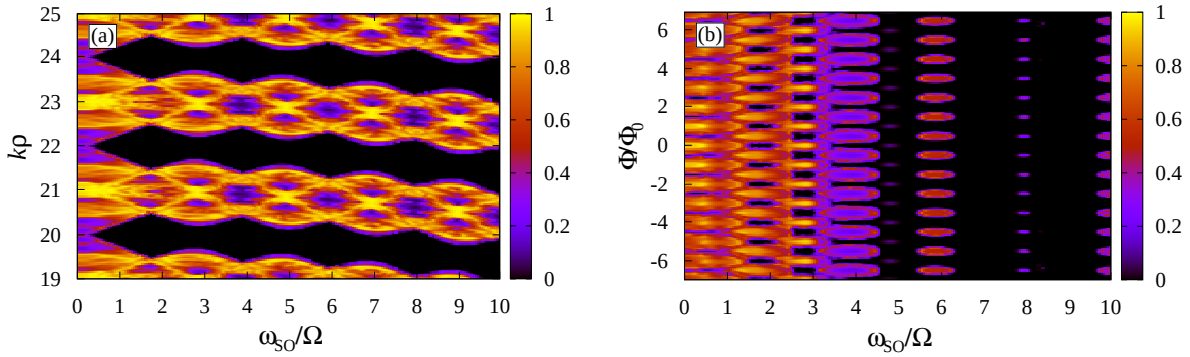

Figure 5.4: The conductance G/G_0 ($G_0 = e^2/h$) of a 5×5 rectangular array with a single input lead attached to ring {31} (a) as a function of the spin-orbit coupling strength $\omega_{\mathrm{SO}}/\Omega$ and $k\rho$ for zero magnetic flux, and (b) as a function of the spin-orbit coupling strength $\omega_{\mathrm{SO}}/\Omega$ and the magnetic flux Φ (in units of Φ_0) for $k\rho = 19.57$.

Figure 5.4 shows the conductance of a 5×5 array with a single input lead in the middle, i.e., attached to ring {31} (using the notations of Fig. 5.1) as a function of $k\rho$, and $\omega_{\rm SO}/\Omega$ (Fig. 5.4(a)), and the magnetic flux and $\omega_{\rm SO}/\Omega$ (Fig. 5.4(b)). The overall structure of these plots remains the same as in the case when the current can enter through all the rings on the left hand side, but the different boundary conditions modify their fine structure.

5.3 Spin transformational properties

Our method allows the calculation of the spin directions for the different output terminals in the arrays. By determining these spin directions we found that spin-dependent interference in the array results in nontrivial spin transformations.

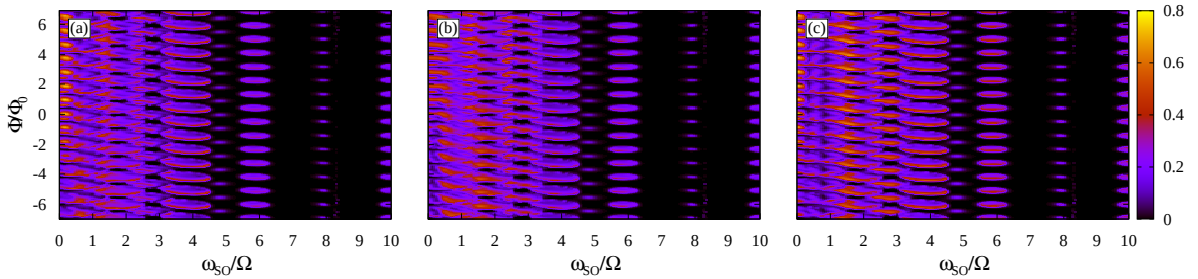

Figure 5.5: The probabilities of the (a) $|\uparrow_x\rangle$, (b) $|\uparrow_y\rangle$, and (c) $|\uparrow_z\rangle$ outputs at ring {55} of a 5×5 array with one input (attached to ring {31}), for $k\rho = 19.6$ as a function of the spin-orbit interaction strength $\omega_{\rm SO}/\Omega$ and the flux Φ (in units of Φ_0). The incoming spin state is $|\uparrow_z\rangle$.

Figure 5.5 shows the spin resolved transmission probabilities for a 5×5 ring array with a single input lead. The incoming spin state is chosen to be $|\uparrow_z\rangle$, i.e., the spin-up eigenstate of σ_z, and the contour plots show the probabilities of the $|\uparrow_x\rangle$, $|\uparrow_y\rangle$ and $|\uparrow_z\rangle$ outputs at ring {55} on the right hand side. We note that the degree of the change in the spin directions in the other output terminals is essentially the same. The fact that the $|\uparrow_z\rangle$ input spinor changes its direction – as it is seen in Figs. 5.5(a), and (b), it can be transformed into $|\uparrow_x\rangle$ or $|\uparrow_y\rangle$) – is due to the spin rotations induced by the spin-orbit interaction. The actual values of the spin resolved transmission probabilities are determined by the spin dependent interference phenomena. The overall dependence of the conductance on the magnetic flux and the Rashba coupling strength can also be seen in the probabilities of the spin directions at each output of the array.

Figure 5.6 shows the z component of the normalized output spinors and visualizes that spin resolved results depend on the input side geometry as well. As we can see, the spin components change in the whole available range between -1 and 1, and their behavior is different for the cases when the electron can enter the array through any of the five terminals, or only through the one attached to ring {31}. Figs. 5.5 and 5.6 suggest that with a given array geometry, in which the spin-orbit interaction strength $\omega_{\rm SO}/\Omega$ is tuned to an appropriate value, the spin of the incoming electron may be rotated to a certain

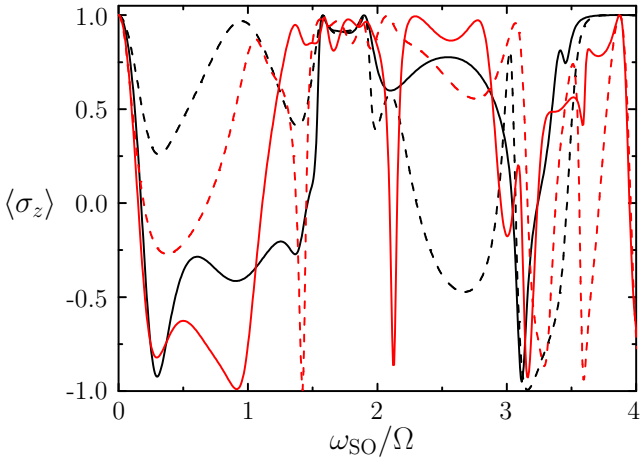

Figure 5.6: The spin transformation properties of a 5×5 array with input leads attached to all rings and only to ring {31} (black and red curves, respectively). The z component of the normalized spin states transmitted via the output terminals attached to ring {25} (solid line) and ring {45} (dashed line). The incoming spin state is chosen to be $|\uparrow_z\rangle$.

direction at a given terminal. This phenomenon together with other spin dependent interference effects [99, 100, 111–117] can lead to spin sensitive quantum networks.

We would like to mention here that beyond the case of rectangular ring arrays with a uniform magnetic field and Rashba spin-orbit coupling, further interesting set-ups can also be imagined, which could be used for a certain purpose in electron spin manipulation. A rectangular array of 3×3 quantum rings with local (ring by ring) modulation of the Rashba spin-orbit interaction strength can be used to direct the input current to any of the output ports, by tuning the spin-orbit coupling strengths in the rings with external gate voltages. This effect is spin independent: the output port is always the same, regardless of the input spin direction, while the output spin states are orthogonal for the $|\uparrow_z\rangle$ and $|\downarrow_z\rangle$ inputs. Arrays of or 5×5 rings with different spin-orbit interaction strengths can be completely analogous to the Stern-Gerlach device: if the input is one of the eigenstates of σ_z, the output will have the same spin direction at a certain output port, while the orthogonal input is directed toward a different output port, with its final direction being the same as the initial one [118]. Two-dimensional ring arrays of different geometry, composed of two- and three-terminal rings of specified spin-transformational operation (determined by the radius of the ring, the positions of the junctions, and the strength of the Rashba coupling), may also be utilized to implement the one-dimensional coined quantum walk with electrons. In this scheme, the coin is represented by the spin of the electron, while the discrete position of the walker corresponds to the label of the rings in one of the spatial directions in the array. Two-terminal rings realize the coin toss i.e., spin flip, while three-terminal rings act either as the step operator of the quantum walk or ensure the addition of probability amplitudes corresponding to stepping back to a previous position in the walk [119].

5.4 The effect of point-like scatterers

In this section we will investigate to what extent the conductance properties are modified by the presence of random scatterers. Considering such effects provides a more realistic description for most cases. To this end we introduce point-like scattering centers between the rings. Note that attaching leads to rings and different rings to each other may lead to scattering, which is why the scattering centers are chosen to be placed in the junctions. We note that the point-like scattering centers we consider may also be identified as the scatterers placed at the junctions in the model presented in Section 2.2.

At each point j where two rings touch each other, we consider an additional Dirac delta potential of the form $U_j(D) = \eta_j(D)\delta$. The strength of the potentials $\eta_j(D)$ are random, they are drawn from independent normal distributions with zero mean and root-mean-square deviation D. That is, the probability for $\eta_j(D)$ to have a value in a small interval around u is given by $p(u)du$, where

$$p(u) = \frac{1}{D\sqrt{2\pi}} e^{-\frac{u^2}{2D^2}}. \tag{5.9}$$

In this way, by tuning D we can model weak disturbances (small D) as well as the case when frequent scattering events completely change the character of the transport process (corresponding to large values of D).

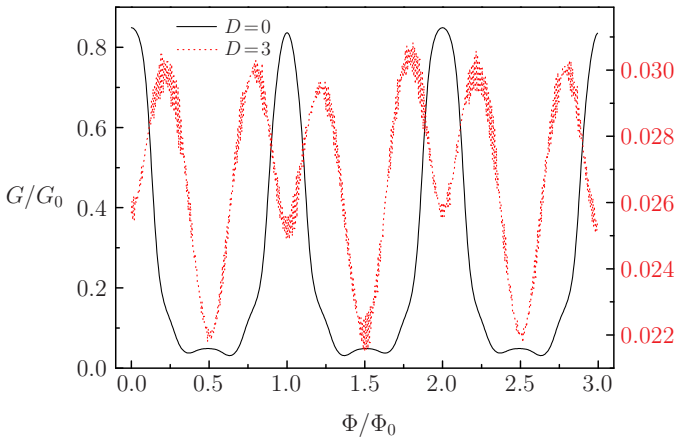

Figure 5.7: The conductance G (in units of $G_0 = e^2/h$) of a 5×5 rectangular array with and without pointlike random scatterers between the rings as a function of the magnetic flux Φ (in units of Φ_0) for $k\rho = 20.2$ and $\omega_{\mathrm{SO}}/\Omega = 13.0$.

As shown in Fig. 5.7, the most general consequence of these random scattering events is the overall decrease in the conductance. However, for strong enough disturbance, more interesting effects can be seen, namely, the splitting of the Aharonov-Bohm peaks. Note that the scattering has the most dramatic effect for the resonances, i.e., $\Phi = n\Phi_0$, and the least for the antiresonance condition, i.e., $\Phi = (n + 1/2)\Phi_0$. We would like

to mention that the model we considered (random elastic scattering processes in single-electron approximation) is similar to the case when the $h/2\,|e| = \Phi_0/2$ oscillations are expected to survive in a single ring – often referred to as the Al'tshuler-Aronov-Spivak effect [71]. Our results for a more complex geometry indicate similar physical consequences of the scattering events: introduction of new peaks in the oscillations as a function of the flux. In fact, the Fourier spectrum of the conductance shown in Fig. 5.8 clearly indicates that for strong enough disturbance, the peaks corresponding to oscillations with a period of $\Phi_0/2$ (that is, with a period that is half of that of the Aharonov-Bohm oscillations, or with a frequency that is twice as much) are stronger than the Aharonov-Bohm peaks. Let us note that phenomena related to the Al'tshuler-Aronov-Spivak effect have recently been predicted for a single ring [120] and were detected in the case of ring arrays [32].

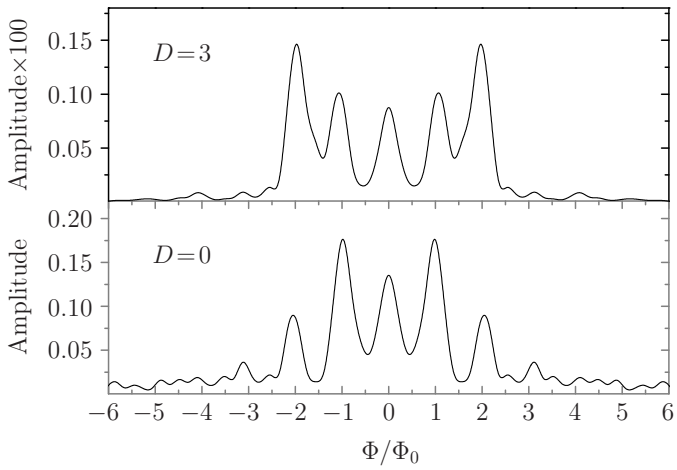

Figure 5.8: Fourier spectra of the data shown in Fig. 5.7. Notice that the relative weight of peaks corresponding to oscillations with $\Phi_0/2$ period increases when scattering effects are introduced.

Finally, we return to the stripes shown in Fig. 5.3, where the conductance is negligible. According to Sec. 5.2, destructive interference is responsible for the appearance of these stripes. Therefore we expect that when scattering events destroy phase coherence, conductance should increase. This effect can be seen in Fig. 5.9, where the conductance is plotted as a function of the spin-orbit interaction strength for different root-mean-square deviations D of the random variables. As it is shown by this figure, for most values of $\omega_{\mathrm{SO}}/\Omega$, the conductance is significantly increased in this region, although it is negligible in the exact ballistic case ($D = 0$). On the other hand, however, G is practically zero around $\omega_{\mathrm{SO}}/\Omega = 7.9$, independently from the strength of the disturbance. This effect is related to single-ring interferences: having investigated the currents and spinor valued wave functions in the array, we found that for this parameter set ($k\rho$, ω_{SO}, and Φ), the input rings ($\{11\} - \{51\}$) are essentially totally opaque for the electrons, i.e., they basically do not enter the second column of the network. Clearly, in this case scattering centers in the junctions cannot modify the transmission properties. However, this kind of effect appears only for certain special parameter sets. We found that the positions of the

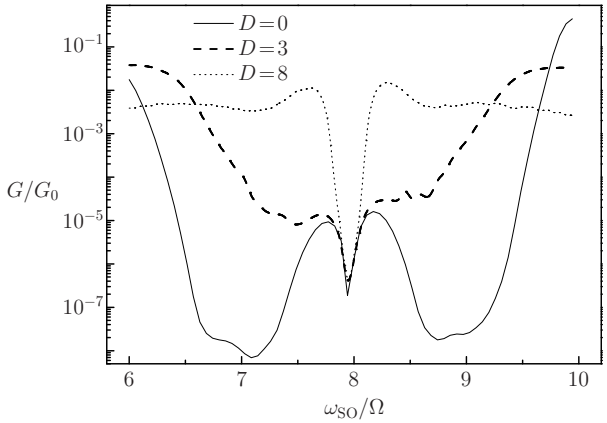

Figure 5.9: The conductance G (in units of $G_0 = e^2/h$) of a 5×5 rectangular array with pointlike random scatterers between the rings for different root-mean-square deviations D as a function of the spin-orbit interaction strength for $k\rho = 19.6$ and $\Phi = 0.3\Phi_0$.

scattering centers for a single ring are important, but in a system of two rings this effect is already remarkably weaker. The transmission properties of larger arrays are usually determined by global (i.e., involving all the rings) interferences when for strong enough disturbance the positions of the scattering centers play usually no significant role.

5.5 Conclusions

In this chapter we calculated the spin-dependent transport properties of two-dimensional rectangular quantum ring arrays. We applied general boundary conditions for the case of single quantum rings, which allowed the construction of arrays of such rings as building blocks. The magnetoconductance of two-dimensional arrays of 3×3, 4×4, and 5×5 quantum rings exhibited oscillations as a function of the magnetic flux, the spin-orbit interaction strength and the wave vector. We also determined the spin-resolved transmission probabilities of the arrays and found significant spin rotations depending on the Rashba coupling strength. We introduced point-like random scattering centers between the rings, which, for strong enough disturbance, resulted in the emergence of higher harmonics in the oscillations as a function of the flux, and led to the increase of the conductance in the regions of the parameters where the array was otherwise opaque for the electrons.

Summary

Introduction

The physics of matter on an intermediate scale between the microscopic and the macroscopic is an increasingly active area of research, which has come to be known as mesoscopic solid state physics. Advances in semiconductor technology have made possible the investigation of artificial structures of reduced dimensionality, which allow the coherent propagation of electrons, thereby leading to novel phenomena, like the quantization of the conductance in narrow wires. Mesoscopic devices are usually fabricated in a thin two-dimensional conducting layer present at the junction of semiconductor heterosrucures, such as GaAs/GaAlAs, where scattering effects may be weak enough to allow for the ballistic transport of electrons. Among these, ring shaped devices (or *quantum rings*) are intensely studied [31, 32, 64–68] due to their ability to reveal various types of quantum interference phenomena, such as the Aharonov-Bohm effect [5].

Electrons possess another inherent quantum property, namely spin. The idea of investigating, and possibly utilizing this additional feature in electronic transport led to the development of a new field of research: *spintronics* [6–9]. The commercially available spintronic devices use spin degree of freedom as a classical resource. The idea of utilizing spin as a quantum resource may be related to the birth of quantum computing [12–15], which suggested the spin of the electron as a possible candidate for the implementation of the qubit, the basic unit of quantum information. One of the resources of spintronics for spin manipluation in semiconductors is the Rashba spin-orbit interaction [22], which has a relativistic origin. This effect is due to the perpendicular electric field present in certain heterointerfaces with which moving electrons interact. Its significance lies in the fact that it can be controlled by external gate voltages [23, 24].

Numerous devices have been proposed [25–28] to utilize the Rashba effect, one of these is a quantum ring connected with two leads [29], in which the phase difference between electron waves traveling clockwise and counterclockwise produces interference effects. It has been shown that these may result in a rotation of the spin state of the electron, being variable by tuning the strength of the Rashba interaction [34].

In this dissertation we focused on quantum rings, in which – provided that transport

is ballistic and phase coherent – the wave function of the electron is able to interfere with itself. In all our calculations, we assumed that only the lowest radial subband takes part in the conduction, that is, the ring can be considered essentially one-dimensional. We used two theoretical models, one of which considers elastic scatterers in the arms of the ring and in the junctions of the leads with the ring, thereby taking into account the imperfectness of the coupling between the current-carrying leads and the ring (Sec. 2.2). The other model (Sec. 2.3) considers the ring to be free from any scatterers and is based on the solution of the time-independent Schrödinger equation and the fitting of the wave functions and the probability currents at the junctions.

Two-terminal quantum rings: Asymmetric injection

We solved the scattering problem of a ring with Aharonov-Bohm flux, in which the injection from the leads into the arms was assumed to be asymmetric [I]. We used the model introduced in Section 2.2, with an appropiate scattering matrix to couple the leads to the ring. The elements of this scattering matrix describing the transmission from the lead into the two arms of the ring were different in order to account for the asymmetry. We determined the transmission probability analitically for a ring with equal length arms, when no scatterers were present in the ring and showed that asymmetric injection increases the transmission probability as a function of the geometric phase accumulated in the arms of the ring. We also showed that the amplitude of the oscillations of the transmission as a function of the magnetic flux is reduced as a result of the asymmetry, the transmission minima shift to higher values due to incomplete destructive interference. We determined the transmission probability analitically through the ring when a scatterer was present in one arm of the ring. We showed that when the scatterer is weak, then the transmission oscillations as a function of the magnetic flux change phase as the phase introduced by the scatterer (relative to the geometric phase acquired in the other arm of the ring) changes. We also showed that asymmetry favoring the arm where the scatterer is present, leads to the increase of transmission minima. In the case of a strong scatterer, we showed that the phase resulting from the presence of the scatterer does not change the phase of the oscillations. We showed that in this case asymmery, which favors the arm in which the strong scatterer is located, leads to the decrease of the transmission probability with respect to the symmetric case.

Three-terminal quantum rings: spin polarization

We presented the solution of the scattering problem in a three-terminal ring, in which both Rashba-type spin-orbit interaction and a magnetic field is present (Sec. 4) [II,III,V].

We showed that a quantum ring with one input and two output leads in the presence of Rashba-type spin-orbit interaction can operate as an electron spin beam splitter [II]. We determined the parameter values, for both symmetric and asymmetric configuration of the leads, within the experimentally feasible range where the ring delivers perfectly polarized output beams of electrons without reflective losses. We found that appropriate spin-polarized input states are transmitted without modification, but it is also possible to prepare inputs, for which the transmission into a given lead is forbidden.

We analyzed the physical origin of the spin polarizational effect, and provided an instructive physical interpretation of the process: for both symmetric and non-symmetric geometries, polarization is due to spatial interference of oppositely directed currents [III]. At a given junction this interference is destructive for a certain spin direction, while constructive for its orthogonal counterpart, which is transmitted into the output lead as a pure state. (Sec. 4.3).

We investigated the nature of the correlation between the output electron spin and its spatial degree of freedom in a three-terminal quantum ring [IV]. We showed that in the case when perfectly polarized outputs are formed from a complete mixture, this correlation is purely classical. However, when the spin state of the input electron is pure, we found that quantum intertwining can be present between the spin direction of the electron and its output path, which is similar to entanglement, but in this case there is a single particle. By calculating the entanglement of formation of the output state we showed that for certain value of the parameters it can be close to its maximal value of unity (Sec. 4.4).

Quantum ring arrays: Conductance properties

We calculated the spin-dependent transport properties of two-dimensional rectangular quantum ring arrays (Chapter 5), that have also been investigated experimentally [32]. We applied general boundary conditions for the case of single quantum rings, which allowed the construction of arrays of such rings as building blocks [V]. The magnetoconductance of two-dimensional arrays of 3×3, 4×4, and 5×5 quantum rings exhibited oscillations as a function of the magnetic flux, the spin-orbit interaction strength, and the wave vector.

We also determined the spin-resolved transmission probabilities of the arrays and found significant spin rotations depending on the strength of the Rashba spin-orbit interaction. In order to provide a more realistic description we introduced point-like random scattering centers between the rings, which, for strong enough disturbance, resulted in the emergence of higher harmonics in the oscillations as a function of the flux, and removed conductance minima as a function of the spin-orbit coupling.

Outlook

We would like to mention that besides the results presented in this dissertation, we have been working on several further questions related to quantum rings with spin-orbit interaction. These studies include the investigation of an array of quantum rings with local (ring by ring) modulation of the Rashba spin-orbit interaction. It turned out that in this device novel effects of spin state transformation of electrons may be expected [VII]. We have proposed a scheme to implement the one-dimensional coined quantum walk with electrons transported through a two-dimensional network of quantum rings [VIII]. We have also addressed the question: to what extent the ideal behavior and functionality of the above mentioned network-based devices are modified by random (spin-dependent) scattering events or finite temperatures [IX]. In a related work a quantum ring with periodically changing spin-orbit interaction strength has also been investigated [X].

Összefoglalás
(Summary in Hungarian)

Ebben a fejezetben a "*Kvantuminterferencia félvezető gyűrűkben*" című doktori disszertációm részletes magyar nyelvű összefoglalása található, amely az angol nyelvű összefoglalásnál jóval bővebben tekinti át a dolgozatban vizsgált kérdéseket és a kapott eredményeket. A fejezet pontjai a disszertáció fejezeteit követik.

Bevezetés

A mindennapi életben használt elektronikai eszközök nagy részében az elektromos áramot elektronok szállítják. Az elektronok azonban, ahogyan azt az elektroninterferenciás kísérletekből tudjuk, nem csak részecske-, hanem hullám természetűek is egyben. Ez a tulajdonság a szokásos vezetékekben, melyek mérete jóval meghaladja az elektronokhoz rendelhető hullámhosszat, nem játszik szerepet. Ha azonban a vezeték vastagsága és hosszúsága összemérhető az említett hullámhosszal, akkor az elektronok koherens terjedése megfigyelhetővé válik. A fizikának azt a területét, amely az ilyen típusú vezetőket vizsgálja, melyek elegendően kicsik ahhoz, hogy rajtuk az elektronok koherensen haladhassanak át, ugyanakkor még elegendően sok számú atomból állnak, *mezoszkópikus sziládtestfizikának* nevezzük. Ebben a mérettartományban egy vezető drót vezetőképessége a kísérletek tanúsága szerint az anyagtól független, univerzális állandók által meghatározott egységekben kvantált, ezért nem írható le a klasszikus fizika törvényeivel. Az ilyen típusú vezetők működése nagyon hasonlít a mikrohullámú technikában használatos hullámvezetők működéséhez, ezért – az angol terminológiában – gyakran nevezik őket elektron-hullámvezetőknek. Mi a továbbiakban ehelyett a szintén használatos "kvantumdrót" kifejezést részesítjük előnyben.

Mezoszkópikus eszközök alapjaként leggyakrabban félvezető heterostruktúrákban (például GaAS/GaAlAs, InGaAs/InAlAs), a különböző félvezető rétegek határfelületén található vékony, kétdimenziós vezető réteg szolgál. Ebben gyakran hoznak létre gyűrű alakú kvantumdrótot (úgynevezett *kvantumgyűrűt*), mely geometriája révén lehetővé teszi, hogy a rajta áthaladó elektron hullámfüggvénye önmagával interferálhasson, majd mérik az

eszköz vezetőképességét a gyűrű síkjára merőleges mágneses tér függvényében. Az ebben az elrendezésben mért vezetőképesség úgynevezett Aharonov-Bohm oszcillációkat mutat, habár a mágneses tér a kísérletekben a gyűrűben is jelen van, szemben a szigorú értelemben vett Aharonov-Bohm effektussal, ahol a tér csak a körbejárt tartomány belsejében van jelen és nulla az elektron pályája mentén.

Az elektron a hullámtermészetén kívül egy másik kvantumos tulajdonsággal is rendelkezik, nevezetesen spinnel. Az elektronspin transzportfolyamatokban játszott szerepének vizsgálatával a spin elektronika (vagy röviden *spintronika* [6–9]) foglalkozik. Számos olyan spintronikai eszköz létezik, amely az elektron spinjét klasszikus erőforrásként hasznosítja, ilyenek például az ,,óriás mágneses ellenállás" jelenségén [10, 11] alapuló ,,spinszelep", amely a merevlemezekben használatos. Azokat a spintronikai kutatásokat, melyek az elektron spinjét, mint kvantumos erőforrást kívánják hasznosítani, talán leginkább a kvantuminformatika motiválta, mely lehetőséget kínál olyan problémák megoldására, amelyek klasszikus számítógéppel nem oldhatóak meg hatékonyan. Itt az információ alapegysége a klasszikus logikai bit kvantumos analógja, egy kétállapotú kvantumrendszer, az úgynevezett qubit valamely állapota. Mivel az elektron spinje is egy kétállapotú kvantumrendszer, ezért alkalmas arra, hogy kvantuminformatikai alkalmazásokban a qubit szerepét betöltse.

A félvezető spintronika egyik legfőbb ,,erőforrása" az a spin-pálya kölcsönhatás, amely bizonyos félvezető heterostruktúrákban azok felépítése révén eredendően jelen van és amelynek erőssége a félvezetőre kapcsolt úgynevezett ,,kapu" elektródákkal (az elnevezés az elektronikában használatos angol ,,gate" kifejezésre utal) hangolható [23]. Több olyan javaslat is született, amely ezt az úgynevezett Rashba-féle spin-pálya kölcsönhatást [22] igyekszik kiaknázni, az elsők között volt például a Datta és Das által felvetett spin tranzisztor [25], illetve Nitta és munkatársai javaslata [29], mely ezt a kölcsönhatást a fentebb említett kvantuminterferenciával együttesen egy kvantumgyűrűben kívánja felhasználni az elektron spinjének forgatására. Ezen utóbbiról később Földi, Molnár, Benedict és Peeters [34] meg is mutatták, hogy elviekben valóban lehetséges az elektron spinjének célzott elforgatása egy kvantumgyűrűvel, amelynél a be- és kimenő drótok helyzete egymáshoz képest változtatható. Arra is rávilágítottak, hogy a külső kapufeszültség, a drótok helyzete, valamint a gyűrű átmérője változtatásával a kvantuminformatikában alapvető forgatások megvalósíthatók.

A dolgozatban bemutatott saját kutatási eredmények létrejöttét a – fentebb felvázolt – kvantumgyűrűk iránti intenzív kísérleti és elméleti érdeklődés motiválta. Kutatásaink során célul tűztük ki olyan kvantumgyűrűk leírását, amelyek esetében az elektron eltérő valószínűséggel juthat a gyűrű két karjába. A spintronikai alkalmazási lehetőségekhez kapcsolódóan meg kívántuk vizsgálni, hogy lehetséges-e az elektron spinjét polarizálni egy olyan kvantumgyűrűvel, amelyben Rashba-féle spin-páya kölcsönhatás van jelen. Célunk volt az is, hogy ilyen típusú gyűrűkből (amelyekben mágneses tér és/vagy spin-pálya

kölcsönhatás van jelen) felépülő rácsok vezetőképességét kiszámítsuk.

A dolgozat első részében, amely az első és második fejezetet foglalja magában, bemutattuk a mezoszkópikus rendszerekben lejátszódó transzport alapvető jellemzőit és a kvantumgyűrűk leírására használatos elméleti modelleket. Ezek összefoglalását tartalmazza az alábbi 1. és 2. pont. A saját kutatási eredményeinket [I-V] a dolgozat második részében részleteztük, ezeket ismertetjük röviden itt a magyar nyelvű összefoglaló 3., 4. és 5. pontjaiban. Emellett azóta is intenzíven kutatjuk a kvantumgyűrűkben Rashba-féle spin-pálya kölcsönhatás jelenlétében lejátszódó jelenségeket és azok érdekes spintronikai felhasználási lehetőségeit [VII-IX].

1. Transzport mezoszkópikus rendszerekben

Az utóbbi évek technológiai fejlődésének köszönhetően megnőtt az érdeklődés az úgynevezett alacsony dimenziós struktúrák felhasználása iránt. Az elnevezés onnan ered, hogy az ilyen eszközökben a vezetésben részt vevő elektronok mozgását potenciálgátak korlátozzák, úgy, hogy azok kettő-, egy-, illetőleg zéró dimenzióban képesek csak szabadon mozogni. Ilyen rendszerek létrehozására főként félvezetők megfelelően egymásra rétegezett heterostruktúrái szolgálnak. Ha például GaAs és GaAlAs (vagy InGaAs és InAlAs) rétegeket illesztünk össze, a határfelületnél potenciálvölgy alakul ki. Itt a Fermi-nívó ,,belelóg" a vezetési sávba, így a környezethez képest erősen megnő az elektronsűrűség. A potenciálvölgy következtében az elektronok mozgása a felületre merőleges irányban kvantálttá válik. Mivel energetikai okokból ezen módusok közül általában csak egy vesz részt a vezetésben ezért ebben az irányban az elektronok lényegében nem, a határfelület mentén azonban szabadon mozoghatnak a mintában. Így a heteroszerkezet határán egy úgynevezett kétdimenziós elektrongáz alakul ki [1]. Az elektronok szabadsági fokainak száma tovább csökkenthető mesterséges potenciálgátaknak például maratással [32, 67], pásztázó atomerő-mikroszkóppal [68], vagy pedig litográfiai eljárásokkal [31] történő kialakításával. Létrehozhatók például keskeny vezető sávok, úgynevezett kvantumdrótok, melyekben a drót hosszanti irányára merőleges, keresztirányú mozgás ismét kvantált. Amennyiben elérhető az, hogy ezek közül a "transzverzális" módusok közül csak egy vegyen részt a vezetésben, akkor egydimenziós kvantumdrótról beszélünk.

Az alacsony dimenziós rendszerek fontos jellemzői az elektronsűrűség és a mozgékonyság. Ezeket rendszerint Hall-méréssel határozzák meg, amely során a minta hosszanti tengelye mentén áramot hoznak létre, majd mérik annak longitudinális, illetve transzverzális (Hall) ellenállását egy külső merőleges mágneses tér változtatása mellett. A mozgékonyságból következtetni lehet az elektronok impulzus relaxációs idejére, azaz arra, hogy az elektronok átlagosan mennyi idő alatt veszítik el az impulzusukat az elszenvedett rugalmatlan ütközések következtében. A mozgékonyság a hőmérséklet csökkenésével

nő, ami a rácsrezgések szerepének a gyengülésével magyarázható. Elegendően alacsony hőmérsékleten már lényegében csak a szennyezések csökkentik a mozgékonyság értékét. Mivel alacsony hőmérsékleten csak azok az elektronok vesznek részt a vezetésben, amelyek energiája közel esik a Fermi-nívóhoz, az elektronsűrűség ismeretében a Fermi-nívóhoz tartozó Fermi-hullámszám értéke meghatározható [1].

A relaxációs idő és a Fermi-hullámszám ismerete további felvilágosítást ad az elektronok átlagos szabad úthosszára vonatkozóan a mintában. Félvezető heterostruktúrákban, ahol a mozgékonyság jóval nagyobb, mint "bulk", azaz nagy térfogatú szennyezett félvezetőkben, a szabad úthossz alacsony hőmérsékleten tipikusan $100 - 1000$ nm. Egy másik fontos fogalom a fáziskoherencia-hossz, amely azt jellemzi, hogy az elektron, mint hullám, mekkora távolságon képes megőrizni az önmagával való interferencia-képességét a mintában történő ütközések ellenére. Nagy mozgékonyságú minták esetén ez általában megegyezik a szabad úthosszal. (Megjegyezzük, hogy hosszabb lehet azonban az úgynevezett spinkoherencia-hossz, melynek értéke elérheti a 100 μm-t is [19].) Amennyiben a vizsgált eszköz mérete összemérhető a fáziskoherencia-hosszal, akkor interferencia-jelenségek megjelenése várható.

Véges méretű ballisztikus (azaz szórásmentes) vezetők vezetőképessége a kísérletek tanúsága szerint a vezető hosszának csökkenésével egy véges értékhez tart [1]. Ez alapvetően annak a következménye, hogy a vezetésben véges számú transzverzális módus vesz részt. Arra az esetre, amikor magában a ballisztikus vezetőben is jelen vannak szórócentrumok, vagy pusztán a vezető geometriája révén szóródhatnak rajta az elektronok, Landauer vezetett be egy formulát (dolgozatunkban az (1.41) képlet), amely szerint a vezetőképesség arányos a vezetésben részt vevő módusok számával és a vezetőn való átjutás kvantummechanikai valószínűségével [46].

Bizonyos félvezető anyagokban fontos szerepet játszik egy relativisztikus effektus, a spin-pálya kölcsönhatás, amely összekapcsolja az elektronok térbeli mozgását a spin irányának változásával. Ez a kölcsönhatás heterostruktúrákban többféle eredetű lehet, a leggyakrabban vizsgált fajtája, az úgynevezett *Rashba-féle spin-pálya csatolás* [22, 55] amely a rétegezés irányában létrejött – az elektronokat mozgásukban korlátozó – potenciálvölgy aszimmetriájának következménye. Az aszimmetrikus potenciál ugyanis egy a határfelületre merőleges elektromos teret kelt, amely kölcsönhat az ott mozgó elektronok spinjével. A Rashba-csatolás különlegessége, hogy a kölcsönhatás erőssége külső kapufeszültség(ek)kel hangolható [23, 24], amely nagyon vonzóvá teszi felhasználását spintronikai eszközökben [6].

2. Kvantumgyűrűk modelljei

Az előzőekben bemutatott félvezető heterostruktúrák határrétegében gyakran hoznak létre gyűrű alakú kvantumdrótokat, úgynevezett *kvantumgyűrűket*, [31, 32, 64–66] melyek mérete összemérhető az elektronok fáziskoherencia-hosszával. Az ilyen kvantumgyűrűkkel lehetőség nyílik különféle interferencia-jelenségek megfigyelésére.

Az egyik gyakran vizsgált jelenség, amikor a gyűrű síkjára merőleges mágneses tér változtatása mellett mérik az eszköz vezetőképességét. A jelentkező oszcillációk a gyűrű által körbevett térrészen áthaladó mágneses fluxus függvényében periodikusak. Ez tulajdonképpen az Aharonov-Bohm effektus [5, 69] következménye, de mint említettük, a félvezető gyűrűkkel végzett kísérletek esetén a mágneses mező a vezetékekben is jelen van, ami az Aharonov és Bohm által megjósolt oszcillációktól való eltérésekhez vezethet.

Ha egy kvantumgyűrűben Rashba-féle spin-pálya kölcsönhatás van jelen, akkor az interferencia a spin-pálya csatolás erősségétől függ [29]. Ez annak a következménye, hogy a gyűrűben mozgó elektron a saját vonatkoztatási rendszerében a határfelületre merőleges elektromos mező mellett mágneses mezőt is ,,lát", ez okozza a spin-pálya kölcsönhatást. A mágneses mezőben az elektronspin precessziót végez, amelynek mértéke arányos a spin-pálya csatolás erősségével. Mivel az elektron által érzékelt mágneses tér iránya merőleges mind a sebességének, mind pedig az elektromos térnek az irányára, ezért az a gyűrű minden egyes pontjában más és más, következésképpen az elektron spinjének elfordulása a gyűrű két ágában különböző lesz (lásd 2.3 ábra). A Rashba-kölcsönhatás erősségét külső kapufeszültséggel változtatva a vezetőképesség a fellépő interferencia miatt oszcillációt mutat [92].

A kvantumgyűrűkben fellépő interferencia-jelenségek elméleti leírása során a gyűrűt gyakran egydimenziósnak tekintik. Ez az egyszerűsítés megtehető amennyiben a gyűrűben valóban egyetlen radiális módus vesz csak részt a vezetésben. Ez a feltétel a kísérletileg vizsgált kvantumgyűrűk egy részénél teljesül. A dolgozatban két ilyen ,,egydimenziós" modellt mutattunk be, amelyek alkalmasak a kvantumgyűrűn való áthaladás valószínűségének – így a Landauer-formula értelmében a gyűrű vezetőképességének – kiszámítására. Az első modell a a mágneses fluxust körülölelő gyűrű karjaiban és a drótokkal való csatlakozási pontjaiban rugalmas szórópotenciálokat tételez fel [62], melyekkel az elektront a gyűrűbe bevezető, illetve onnan kivezető drót és a gyűrű közti csatolás nemidális voltát képes figyelembe venni. Saját kutatásaink során ezt az általános modellt módosítottuk annak érdekében, hogy figyelembe vegyük a gyűrű két karja közti aszimmetria lehetőségét [93].

A másik modell némileg egyszerűbb az elsőnél és spinfüggő terjedés esetére is alkalmazható. A gyűrűn mozgó elektron Hamilton-operátorának sajátérték-egyenletét megoldva a sajátállapotok szuperpozíójaként írjuk fel a gyűrűbeli hullámfüggvényt úgy, hogy nem tételezünk fel szórópotenciált a gyűrűben – bár megjegyezzük, hogy a modell általánosít-

ható arra az esetre is. A be- és kivezető drótokat úgy kapcsoljuk a gyűrűhöz unitér módon, hogy a hullámfüggvényeket illesztjük a csatlakozási pontokban, az áramokra pedig egy a klasszikus Kirchhoff-törvénnyel analóg feltételt írunk elő: a csatlakozási pontokban a valószínűségi áramsűrűségek eredője zérus legyen. Spinfüggő interferencia esetében annak a Hamilton-operátornak a sajátérték-problémáját kell megoldanunk, mely a Rashba-féle spin-pálya kölcsönhatási tagot is tartalmazza. Itt lényeges, hogy a gyűrű Hamilton-operátorának minden energiasajátértéke négyszeresen elfajult. Az áramokra vonatkozó feltételeket ebben az esetben a valószínűségi spin-áramsűrűségekkel kell felírnunk [89, 92]. A megoldást az egy bemenettel és egy kimenettel rendelkező gyűrű esetén be is mutattuk. Láthattuk, hogy alkalmasan megválasztva a spin-pálya csatolás erősségét, a bemenet és kimenet egymáshoz viszonyított helyzetét, valamint a gyűrű sugarát, különféle spin-forgatások valósíthatók meg [34].

3. Aszimmetrikus injektálás

A kísérletekben vizsgált kvantumgyűrűk esetében az elektront a gyűrűhöz és abból kivezető drótok kapcsolata a gyűrűvel nem tökéletesen ideális. A drótok és a gyűrű csatlakozási pontjaiban reflexió léphet fel, illetőleg nem feltétlenül igaz, hogy a gyűrű karjaiba az elektron azonos valószínűséggel juthat be. Ez a fajta aszimmetria több okból is felléphet. Egyrészt lehet a következménye annak, hogy a gyűrű és a drótok kialakítása nem tökéletes, de amiatt is jelentkezhet, hogy az alkalmazott mágneses tér hatására fellépő Lorentz-erő a gyűrű véges vastagsága révén azt eredményezi, hogy a két karba eltérő valószínűséggel jut be (injektálódik) az elektron [35, 94].

Ebben a fejezetben az aszimmetrikus injektálást egy egydimenziós modell segítségével írtuk le, melyet a rugalmas szórópotenciálokat tartalmazó modell megfelelő általánosításaként kaptunk [I]. A gyűrű két karjába jutás valószínűségei közti különbséget úgy vettük figyelembe, hogy a vezető drótok és a gyűrű csatlakozási pontjában a be- és kimenő amplitúdók közti kapcsolatot leíró unitér mátrixban a két karra vonatkozó elemek között egy arányossági tényezőt vezettünk be. A bemenő drót és a gyűrű közti illesztést egy másik paraméterrel vettük figyelembe. Az így kapott mátrixról megmutattuk, hogy határesetben visszaadja a szimmetrikus injektálást leíró, korábban bemutatott mátrixot.

Az említett mátrix felhasználásával analitikusan kiszámítottuk egy olyan két dróttal rendelkező kvantumgyűrűn való áthaladás valószínűségét, amely által körbevett térrészen mágneses fluxus halad át és amelynek karjai egyenlő hosszúságúak [I]. Két esetet vizsgáltunk: amikor nincsenek jelen szórócentrumok a gyűrűben és amikor az egyik karban szórócentrum található. Megmutattuk, hogy ha nincs jelen szórócentrum a gyűrűben, akkor a transzmissziós valószínűség mágneses fluxus függvényében jelentkező oszcillációinak amplitúdója a gyűrű két karja közti aszimmetria hatására csökken, és a minimumai

magasabbra tolódnak (3.2(b) ábra), mivel ekkor nem teljes a destruktív interferencia. Megvizsgáltuk a gyűrű és a drótok közti csatolás csökkentésének hatását abban az esetben, amikor az elektron a gyűrű két karjába aszimmetrikusan injektálódik. Megmutattuk, hogy a transzmissziós valószínűség a geometriai fázis függvényében lecsökken, kivéve néhány esetet, amelyekre a gyűrű továbbra is teljesen átlátszó marad az elektronok számára (3.3(a) ábra). A geometriai fázis egyéb értékei esetén a csatolás romlásával a transzmisziós valószínűség a mágneses fluxus függvényében lecsökken, csakúgy, mint az oszcillációk amplitúdója (3.3(b) ábra). Megvizsgáltuk, hogy mi tapasztalható a transzmissziós valószínűság mágneses fluxus függvényében jelentkező oszcillációiban, ha a gyűrű aszimmetria által kitüntetett karjában szórócentrum található, amely csak bizonyos valószínűséggel engedi át az elektront és a másik karban szerzett geometriai fázishoz képest egy további fázistolást eredményez. Megmutattuk, hogy amennyiben a szórócentrum gyenge (azaz nagy valószínűséggel átengedi az elektront), az oszcillációk fázisa eltolódik, amplitúdójuk megváltozik a szórócentrum által bevezetett fázis változtatásával, az aszimmetria hatására pedig a transzmissziós minimumok magasabbra tolódnak (3.4 ábra). Azt is megmutattuk, hogy ha az aszimmetria által preferált karban erős (azaz az elektront kicsiny valószínűséggel átengedő) szórócentrum van jelen, akkor a transzmisszió oszcillációinak fázisa nem érzékeny a szórócentrum által okozott fázistolás változtatására. A gyűrű karjai közti aszimmetria ekkor – a szimmetrikus esethez képest – a transzmissziós valószínűség lecsökkenését eredményezi.

4. Kvantumgyűrű három dróttal

4.1. A feladathoz tartozó szórásprobléma megoldása

A spintronikai alkalmazási lehetőségekhez kapcsolódóan kiszámítottuk egy olyan kvantumgyűrűn való átjutás valószínűségét, amelyben Rashba-féle spin-pálya kölcsönhatás – és a későbbi, 5. fejezet témájának megalapozása érdekében mágneses tér is – jelen van és amelyhez három kvantumdrót kapcsolódik [II,III,V]. Feltettük, hogy a mágneses tér elegendően gyenge, és hatását perturbációként vettük figyelembe. A megoldást a legáltalánosabb határfeltétel esetére – miszerint minden kvantumdróton megengedett bemenő és kimenő (spinfüggő) hullám is – a 2.3. fejezetben bemutatott egyszerű egydimenziós modell segítségével végeztük el. Megmutattuk, hogy egy adott drótban a kimenet meghatározásához a gyűrű szimmetriája révén elegendő annak a problémának a megoldása, amikor a drótok közül az egyik csak bemenetként a másik kettő pedig csak kimenetként szolgál. Minden bemenet hozzájárul ugyanis minden kimenet létrejöttéhez egymástól függetlenül. Ha ismerjük egy adott bemenetre a visszavert állapotot meghatározó reflexiós mátrixot, illetőleg a két kimenetet meghatározó transzmissziós mátrixokat, akkor a többi bemenetre vonatkozó reflexiós és transzmissziós mátrix is meghatározható

olyan módon, hogy az ismert mátrixokban a drótok közti szögeket a megfelelő módon kicseréljük. Ahhoz, hogy az így nyert mátrixok mind ugyanabban a bázisban legyenek felírva, mint az ismert probléma mátrixai, még a megfelelő hasonlósági transzformációkat (az ismert probléma bemenő drótjától mért szöggel való forgatásokat) el kell végeznünk.

4.2. A háromdrótos kvantumgyűrű mint spin-polarizáló eszköz

A fentiekben ismertetett kvantumgyűrű esetén részletesebben is megvizsgáltuk azt az esetet, amikor a gyűrűbe az elektron csak egy dróton keresztül juthat, de két drót áll rendelkezére a távozásra. Megmutattuk, hogy ha a bejövő elektron spin-állapota maximálisan kevert, akkor ahhoz, hogy a két kimeneten tiszta állapot jöjjön létre, a megfelelő transzmissziós mátrixok determinánsa ell kell tűnjék [II]. Amint azt a 4.2 fejezetben részleteztük, ez két esetben is elérhető. Mindkét esetben több feltétel együttes teljesülését kell elérnünk a drótok egymáshoz viszonyított helyzetére, a spin-pálya kölcsönhatás erősségére, és a gyűrű sugarára vonatkozóan. Megmutattuk, hogy az említett feltételek egyszerre történő teljesítése lehetséges (4.2 ábra) mind szimmetrikus, mind aszimmetrikus helyzetű kimenő drótok esetén, vagyis a gyűrű alkalmas az elektron spinjének polarizálására. Megvizsgálva egy ilyen polarizáló gyűrű kimenetein a transzmissziós valószínűségeket azt találtuk, hogy azok a két kimeneten megegyeznek és elérhető az is, hogy értékük maximális legyen, vagyis a gyűrűn ne keletkezzék reflexiós veszteség. A polarizáció mindkét esetében meghatároztuk a kimeneten lévő spin-állapotokat és azt találtuk, hogy azok megegyeznek a gyűrű ezen pontjaihoz tartozó két sajátspinor egyikével úgy, hogy az egyik kimeneten az egyik, a másikon a másik jelenik meg (a két esetben felcserélve). Megmutatható, hogy vannak olyan spinirányok, melyek bemenete esetén az egyik kimenetre biztosan nem kerül az elektron. Mindezek alapján elmondhatjuk, hogy egy ilyen gyűrű nagyon hasonlóan viselkedik, mint a Stern-Gerlach berendezés, ugyanis polarizálatlan bemenetből polarizált spinállapotokat hoz létre a kimeneteken.

4.3. A spin-polarizáció fizikai háttere

Ebben a fejezetben a spin-polarizációs effektus fizikai hátterét tártuk fel [III]. A maximálisan spin-polarizálatlan bemenő állapotot a bemenő drót helyéhez tartozó gyűrűbeli sajátspinorokkal felírva meghatároztuk a gyűrűben létrejövő állapotot, amely a gyűrűben is a megfelelő sajátspinorú hullámok (minden sajátspinorhoz tartozik két ellentétes irányú áramot eredményező hullám) keveréke. Mivel az előző fejezetben láttuk, hogy a polarizációs feltételek teljesülése esetén az egyik kimeneten az egyik, a másik kimeneten a másik típusú sajátspinor jelenik meg, megvizsgáltuk, hogy mikor lesz az adott sajátspinorú állapotok megtalálási valószínűsége zérus a kimeneteken, mivel ezekben az esetekben várható, hogy a gyűrűbeli kevert állapot tiszta (azaz projektor) legyen. Azt találtuk,

hogy egy adott sajátspinorú állapot egy adott kimeneten való eltűnését ugyanazok a polarizációs feltételek írják le, mint amelyeket az előző fejezetben – más gondolatmenet alapján – írtunk fel. Mindezek alaján könnyen érthetővé válik, hogy a polarizációs effektus azért jön létre, mert az azonos sajátspinorú, de ellentétes keringési iránynak megfelelő hullámok egymással destruktívan interferálnak a kimeneteken (az egyik kimeneten az egyik típusú, a másik kimeneten a másik típusú sajátspinorra történik ez meg).

Abban az esetben, ha a bejövő maximálisan kevert spin-állapotot a z irányban $|\uparrow\rangle$ és $|\downarrow\rangle$ állapotok keverékeként írjuk fel, a polarizációs effektus a 4.5 ábra alapján érthető meg a legkönnyebben: a gyűrű minden egyes pontjában külön-külön felrajzolva a $|\uparrow\rangle$ és $|\uparrow\rangle$ bemenetek esetén létrejövő spinirányokat látható, hogy a kimeneteken azért jönnek létre a polarizált állapotok, mert a kétfajta bemenet a kimenetekre érve ugyanabba az irányba fordul.

4.4. A térbeli- és spin szabadsági fokok összefonódása

Ebben a fejezetben azt vizsgáltuk meg, hogy egy egy bemenettel és két kimenettel rendelkező gyűrűben a kimenet, mint egyik szabadsági fok és a kimenő spin, mint másik szabadsági fok közötti korrelációk milyen típusúak lehetnek [IV]. A kérdést a speciális spin-polarizáló esetben és általában is elemeztük. Ahhoz, hogy az említett korrelációkat megvizsgálhassuk, a kimeneteket ,,globálisan" kell tekintenünk, azaz abban a Hilbert-térben kell dolgoznunk, amely a lehetséges kimenetek, mint térbeli bázis és valamilyen spin-bázis, például a z irányú $|\uparrow\rangle$ és $|\downarrow\rangle$ állapotok által kifeszített Hilbert-terek tenzori szorzataként áll elő.

Megmutattuk, hogy abban az esetben, amikor a gyűrű polarizál a két szabadsági fok között a korreláció kizárólag klasszikus: a bemenő maximálisan kevert állapot a kimeneteken ugyan külön-külön tiszta állapotokat eredményez, globálisan mégis maximálisan kevert az elektron állapota a kimeneten. Akkor azonban, ha a bemenő elektron spinje tiszta állapotú azt találtuk, hogy a globális kimenő állapotban lehet összefonódás (azaz kvantumos korreláció) a kétféle szabadsági fok között. Megmutattuk, hogy bizonyos bemenetek esetén az összefonódás maximális is lehet.

5. Kvantumgyűrűk rácsai

Ebben a fejezetben kvantumgyűrűkből képzett négyzetes rácsok vezetőképességét határoztuk meg, melyekről feltettük, hogy bennük Rashba-féle spin-pálya kölcsönhatás és a gyűrűk síkjára megőleges mágneses tér is jelen van [V]. Olyan, egymással érintkező gyűrűkből álló 3×3-as, 4×4-es és 5×5-ös rácsokat vizsgáltunk, melyek a függőleges irányban zártak, a vízszintes irányban viszont lehetővé teszik az elektronok terjedését, ahogyan azt az 5.1 ábra is mutatja. Ilyen típusú rácsokat kísérletileg is előállítottak [32].

Bemutattunk egy olyan módszert, amelynek a segítségével az egyes gyűrűkkel kapcsolatos problémák megoldásának ismeretében a rácson való átjutás valószínűsége kiszámítható. Mivel a rácsot olyan gyűrűk építik fel, melyek két, három, illetve négy másik gyűrűvel érintkeznek, a kettő, illetve négy dróttal rendelkező gyűrűk problémáinak megoldását is felvázoltuk (a háromdrótos gyűrű problémáját már a 4.1. fejezetben megoldottuk). A gyűrűk érintkezési ponjaiban ezután előírtuk a hullámfüggvények, valamint deriváltjaik folytonosságát. Az így kapott (nagyszámú egyenletből álló) egyenletrendszer numerikus megoldásával meghatároztuk a rács kimenetein fellépő spin-állapotokat, amelyekből azután a Landauer-formula segítségével kiszámítottuk a rács vezetőképességét.

A vezetőképességet a mágneses tér, a Rashba-csatolás erőssége és az elektron hullámszámából, valamint a gyűrű sugarából képzett $k\rho$ paraméter függvényében ábrázolva megmutattuk, hogy a különféle méretű rácsok vezetőképessége mindhárom paraméter függvényében oszcillációkat mutat. A $k\rho$ paraméter bizonyos értékeire a rács teljesen átlátszatlan az elektronok számára (5.3 ábra). Ez az effektus a rácsot alkotó gyűrűk szintjén lejátszódó többszörös destruktív interferencia hatására következik be. A spin-pálya kölcsönhatás nélküli esetben a nemvezető sávok eltűnnek, a vezetőképességben jelentkező oszcillációk periódusát a gyűrűk száma határozza meg. Az említett nemvezető sávok a vezetőképességben a mágneses tér és a spin-pálya kölcsönhatás erőssége függvényében is megjelentek (5.3 ábra). Megvizsgáltuk az egy bemenettel rendelkező ugyanolyan méretű rácsok vezetőképességét is, ahol lényegében ugyanazok az effektusok lépnek fel, mint a több bemenetű rácsok esetén (5.4 ábra).

A vezetőképesség kiszámítására használt módszerünk azt is lehetővé tette, hogy a rácsok egyes kimenetein kialakuló spinirányokat is megvizsgáljuk az alkalmazott mágneses tér és spin-pálya erősség függvényében. Megmutattuk, hogy a bemenő spinállapot a különböző kimenetekre érve különböző módon fordul el és a megvalósítható spin-forgatások széles tartományban mozognak (5.5 és 5.6 ábra).

A realisztikusabb leírás érdekében kiszámítottuk a rácsok vezetőképességét abban az esetben is, amikor a gyűrűk között pontszerű szórócentrumok lehetnek jelen, melyek erősségét egy adott szórással rendelkező normális eloszlás határozza meg. Megmutattuk, hogy a szórócentrumok legfőbb hatása, hogy jelenlétükben a vezetőképesség átlagosan lecsökken (5.7 ábra). A másik fontos hatásuk, hogy a mágneses tér függvényében az Aharonov-Bohm (AB) oszcillációk első felharmonikusai (az úgynevezett Al'tshuler-Aronov-Spivak rezgések) felerősödnek (5.8 ábra). Azt is megmutattuk, hogy a szórócentrumok hatásának következtében, az egyébként nem vezető tartományokban a vezetőképesség megnőhet a szóródások következtében (5.9). Ez azért lehetséges, mert a szórócentrumok képesek elrontani a destruktív interferenciához szükséges fáziskoherenciát. Bizonyos paraméterek esetén azonban a szórócentrumok hatására sem növekszik meg a vezetőképesség. Ezekről az esetekről megmutattuk, hogy ilyenkor már a bejövő oldalon lévő első gyűrűk teljesen reflektálják az elektront.

List of publications

Related publications

[I] P. Vasilopoulos, **O. Kálmán**, F. M. Peeters, and M. G. Benedict: *Aharonov-Bohm oscillations in a mesoscopic ring with asymmetric arm-dependent injection*, Phys. Rev. B **75**, 035304 (2007).

[II] P. Földi, **O. Kálmán**, M. G. Benedict, and F. M. Peeters: *Quantum rings as electron spin beam splitters*, Phys. Rev. B **73**, 155325 (2006).

[III] **O. Kálmán**, P. Földi, M. G. Benedict, and F. M. Peeters: *Spatial interference induced spin polarization in a three-terminal quantum ring*, Physica E **40**, 567 (2008).

[IV] **O. Kálmán**, P. Földi, and M. G. Benedict: *Quantum and classical correlations of spatial and spin degrees of freedom in quantum rings*, Open Syst. Inf. Dyn. **13**, 455 (2006).

[V] **O. Kálmán**, P. Földi, M. G. Benedict, and F. M. Peeters: *Magnetoconductance of rectangular arrays of quantum rings*, Phys. Rev. B **78**, 125306 (2008).

Other publications

[VI] **O. Kálmán**, and M. G. Benedict: *Quantum gates and protocols with spherical Wigner functions*, Int. J. Quantum Inf. **3**, 501 (2005).

[VII] P. Földi, **O. Kálmán**, M. G. Benedict, and F. M. Peeters: *Networks of quantum nanorings: Programmable spintronic devices*, Nano Lett. **8**, 2556 (2008).

[VIII] **O. Kálmán**, T. Kiss, and P. Földi: *Quantum walk on the line with quantum rings*, Phys. Rev. B **80**, 035327 (2009).

[IX] P. Földi, **O. Kálmán**, and F. M. Peeters: *Stability of spintronic devices based on quantum ring networks*, Phys. Rev. B **80**, 125324 (2009).

[X] P. Földi, M. G. Benedict, **O. Kálmán**, and F. M. Peeters: *Quantum rings with time-dependent spin-orbit coupling: Spintronic Rabi oscillations and conductance properties*, Phys. Rev. B **80**, 165303 (2009).

Acknowlegdement

I would like to thank my supervisors, Mihály G. Benedict and Péter Földi for their guidance throughout my years as a PhD student at the University of Szeged and even after I started working at The Research Institute for Solid State Physics and Optics as a young researcher. Without their professional and personal support this work could not have been completed. I would also like to thank Francois M. Peeters and Partakolis Vasilopoulos, with whom the majority of the work in Chapter 3 had been done during my visit to the University of Antwerp.

I would like to express my gratitude towards Attila Czirják, Piroska Dömötör and every member of the Department of Theoretical Physics, for their professional inspiration, personal encouragment, and their contribution to making a very friendly atmosphere at the University of Szeged.

I would also like to thank all the members of the Department of Quantum Optics and Quantum Information whom I had the opportunity to work with, for creating and maintaining an inspiring atmosphere. In particular, I would like to thank our head, Péter Ádám, who has a great share in creating this atmosphere. I would also like to express my gratitude towards Tamás Kiss, who dedicated his valuable time to carefully reading the manuscript and adding his indispensable comments and suggestions to it.

Last, but not least, I would like to thank my parents, grandparents, and my husband for believing in me, encouraging me, and providing their loving understanding and generous support without which I could not have been able to get this far.

Appendix

Here we present the analytic expressions for the reflection and transmission matrices, obtained from the solution of the scattering problem of general two- and four-terminal rings, in which Rashba-type spin-orbit interaction and a perpendicular magnetic field are present, the latter of which is treated as a perturbation. We have shown in Section 4.1 that it is sufficient to obtain the solution for the boundary condition when only one of the terminals acts as an input, since the more general boundary condition of having inputs on all terminals is just a superposition of such cases with an appropriate rotation of the matrices [see Eqs. (4.27) and (4.28)]. Considering f_{I} as the only input [i.e., $f_{i\neq \mathrm{I}} = 0$ in Fig. 5.2], requiring the continuity of the wave functions, and applying Griffith's boundary conditions at the junctions in both cases (see Section 2.3), we can determine the reflection matrices $R^{f_{\mathrm{I}}}$ and $\tilde{R}^{f_{\mathrm{I}}}$ of the two-terminal ring and of the four-terminal ring, respectively. Both of these matrices can be written in a form analogous to that of $\hat{R}^{f_{\mathrm{I}}}$ of the three-terminal case given by Eq. (4.21) with $\hat{\varrho}^{(\mu)}$ ($\mu = 1, 2$) being replaced by

$$\varrho^{(\mu)} = \frac{4k\rho}{y^{(\mu)}} \left\{ k\rho \sin(q^{(\mu)}\gamma_1) \sin(q^{(\mu)}(2\pi - \gamma_1)) + \mathrm{i} q^{(\mu)} \sin(2q^{(\mu)}\pi) \right\}, \tag{A-1}$$

and

$$\begin{aligned}
\tilde{\varrho}^{(\mu)} \;=\; & \frac{2k\rho}{\tilde{y}^{(\mu)}} \Big\{ k^3\rho^3 \Big[\cos\big(2q^{(\mu)}\pi\big) + \cos\big(2q^{(\mu)}(\pi - \gamma_3 + \gamma_2 - \gamma_1)\big) - \cos\big(2q^{(\mu)}(\pi - \gamma_3 + \gamma_2)\big) \\
& + \cos\big(2q^{(\mu)}(\pi - \gamma_3 + \gamma_1)\big) - \cos\big(2q^{(\mu)}(\pi - \gamma_2 + \gamma_1)\big) - \cos\big(2q^{(\mu)}(\pi - \gamma_3)\big) \\
& + \cos\big(2q^{(\mu)}(\pi - \gamma_2)\big) - \cos\big(2q^{(\mu)}(\pi - \gamma_1)\big) \Big] - 8\mathrm{i}(q^{(\mu)})^3 \sin\big(2q^{(\mu)}\pi\big) \\
& + 2\mathrm{i}k^2\rho^2 q^{(\mu)} \Big[\sin\big(2q^{(\mu)}(\pi - \gamma_3 + \gamma_2)\big) + \sin\big(2q^{(\mu)}(\pi - \gamma_3 + \gamma_1)\big) - 3\sin\big(2q^{(\mu)}\pi\big) \\
& + \sin\big(2q^{(\mu)}(\pi - \gamma_2 + \gamma_1)\big) \Big] + 4\mathrm{i}k^2\rho^2 q^{(\mu)} \Big[\sin\big(2q^{(\mu)}(\pi - \gamma_1)\big) - \sin\big(2q^{(\mu)}(\pi - \gamma_3)\big) \Big] \\
& - 4k\rho(q^{(\mu)})^2 \Big[\cos\big(2q^{(\mu)}(\pi - \gamma_3)\big) + \cos\big(2q^{(\mu)}(\pi - \gamma_2)\big) + \cos\big(2q^{(\mu)}(\pi - \gamma_1)\big) \\
& - 3\cos\big(2q^{(\mu)}\pi\big) \Big] \Big\},
\end{aligned} \tag{A-2}$$

respectively, where

$$\begin{aligned}
y^{(\mu)} \;=\; & k^2\rho^2 \left[\cos(2q^{(\mu)}(\pi - \gamma_1)) - \cos(2q^{(\mu)}\pi) \right] + 4\mathrm{i}kaq^{(\mu)} \sin(2q^{(\mu)}\pi) \\
& - 4(q^{(\mu)})^2 \left[\cos\left[((-1)^{\mu+1} w + 2\phi)\pi \right] + \cos(2q^{(\mu)}\pi) \right],
\end{aligned} \tag{A-3}$$

$$
\begin{aligned}
\tilde{y}^{(\mu)} &= 16\left(q^{(\mu)}\right)^4\left\{\cos\left[((-1)^{\mu+1}w+2\phi)\pi\right]+\cos\left(2q^{(\mu)}\pi\right)\right\}-32\mathrm{i}k\rho\left(q^{(\mu)}\right)^3\sin\left(2q^{(\mu)}\pi\right)\\
&\quad -4k^2\rho^2\left(q^{(\mu)}\right)^2\left[\cos\left(2q^{(\mu)}(\pi-\gamma_3)\right)+\cos\left(2q^{(\mu)}(\pi-\gamma_2)\right)+\cos\left(2q^{(\mu)}(\pi-\gamma_1)\right)\right.\\
&\quad +\cos\left(2q^{(\mu)}(\pi-\gamma_3+\gamma_1)\right)+\cos\left(2q^{(\mu)}(\pi-\gamma_3+\gamma_2)\right)+\cos\left(2q^{(\mu)}(\pi-\gamma_2+\gamma_1)\right)\\
&\quad \left.-6\cos\left(2q^{(\mu)}\pi\right)\right]+4\mathrm{i}k^3\rho^3q^{(\mu)}\left[\sin\left(2q^{(\mu)}(\pi-\gamma_3+\gamma_2)\right)+\sin\left(2q^{(\mu)}(\pi-\gamma_2+\gamma_1)\right)\right.\\
&\quad \left.-\sin\left(2q^{(\mu)}(\pi-\gamma_3)\right)+\sin\left(2q^{(\mu)}(\pi-\gamma_1)\right)\right]-2\sin\left(2q^{(\mu)}\pi\right)+k^4\rho^4\left[\cos\left(2q^{(\mu)}\pi\right)\right.\\
&\quad +\cos\left(2q^{(\mu)}(\pi-\gamma_3+\gamma_2-\gamma_1)\right)-\cos\left(2q^{(\mu)}(\pi-\gamma_3+\gamma_2)\right)-\cos\left(2q^{(\mu)}(\pi-\gamma_3)\right)\\
&\quad +\cos\left(2q^{(\mu)}(\pi-\gamma_3+\gamma_1)\right)-\cos\left(2q^{(\mu)}(\pi-\gamma_2+\gamma_1)\right)+\cos\left(2q^{(\mu)}(\pi-\gamma_2)\right)\\
&\quad \left.-\cos\left(2q^{(\mu)}(\pi-\gamma_1)\right)\right]. \qquad \text{(A-4)}
\end{aligned}
$$

Here $\phi=\Phi/\Phi_0$, w and $q^{(\mu)}$ are given by Eq. (4.4) and (4.13), respectively.

The transmission matrices $T^{f_{\mathrm{I}}}$ of the two-terminal ring and $\tilde{T}_n^{f_{\mathrm{I}}}$ $(n=1,2,3)$ of the four terminal ring can be given in an analogous form to that of the transmission matrices $\hat{T}_n^{f_{\mathrm{I}}}$ of the three-terminal one given by Eq. (4.24), with $\hat{\tau}_n^{(\mu)}$ being replaced by

$$
\tau^{(\mu)}=\frac{4\mathrm{i}k\rho q^{(\mu)}}{y^{(\mu)}}e^{\mathrm{i}\gamma\left((-1)^{\mu+1}w/2+\phi\right)}\left[\sin(q^{(\mu)}(2\pi-\gamma))-e^{-\mathrm{i}\pi\left((-1)^{\mu+1}w+2\phi\right)}\sin(q^{(\mu)}\gamma)\right], \qquad \text{(A-5)}
$$

and

$$
\begin{aligned}
\tilde{\tau}_1^{(\mu)} &= \frac{4k\rho q^{(\mu)}}{\tilde{y}^{(\mu)}}e^{\mathrm{i}\frac{\gamma_1}{2}\left((-1)^{\mu+1}w+2\phi\right)}\left\{\mathrm{i}k^2\rho^2\left[\sin\left(q^{(\mu)}(2\pi-2\gamma_3+2\gamma_2-\gamma_1)\right)-\sin\left(q^{(\mu)}(2\pi-\gamma_1)\right)\right.\right.\\
&\quad \left.+\sin\left(q^{(\mu)}(2\pi-\gamma_2+\gamma_1)\right)-\sin\left(q^{(\mu)}(2\pi-\gamma_3+\gamma_1)\right)\right]+2k\rho q^{(\mu)}\left[2\cos\left(q^{(\mu)}(2\pi-\gamma_1)\right)\right.\\
&\quad \left.-\cos\left(q^{(\mu)}(2\pi-2\gamma_2+\gamma_1)\right)-\cos\left(q^{(\mu)}(2\pi-2\gamma_3+\gamma_1)\right)\right]\\
&\quad \left.+4\mathrm{i}(q^{(\mu)})^2\left[e^{-\mathrm{i}\pi\left((-1)^{\mu+1}w+2\phi\right)}\sin\left(q^{(\mu)}\gamma_1\right)-\sin\left(q^{(\mu)}(2\pi-\gamma_1)\right)\right]\right\}, \qquad \text{(A-6)}
\end{aligned}
$$

$$
\begin{aligned}
\tilde{\tau}_2^{(\mu)} &= \frac{4k\rho q^{(\mu)}}{\tilde{y}^{(\mu)}}e^{\mathrm{i}\frac{\gamma_2}{2}\left((-1)^{\mu+1}w+2\phi\right)}\left\{2k\rho q^{(\mu)}\left[\cos\left(q^{(\mu)}(2\pi-\gamma_2)\right)-e^{-\mathrm{i}\pi\left((-1)^{\mu+1}w+2\phi\right)}\cos\left(q^{(\mu)}\gamma_2\right)\right.\right.\\
&\quad \left.+e^{-\mathrm{i}\pi\left((-1)^{\mu+1}w+2\phi\right)}\cos\left(q^{(\mu)}(2\gamma_1-\gamma_2)\right)-\cos\left(q^{(\mu)}(2\pi-2\gamma_3+\gamma_2)\right)\right]\\
&\quad \left.+4\mathrm{i}\left(q^{(\mu)}\right)^2\left[e^{-\mathrm{i}\pi\left((-1)^{\mu+1}w+2\phi\right)}\sin\left(q^{(\mu)}\gamma_2\right)-\sin\left(q^{(\mu)}(2\pi-\gamma_2)\right)\right]\right\}, \qquad \text{(A-7)}
\end{aligned}
$$

$$
\begin{aligned}
\tilde{\tau}_3^{(\mu)} &= \frac{4k\rho q^{(\mu)}}{\tilde{y}^{(\mu)}}e^{\mathrm{i}\frac{\gamma_3}{2}\left((-1)^{\mu+1}w+2\phi\right)}\left\{\mathrm{i}k^2\rho^2e^{-\mathrm{i}\pi\left((-1)^{\mu+1}w+2\phi\right)}\left[\sin\left(q^{(\mu)}\gamma_3\right)+\sin\left(q^{(\mu)}(2\gamma_1-\gamma_3)\right)\right.\right.\\
&\quad \left.-\sin\left(q^{(\mu)}(2\gamma_2-\gamma_3)\right)+\sin\left(q^{(\mu)}(2\gamma_2-2\gamma_1-\gamma_3)\right)\right]\\
&\quad -2k\rho q^{(\mu)}e^{-\mathrm{i}\pi\left((-1)^{\mu+1}w+2\phi\right)}\left[2\cos\left(q^{(\mu)}\gamma_3\right)-\cos\left(q^{(\mu)}(2\gamma_1-\gamma_3)\right)-\cos\left(q^{(\mu)}(2\gamma_2-\gamma_3)\right)\right]\\
&\quad \left.+4\mathrm{i}\left(q^{(\mu)}\right)^2\left[e^{-\mathrm{i}\pi\left((-1)^{\mu+1}w+2\phi\right)}\sin\left(q^{(\mu)}\gamma_3\right)-\sin\left(q^{(\mu)}(2\pi-\gamma_3)\right)\right]\right\}, \qquad \text{(A-8)}
\end{aligned}
$$

respectively.

Bibliography

[1] S. Datta, *Electronic Transport in Mesoscopic Systems* (Cambridge Univ. Press, Cambridge, 1995).

[2] C. W. J. Beenakker and H. van Houten, Solid State Physics **44**, 1 (1991).

[3] B. J. van Wees, H. van Houten, C. W. J. Beenakker et al., Phys. Rev. Lett. **60**, 848 (1988).

[4] R. A. Webb, S. Washburn, C. P. Umbach et al., Phys. Rev. Lett. **54**, 2696 (1985).

[5] Y. Aharonov and D. Bohm, Phys. Rev. **115**, 485 (1959).

[6] D. D. Awschalom, D. Loss and N. Samarth, *Semiconductor Spintronics and Quantum Computation* (Springer, Berlin, 2002).

[7] I. Žutić, J. Fabian and S. D. Sarma, Rev. Mod. Phys. **76**, 323 (2004).

[8] J. Cserti, Természet Világa **136**, 9 (2005).

[9] S. Bandyopadhyay and M. Cahay, *Introduction to Spintronics* (CRC Press, 2008).

[10] M. N. Baibich, J. M. Broto, A. Fert et al., Phys. Rev. Lett. **61**, 2472 (1988).

[11] G. Binasch, P. Grünberg, F. Saurenbach et al., Phys. Rev. B **39**, 4828 (1989).

[12] S. Imre and F. Balázs, *Quantum Computing and Communications An Engineering Approach* (John Wiley & Sons, Chichester, West Sussex, 2005).

[13] D. Bouwmeester, A. Eckert and A. Z. (Eds.), *The Physics of Quantum Information* (Springer, Berlin, 2001).

[14] S. Stenholm and K.-A. Souminen, *Quantum Approach to Informatics* (John Wiley & Sons, Hoboken, New Jersey, 2005).

[15] L. Diósi, *A Short Course in Quantum Information Theory An Approach From Theoretical Physics in Lecture Notes in Physics, Vol. 713* (Springer, Berlin, 2007).

[16] D. Deutsch and R. Jozsa, Proc. Math. Phys. Sci. **439**, 553 (1992).

[17] P. W. Shor, SIAM J.Sci.Statist.Comput. **26**, 1484 (1997).

[18] M. A. Nielsen and I. L. Chuang, *Quantum Computation and Quantum Information* (Cambridge Univ. Press, Cambridge, 2000).

[19] J. M. Kikkawa and D. D. Awschalom, Phys. Rev. Lett. **80**, 4313 (1998).

[20] J. M. Kikkawa and D. D. Awschalom, Nature **397**, 139 (1999).

[21] B. Huang, D. J. Monsma and I. Appelbaum, Phys. Rev. Lett. **99**, 177209 (2007).

[22] E. I. Rashba, Sov. Phys. Solid State **2**, 1109 (1960).

[23] J. Nitta, T. Akazaki, H. Takayanagi et al., Phys. Rev. Lett. **78**, 1335 (1997).

[24] D. Grundler, Phys. Rev. Lett. **84**, 6074 (2000).

[25] S. Datta and B. Das, Appl. Phys. Lett. **56**, 665 (1990).

[26] M. Popp, D. Frustaglia and K. Richter, Nanotechnology **14**, 347 (2003).

[27] R. Ionicioiu and I. D'Amico, Phys. Rev. B **67**, 041307(R) (2003).

[28] D. Frustaglia, M. Hentschel and K. Richter, Phys. Rev. Lett. **87**, 256602 (2001).

[29] J. Nitta, F. E. Meijer and H. Takayanagi, Appl. Phys. Lett. **75**, 695 (1999).

[30] J. Nitta, T. Koga and H. Takayanagi, Physica E **12**, 753 (2002).

[31] M. König, A. Tschetschetkin, E. M. Hankiewicz et al., Phys. Rev. Lett. **96**, 076804 (2006).

[32] T. Bergsten, T. Kobayashi, Y. Sekine et al., Phys. Rev. Lett. **97**, 196803 (2006).

[33] J. Nitta and T. Bergsten, New J. Phys. **9**, 341 (2007).

[34] P. Földi, B. Molnár, M. G. Benedict et al., Phys. Rev. B **71**, 033309 (2005).

[35] B. Szafran and F. M. Peeters, Phys. Rev. B **72**, 165301 (2005).

[36] J. S. Sheng and K. Chang, Phys. Rev. B **74**, 235315 (2006).

[37] S. Bellucci and P. Onorato, J. Phys.: Condens. Matter **19**, 395020 (2007).

[38] H. L. Störmer, Surf. Sci. **132**, 519 (1983).

[39] J. J. Harris, J. A. Pals and R. Woltjer, Rep. Prog. Phys. **52**, 1217 (1989).

[40] D. J. Newson, K. F. Berggren, M. Pepper et al., J. Phys. C: Solid State Phys. **19**, L403 (1986).

[41] J. Singleton, R. J. Nicholas, F. Nasir et al., J. Phys. C: Solid State Phys. **19**, 35 (1986).

[42] L. I. Schiff, *Quantum Mechanics 3rd ed.* (McGraw-Hill, New York, 1968).

[43] M. E. Cage, R. F. Dziuba and B. F. Field, IEEE Trans. Instrum. Meas. **34**, 301 (1985).

[44] J. M. Ziman, *Principles of the theory of solids* (Cambridge University Press, Cambridge, 1972).

[45] J. H. Davies, *The physics of low-dimensional semiconductors* (Cambridge University Press, Cambridge, 1998).

[46] R. Landauer, IBM J. Res. Dev. **32**, 306 (1988).

[47] V. B. Berestetskii, E. M. Lifshitz and L. P. Pitaevskii, *Landau and Lifshitz Course of Theoretical Physics Vol. 4: Quantum Electrodynamics 2nd Ed.* (Pergamon Press, Oxford, 1922).

[48] J. J. Sakurai, *Advanced Quantum Mechanics* (Addison-Wesley, 1967).

[49] J. Singh, *Physics of Semiconductors and their Heterostructures* (McGraw-Hill, New York, 1993).

[50] G. Dresselhaus, Phys. Rev. **100**, 580 (1955).

[51] R. Winkler, *Spin-Orbit Coupling Effects in Two-Dimensional Electron and Hole Systems* (Springer, Berlin, 2003).

[52] H.-A. Engel, E. I. Rashba and B. I. Halperin, *Theory of Spin Hall Effects in Semiconductors, in Handbook of Magnetism and Advanced Magnetic Materials* (Wiley & Sons Ltd., Chichester, UK, 2006).

[53] Y. A. Bychkov and E. I. Rashba, J. Phys. C **17**, 6039 (1984).

[54] E. A. de Andrada e Silva, G. C. L. Rocca and F. Bassani, Phys. Rev. B **50**, 8523 (1994).

[55] J. Fabian, A. Matos-Abiague, C. Ertler et al., Act. Phys. Slov. **57**, 565 (2007).

[56] G. Lommer, F. Malcher and U. Rössler, Phys. Rev. Lett. **60**, 728 (1988).

[57] E. A. de Andrada e Silva, Phys. Rev. B **46**, 1921 (1992).

[58] B. Das, S. Datta and R. Reifenberger, Phys. Rev. B **41**, 8278 (1990).

[59] G. Engels, J. Lange, T. Schäpers et al., Phys. Rev. B **55**, R1958 (1997).

[60] X. C. Zhang, A. Pfeuffer-Jeschke, K. Ortner et al., Phys. Rev. B **63**, 245305 (2001).

[61] J. Nitta, T. Akazaki, H. Takayanagi et al., Physica E **2**, 527 (1998).

[62] M. Büttiker, Y. Imry and M. Y. Azbel, Phys. Rev. A **30**, 1982 (1984).

[63] A. D. Stone and Y. Imry, Phys. Rev. Lett. **56**, 189 (1986).

[64] G. Timp, A. M. Chang, J. E. Cunningham et al., Phys. Rev. Lett. **58**, 2824 (1987).

[65] K. Ismail, S. Washburn and K. Y. Lee, Appl. Phys. Lett. **59**, 1998 (1991).

[66] C. J. B. Ford, A. B. Fowler, J. M. Hong et al., Surf. Sci. **229**, 307 (1990).

[67] S. Pedersen, A. E. Hansen, A. Kristensen et al., Phys. Rev. B **61**, 5457 (2000).

[68] T. Ihn, A. Fuhrer, M. Sigrist et al., Adv. in Solid State Phys. **43**, 139 (2003).

[69] M. Peshkin and A. Tonomura, Lecture Notes in Physics **340** (1989).

[70] C. P. Umbach, C. V. Haesendonck, R. B. Laibowitz et al., Phys. Rev. Lett. **56**, 386 (1986).

[71] B. L. Al'tshuler, A. G. Aronov and B. F. Spivak, JETP Lett. **33**, 94 (1981).

[72] J. Sólyom, *A Modern Szilárdtestfizika Alapjai III.* (ELTE Eötvös Kiadó Kft., Budapest, 2003).

[73] D. Y. Sharvin and Y. V. Sharvin, JETP Lett. **34**, 272 (1981).

[74] B. L. Al'tshuler, A. G. Aronov, B. Z. Spivak et al., JETP Lett. **35**, 588 (1982).

[75] B. Pannetier, J. Chaussy, R. Rammal et al., Phys. Rev. Lett. **53**, 718 (1984).

[76] B. Pannetier, J. Chaussy, R. Rammal et al., Phys. Rev. B **31**, 3209 (1985).

[77] T. Koga, Y. Sekine and J. Nitta, Phys. Rev. B **74**, 041302(R) (2006).

[78] J. Luo, H. Munekata, F. F. Fang et al., Phys. Rev. B **41**, 7685 (1990).

[79] S. A. Wolf, D. D. Awschalom, R. A. Buhrman et al., Science **294**, 1488 (2001).

[80] I. Žutić, J. Fabian and S. D. Sarma, Rev. Mod. Phys. **76**, 323 (2004).

[81] J. Nitta, NTT Technical Review **2**, 31 (2004).

[82] C. Benjamin and A. M. Jayannavar, Phys. Rev. B **65**, 153309 (2002).

[83] S. Bandopadhyay, P. S. Deo and A. M. Jayannavar, Phys. Rev. B **70**, 075315 (2004).

[84] A. Yacoby, M. Heiblum, D. Mahalu et al., Phys. Rev. Lett. **74**, 4047 (1995).

[85] G. Cernicchiaro, T. Martin, K. Hasselbach et al., Phys. Rev. Lett. **79**, 273 (1997).

[86] Y. Gefen, Y. Imry and M. Y. Azbel, Phys. Rev. Lett. **52**, 129 (1984).

[87] E. Merzbacher, *Quantum Mechanics 2nd ed.* (John Wiley & Sons, New York, 1970).

[88] D. J. Griffith, *Introduction to Quantum Mechanics* (Prentice Hall, Upper Saddle River, New Jersey, 1995).

[89] S. Griffith, Trans. Faraday Soc. **49**, 345 (1953).

[90] F. E. Meijer, A. F. Morpugo and T. M. Klapwijk, Phys. Rev. B **66**, 033107 (2002).

[91] D. Frustaglia and K. Richter, Phys. Rev. B **69**, 235310 (2004).

[92] B. Molnár, F. M. Peeters and P. Vasilopoulos, Phys. Rev. B **69**, 155335 (2004).

[93] P. Vasilopoulos, O. Kálmán, F. M. Peeters et al., Phys. Rev. B **75**, 035304 (2007).

[94] K. N. Pichugin and A. F. Sadreev, Phys. Rev. B **56**, 9662 (1997).

[95] O. Kálmán, P. Földi, M. G. Benedict et al., Phys. Rev. B **78**, 125306 (2008).

[96] P. Földi, O. Kálmán, M. G. Benedict et al., Phys. Rev. B **73**, 155325 (2006).

[97] O. Kálmán, P. Földi, M. G. Benedict et al., Physica E **40**, 567 (2008).

[98] O. Kálmán, P. Földi and M. G. Benedict, Open Sys. and Inf. Dyn. **13**, 455 (2006).

[99] R. Ionicioiu and I. D'Amico, Phys. Rev. B **67**, 041307 (R) (2003).

[100] A. W. Cummings, R. Akis and D. K. Ferry, Appl. Phys. Lett. **89**, 172115 (2006).

[101] A. G. Mal'shukov, C. S. Tang, C. S. Chu et al., Phys. Rev. B **68**, 233307 (2003).

[102] M. Governale, D. Boese, U. Zülicke et al., Phys. Rev. B **65**, 140403(R) (2002).

[103] A. Pályi, C. Péterfalvi and J. Cserti, Phys. Rev. B **74**, 073305 (2006).

[104] G. Papp, P. Vasilopoulos and F. M. Peeters, Phys. Rev. B **72**, 115315 (2005).

[105] R. Loudon, *The Quantum Theory of Light 3rd ed.* (Cambridge Univ. Press, Cambridge, 2000).

[106] J. K. Asbóth, P. Adam, M. Koniorczyk et al., Eur. Phys. J. D **30**, 403410 (2004).

[107] Y. Hasegawa, R. Loidl, G. Badurek et al., Nature (London) **425**, 45 (2003).

[108] S. Hill and W. K. Wootters, Phys. Rev. Lett. **78**, 5022 (1997).

[109] W. K. Wootters, Phys. Rev. Lett. **80**, 2245 (1998).

[110] B. Molnár and P. V. F. M. Peeters, Phys. Rev. B **72**, 075330 (2005).

[111] A. Pályi and J. Cserti, Phys. Rev. B **76**, 035331 (2007).

[112] A. Pályi and J. Cserti, Phys. Rev. B **78**, 241304(R) (2008).

[113] J. Cserti, A. Csordás and U. Zülicke, Phys. Rev. B **70**, 233307 (2004).

[114] T. Koga, J. Nitta and M. van Veenhuizen, Phys. Rev. B **70**, 161302(R) (2004).

[115] U. Zülicke and A. I. Signal, Solid State Commun. **144**, 529 (2007).

[116] S. Bellucci and P. Onorato, Phys. Rev. B **77**, 165305 (2008).

[117] G. Papp, S. Borza and F. M. Peeters, J. Appl. Phys. **97**, 113901 (2005).

[118] P. Földi, O. Kálmán, M. G. Benedict et al., Nano Lett. **8**, 2556 (2008).

[119] O. Kálmán, T. Kiss and P. Földi, Phys. Rev. B **80**, 035327 (2009).

[120] M. J. van Veenhuizen, T. Koga and J. Nitta, Phys. Rev. B **73**, 235315 (2006).